ANNUAL REPORT

Center for Experimental Nuclear Physics and Astrophysics
University of Washington
May, 2003

Sponsored in part by the United States Department of Energy under Grant #DE-FG03-97ER41020/A000.

Cover photos, clockwise from upper left: One of the SNO NCD welding teams, Sean McGee, Tom Burritt, Ian Lawson (Guelph) and Peter Doe, preparing a pre-deployment-welded NCD segment for storage in the mine at Sudbury. Kareem Kazkaz and Jeremy Kephart(NC State) verifying the performance of the SEGA crystal after taking possession of it from Ortec. Smarajit Triambak and Cristina Bordeanu, adjusting the target position for a Tandem experiment. The fixture for welding the NCDs.

INTRODUCTION

CENPA pursues a broad program of research in nuclear physics, astrophysics and related fields. Research activities are conducted locally and at remote sites. The current program includes "in-house" research on nuclear collisions and fundamental interactions using the local tandem Van de Graaff, as well as local and remote non-accelerator research on fundamental interactions and user-mode research on relativistic heavy ions at large accelerator facilities in the U.S. and Europe. We are pleased to welcome Professor Alejandro García, who joined our faculty in September 2002, and Professor Askel Hallin, on sabbatical from Queen's University.

We have completed our "Phase II" ^{7}Be(p,γ)^{8}B measurements, extending our earlier work to lower energy and reducing our systematic errors. Our new $S_{17}(0)$ determination is in excellent agreement with our Phase I value published in 2002. Our measurements remain the most precise determination to date of this important reaction rate.

We have developed a ^{8}B radioactive beam at the Tandem with a flux of half a dozen ^{8}B per second, and have accumulated about 3×10^{5} coincidence-tagged ^{8}B decays, in an experiment searching for a branch to the ground state of ^{8}Be. We are presently analyzing these data, searching for a signal from the 92-keV alpha particles from the ground state of ^{8}Be.

Event structure analysis of RHIC Au-Au collisions has revealed a number of new correlation phenomena related to 1) initial-state multiple scattering and its variation with event centrality and 2) local measure conservation at hadronization and its variation with changes in the prehadronic medium, both indicating the development of a collective medium with dissipative properties. Fluctuation scaling results have been successfully inverted by a numerical process to construct autocorrelation distributions which are directly interpretable in terms of physical models.

HBT interferometry with STAR data at RHIC have in the past three years provided significant challenges to conventional theoretical models of RHIC physics. The latest such challenges, reported here, show rising pion phase space density and decreasing entropy per particle with centrality, both results suggesting the onset of some unknown low entropy process in central RHIC collisions.

The SNO detector has been in operation since June 2001 with 0.2% NaCl added to the heavy water to enhance detection of neutrons released by neutral current interactions. Analysis of 254 live days of that data set is nearly complete and a paper is being prepared for publication in the summer of 2003. As expected, a strong neutron peak is seen, but because a "blind" analysis is being performed the implied NC rate is not yet known. Quite good statistical separation of NC events from charged-current ones based on the differences in anisotropy of Čerenkov light is being realized.

The neutral current detector array is complete, and the detectors have been welded together in preparation for deployment. Deployment hardware is in hand and deployment crews are trained in readiness for installation of the array in late 2003.

The MOON ^{100}Mo double beta decay experiment research at CENPA is now focused on development of a bolometric method that could provide high energy resolution and the ability to tag double-beta transitions to excited states in ^{100}Ru. In collaboration with UW condensed-matter physicists a dilution refrigerator is being set up to make preliminary measurements of the specific heat and thermal diffusivity of superconducting and normal Mo at millikelvin temperatures.

The emiT experiment, a search for time violation in neutron beta decay, has been collecting data at the NIST Center for Neutron Research since the fall of 2002. To date, it has been a highly successful run, collecting over 150 million coincidences. The collaboration plans to continue acquiring data and studying potential systematics through the end of 2003.

Development of the world's most sensitive direct kinematical neutrino-mass measurement, via tritium beta-decay, has been proceeding rapidly. The University of Washington intends to provide the detector system for this international experiment that will be constructed at the Forschungszentrum Karlsruhe in Germany.

The Majorana collaboration hopes to construct a ^{76}Ge-based next generation 0-neutrino double-beta-decay detector. Our efforts have concentrated on collaborating with scientists at Pacific Northwest National Laboratories to construct a prototype Multiple-Element Germanium Assay (MEGA) detector that consists of an array of 18 high purity Ge detectors.

Progress on the ^{199}Hg EDM experiment includes increased reliability of the 254-nm laser system and a reduction in discharges occurring in the high-voltage cables. Data are currently being taken towards a new measurement.

We are developing an experiment to measure the beta asymmetry from neutron beta decay with high accuracy to elucidate the apparent non-unitarity of the CKM matrix.

We have started experiments at CENPA to reduce uncertainties regarding high-precision measurements to determine the positron-neutrino correlation and the log(ft) value for the $0^+ \rightarrow 0^+$ decay of ^{32}Ar.

Torsion-balance experiments have demonstrated that, for distances down to 90 μm, there is no force that violates Newton's inverse square law coupling to mass with equal or larger strength than gravity. New developments include 1) a pendulum for testing coupling to spin, 2) a new equivalence principle test, and 3) an 'anapole' pendulum for an axion search.

As always, we encourage outside applications for the use of our facilities. As a convenient reference for potential users, the table on the following page lists the capabilities of our accelerators. For further information, please contact Prof. Derek W. Storm, Executive Director, CENPA, Box 354290, University of Washington, Seattle, WA 98195; (206) 543-4080, or storm@npl.washington.edu. Further information is also available on our web page: http://www.npl.washington.edu.

We close this introduction with a reminder that the articles in this report describe work in progress and are not to be regarded as publications or to be quoted without permission of the authors. In each article the names of the investigators are listed alphabetically, with the primary author underlined, to whom inquiries should be addressed.

Derek Storm, Editor — Barbara Fulton, Assistant Editor

TANDEM VAN DE GRAAFF ACCELERATOR

A High Voltage Engineering Corporation Model FN purchased in 1966 with NSF funds, operation funded primarily by the U.S. Department of Energy. See W. G. Weitkamp and F. H. Schmidt, "The University of Washington Three Stage Van de Graaff Accelerator," Nucl. Instrum. Meth. **122**, 65 (1974). Recently adapted to an (optional) terminal ion source and a non-inclined tube #3, which enables the accelerator to produce high intensity beams of helium and hydrogen isotopes at energies from 100 keV to 5.5 MeV.

Some Available Energy Analyzed Beams

Ion	Max. Current (particle μA)	Max. Energy (MeV)	Ion Source
^{1}H or ^{2}H	50	18	DEIS or 860
^{3}He or ^{4}He	2	27	Double Charge-Exchange Source
^{3}He or ^{4}He	30	7.5	Tandem Terminal Source
^{6}Li or ^{7}Li	1	36	860
^{11}B	5	54	860
^{12}C or ^{13}C	10	63	860
*^{14}N	1	63	DEIS or 860
^{16}O or ^{18}O	10	72	DEIS or 860
F	10	72	DEIS or 860
* Ca	0.5	99	860
Ni	0.2	99	860
I	0.001	108	860

*Negative ion is the hydride, dihydride, or trihydride.

Additional ion species available including the following: Mg, Al, Si, P, S, Cl, Fe, Cu, Ge, Se, Br and Ag. Less common isotopes are generated from enriched material.
In addition, we are now producing a separated beam of 15-MeV ^{8}B at 6 particles/second.

BOOSTER ACCELERATOR

See "Status of and Operating Experience with the University of Washington Superconducting Booster Linac," D. W. Storm *et al.*, Nucl. Instrum. Meth. A **287**, 247 (1990). The Booster is presently in a "mothballed" state.

Contents

1 Fundamental Symmetries and Weak Interactions

Weak Interactions

1.1 A second run of the emiT experiment

J. F. Amsbaugh, L. Grout,* H. P. Mumm, A. W. Myers, P. Parazzoli,†
R. G. H. Robertson, K. Sundqvist,‡ T. D. Van Wechel, D. I. Will and J. F. Wilkerson

The emiT experiment is a search for time-reversal (T) invariance violation in the beta decay of free neutrons. Current observations of CP(T) violation in the Kaon and B-meson systems can be accommodated within the standard model of particle physics. However, baryogensis as well as attempts to develop unified theories, indicate that additional sources are required. The standard model predicts T-violating observables in beta decay to be extremely small (second order in the weak coupling constant) and hence to be beyond the reach of modern experiments.[1] However, potentially measurable T-violating effects are predicted to occur in some non-standard models such as those with left-right symmetry, exotic fermions, or lepto-quarks.[2,3] Thus a precision search for T-violation in neutron beta decay provides an excellent test of physics beyond the Standard Model.

The emiT experiment in sensitive to the T-odd P-even triple correlation between the neutron spin and the momenta of the neutrino and electron, $D\boldsymbol{\sigma_n} \cdot \boldsymbol{P_e} \times \boldsymbol{P_\nu}$, in the neutron beta-decay distribution. The coefficient of this correlation, D, is measured by detecting decay electrons in coincidence with recoil protons from a polarized beam of cold (2.7 meV) neutrons. Four electron detectors (plastic scintillators) and four proton detectors (large-area diode arrays) are arranged in an alternating octagonal array concentric with the neutron beam.

During the first run, high voltage related problems damaged electronic components, led to high background rates and ultimately produced a non-symmetric detector. Systematic effects were less effectively canceled due to the lack of full detector symmetry and a more complex data analysis scheme was required. The result, $D = -0.1 \pm 1.3 \times 10^{-3}$, represents a small improvement over the current world average.[4] To solve these problems, a major overhaul of the emiT detector was started in 1999. A full redesign of the proton focusing assembly maintained focusing efficiency, while reducing high field regions and minimizing the associated field emission, the dominant background during the first run. To reduce dead-layer-proton-energy loss, surface barrier detectors having a Au layer of 20 μg/cm^2, a depletion

*Presently at MIT Lincoln Labs, Lexington, MA 02420.
†Presently at Los Alamos National Laboratory, Los Alamos, NM 87545.
‡Presently at Department of Physics, University of California, Berkeley, CA 94720.
[1] M. Kobayashi and T. Maskawa, Prog. Theor. Phys. **49**, 652 (1973).
[2] P. Herczeg, *Progress in Nuclear Physics*, W.-Y. P. Hwang, ed., Elsevier Sciences Publishing Co. Inc. (1991) p. 171.
[3] E. G. Wasserman, *Time Reversal Invariance in Polarized Neutron Decay*, Ph.D. thesis, Harvard University, (1994).
[4] L. J. Lising *et al*, Phys. Rev. C **62**, 055501 (2000).

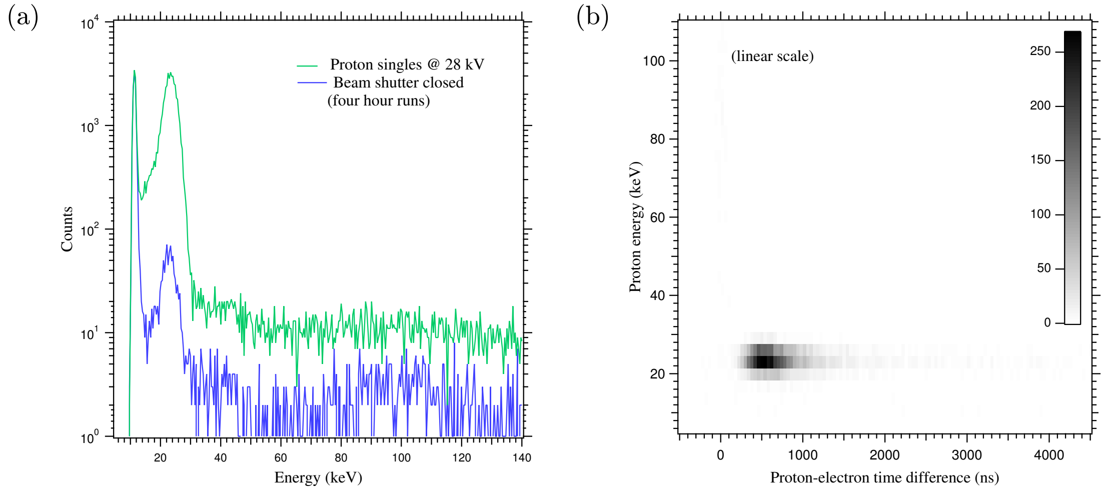

Figure 1.1-1. Raw proton data for surface barrier A16. (a) Pulse height singles spectrum of decay protons for a typical four hour run. The FWHM is 4.78 keV. The peak near 25 keV in the 'beam shutter closed' data, which is the smaller amplitude graph, is from protons and is below 0.6 Hz in all channels. The low energy peak is the minimum ionizing peak in silicon. (b) Coincidence plot of the same data, proton energy vs delay time. Note very low backgrounds.

region of 300 microns and an active area of 300 mm^2 are being used for the second run. A new liquid nitrogen based system was installed and was critical to achieving acceptable energy resolution. Major upgrades to the preamps, shaper/ADC boards, timing electronics and data acquisition code have been completed. A low-energy < 800 eV, low-intensity proton source, was constructed to facilitate *in situ* characterization of our detectors.[5] Finally, measurements indicate that NIST's Center for Neutron Research reactor upgrade has yielded the expected factor of 1.8 increase in flux.

In June of 2002, the emiT detector was moved to NIST's Center for Neutron Research. A test stand was set up to allow testing of the individual proton and electron detectors off-line. While final beamline development and magnetic field alignment were being carried out a number of independent detector validation tasks were carried out. While the high voltage behavior was much improved since emiT's last run, see Fig. 1.1-1, tests lead to a repolishing of the electrodes and minor modifications of the electrode hardware. Cooling tests indicated that surface barrier leakage current was higher than expected. To mitigate the negative effects on resolution, preamp supply voltage was lowered, reducing heat load. Some alterations were also made to the cooling hardware.

By September, the detector was installed on the neutron beamline and was fully functional. The proton and electron detectors were each calibrated with a selection of gamma sources. At this point it became clear that high background rates were leading to an unacceptably high dead time. This problem was attacked from a number of angles. First, timing and gate widths in both the proton and electron electronics chains were optimized. Second, by moving the neutron beam stop half a meter downstream, using lithium plastic in place

[5] F. Naab *et al.*, Nucl. Instrum. Methods B, **197**, 278 (2002).

of boroflex, and by careful shielding of the spin flipper, background rates in the beta detectors was reduced by fifty percent. Attempts were also made to improve the data acquisition software performance.

EmiT is now collecting data at a coincidence rate of 28 Hz. Approximately 15 million events have been collected, giving a statistical sensitivity superior to all previous measurements. A preliminary test of the dominant systematic effect has been conducted and indicates that systematics are below the expected sensitivity of the apparatus. EmiT will continue to take data through August of 2003 and expects to reach the design sensitivity of $D \approx 2 \times 10^{-4}$.

1.2 Status and updates to emiT DAQ

M. A. Howe and J. F. Wilkerson

The emiT data acquisition (emiTDAQ) software that is being used to collect data for the emiT experiment was installed at NIST during the summer of 2002. Since the emiTDAQ software was described in last year's annual report,[1] only a brief overview of the most significant updates and operational status is provided here.

One of the first major upgrades to emiTDAQ after installation was to move the event readout off the Mac and into a VME-based embedded CPU (eCPU). The eCPU runs a small stand-alone application that monitors the CENPA-built 100-MHz latched clock for event signals, reads out hardware as required, bundles the data together with the timing information from the latched clock, and finally places the data into dual memory. The main system reads the data from dual port memory, builds events that fall within a slow coincidence-timing window by using the timing information, and stores the built data to disk. A user specified fraction of non-coincidence data are recorded to disk as well.

Data quality and monitoring tools were developed to allow the quality of the data stream to be monitored online in real-time. Histograms of all the shaper ADC, TDC, and QDC data are kept as well as 2D histograms of the coincidence data. Data rates are also calculated and displayed so that the operator can quickly visualize the overall state of the detector, find dead channels, diagnose gain/threshold problems, etc.

Integrated control of various system parameters is done using an Acromag IP220 DAC module. One of the parameters controlled is the neutron beam polarization spin direction which is flipped every ten seconds.

Analog parameters such as detector temperatures are readout using an Acromag IP320 I/O module and an 1151N scaler module. For monitoring the health of the detector, all the analog data can be displayed, both in table form as well as in strip-chart form. High/Low alarm limits can be set on all parameters. In addition to sounding audible alarms, notifications can be e-mailed to the cell phones or pagers of interested parties. Constraints can be specified for which alarms are sent and acceptable time windows during which to send them. Since the emiT detector is not manned over-night, the email alarm system has helped alert on call operators to serious incipient problems with the detector which would have resulted in detector downtime and/or actual harm to the detector.

A completely separate system was added to read out the magnetometer data using LabView. The magnetometer data are transferred to the emiTDAQ approximately once per minute and are stored in the data stream.

The emiT DAQ system has been running almost continuously since installation and continues to perform reliably. No further upgrades are expected.

[1] CENPA Annual Report, University of Washington (2002) p. 1.

1.3 Parity non-conserving neutron spin rotation in liquid helium

E. G. Adelberger, A. García, B. R. Heckel and H. E. Swanson

We have undertaken a project to measure the PNC neutron spin rotation in a 50 cm long liquid helium target to a precision of 10^{-7} rad and to explore the possibility of measuring the PNC interaction between bare neutrons and protons. This project has been supported by the NSF in addition to the support received from the DOE through CENPA. The collaboration for this project includes E. Adelberger, A. Garcia, B. Heckel and E. Swanson from CENPA, M. Snow and C. Bass from Indiana University, and D. Haase and D. Markoff from TUNL.

Despite a considerable body of data of PNC measurements in nuclei, it has not been possible to extract a consistent picture of the weak force between nucleons. Uncertainties about the nuclear wave functions make it difficult to compare experiment to theory unambiguously. The weak isovector coupling constant, f_π, is of particular interest because it is strongly influenced by the neutral current Z^0 exchange, yet it has proven to be very difficult to measure.

We have proposed to measure f_π in PNC $n-alpha$ scattering, a few-body nucleon system that may be calculated with relative confidence. The PNC rotation of the spin vector of a neutron beam as it traverses a liquid helium target, ϕ_{pnc}, provides a measurable observable:

$$\phi_{pnc}(n-\alpha) \quad \propto \quad +f_\pi + .33h^0_\rho + .23h^0_\omega - .11h^1_\rho - .23h^1_\omega - .02h'^1_\rho$$

where the coupling constants are the standard DDH amplitudes.[1] If f_π vanishes, then PNC p-α measurements, the isospin conjugate system to n-alpha, predict a value for ϕ_{pnc} of approximately 5×10^{-7} rad in a 50-cm long liquid-helium target, five times larger than the experimental limit we propose to achieve.

Cold neutrons, having de Broglie wavelengths longer than 0.4 nm, propagate through material targets as neutron waves. The target averaged interaction with the neutrons creates a neutron index of refraction. PNC neutron spin rotation arises from a term $G'\vec{\sigma}\cdot\vec{p}$ in the index of refraction that is generated by the weak interaction (where $\vec{\sigma}$ is the Pauli spin and $\vec{p}$ is the momentum of the neutron, and G' is proportional to the universal weak coupling constant.) The spins in a neutron beam whose polarization vector is transverse to $\vec{p}$ will experience a torque about $\vec{p}$, resulting in a total rotation angle of:

$$\phi_{pnc} \quad = \quad -4\pi NLRe(G')$$

independent of neutron momentum, where N is the number density of target nuclei and L the target length.

The experimental challenge is to distinguish the small PNC rotations from much larger neutron spin rotations due to residual magnetic fields. We have constructed a neutron spin polarimeter that includes a cryostat surrounding a liquid helium target region and have performed the first measurement of the pnc neutron spin rotation in a liquid helium target.

[1] V. F. Dmitriev, V. V. Flambaum, O. P. Sushkov and V. B. Telitsin, Phys. Lett. **125**, 1 (1983).

The first data runs with the cryogenic polarimeter, taken at the NIST reactor, achieved a result of $\phi_{pnc} = (3.8 \pm 6.5) \times 10^{-7}$ rad, limited by count rate shot noise.[2]

To achieve an additional factor of five in experimental sensitivity, we are in the process of rebuilding the polarimeter. There are three essential improvements. The first is to redesign the cryostat so that superfluid helium can be used as a target. Superfluid helium has a density 20% higher than normal liquid helium; it will scatter 30% less neutrons out of the beam; and it provides better thermal conductivity to reduce systematic errors. The second improvement is to employ a long wavelength neutron filter in the beam to remove the longest wavelength neutrons. This is expected to increase the detected beam polarization by 50%. Finally, the beam collimation will be opened to allow a larger count rate.

In the past year, we have completed the design for a superfluid-helium target chamber and the construction of the modified cryostat is underway. We have purchased the associated vacuum hardware and the components for a new data acquisition system. After the emiT experiment completes its run at the NIST reactor, we expect to begin mounting the apparatus for the spin rotation measurement. In 18 weeks of beam time, we should have the statistics to measure ϕ_{pnc} at the level of 10^{-7} rad.

[2]D. Markoff, Ph.D. thesis, University of Washington, (1997).

1.4 Beta asymmetry from ultra-cold neutrons

A. García, A. Sallaska and E. Tatar*

Neutron β decay presents a unique opportunity to test the present evidence for the non-unitarity of the CKM matrix:[1] Here isospin-breaking corrections are negligible and radiative corrections are well understood. However, because neutron decay is a mixed (Gamow-Teller and Fermi) β decay, one needs to measure, in addition to the half life, some other quantity, like the β asymmetry. Several previous measurements of the β asymmetry have disagreements that go beyond their claimed uncertainties, indicating that some of those experiments have unknown systematic errors. One main source of problems in neutron β-asymmetry measurements is that the polarization of neutrons needs to be known with very high accuracy.

We have joined a collaboration[2] to produce a measurement of the β asymmetry in neutron decay using ultra-cold neutrons (UCN). Neutrons are produced at LANL by spallation and then moderated by scattering on graphite and solid deuterium. Once the velocities of neutrons are on the order of a few m/s they reflect off the walls of guides and are sent through a 7-Tesla solenoidal field that fully polarizes them. UCN production has been successfully tested at LANL, and an improved version of the moderator is under construction.

The UCNs will be sent to a spectrometer consisting of a $\approx$ 1 Tesla holding field (with non-uniformities of less than 10^{-3}). There the UCNs will be contained by a neutron guide made of quartz with diamond coating (to avoid de-polarization and losses) in a volume of $\approx$ 3 meters of length and 10 cm in diameter where they will be left to decay and observed by two detectors on both ends. The detectors will be a combination of a position-sensitive gas ΔE plus a plastic scintillator or a position-sensitive Si detector.

A proposal to NSF and DOE has been reviewed and the project has been funded. Presently we are working on performing Monte Carlo calculations to understand how to minimize potential backgrounds, designing a system to monitor the intensities of UCNs inside the spectrometer, and putting together a system to perform measurements potential backgrounds in the area of the experiment.

*Idaho State University, Department of Physics, Pocatello, ID 83209.

[1] I. S. Towner and J. C. Hardy, Phys. Rev. C **66**, 035501 (2002) and references therein.

[2] The collaboration is composed mainly of people from Caltech, LANL, NCSU, Virginia Tech, and UW.

1.5 Limits on scalar currents from the decay of ^{32}Ar

E. G. Adelberger, A. García and H. E. Swanson

The determination of the $e-\nu$ correlation in the $0^+ \rightarrow 0^+$ β decay of ^{32}Ar allows for placing limits on scalar contributions to the weak interactions, which appear naturally in extensions of the Standard Model, such as Lepto-quarks, and Supersymmetries.[1] In our experiment[1] for determining the $e-\nu$ correlation by measuring the beta-delayed protons from ^{32}Ar,we used as a calibration protons emitted from the T=3/2 state in ^{33}Cl. In Section 4.1, we briefly describe recent developments with respect to the mass of this state. We are presently re-analyzing the data from the ^{32}Ar experiment taking into account these developments.

Briefly, the mass of the calibration point from ^{33}Cl has shifted up by about 5 keV.[2] Because this was the only calibration point available at proton energies above 2 MeV and the other calibration points remained at their former values, this implies a change in the energy calibration of the spectrum. The latter, by itself, would change the conclusions from our data drastically. However, this change also implies a change in the mass of the T=2 daughter state in ^{32}Cl which modifies the Q-value, and changes the proton's energy, both of which modify the expected shape of the proton line. These factors end up canceling each other and the answer remains in agreement with the predictions of the Standard Model. However, the correct determination of the uncertainties and limits on the scalar couplings require careful consideration of many factors, and this is in the works. In addition, we are working on a careful analysis of the data to determine evidence for isospin breaking.

[1] E. G. Adelberger *et al.*, Phys. Rev. Lett. **83**, 1299 (1999).
[2] Pyle *et al.*, Phys. Rev. Lett. **88**, 122501-1 (2002).

1.6 Search for a permanent electric dipole moment of ^{199}Hg

W. C. Griffith, M. D. Swallows,* M. V. Romalis† and E. N. Fortson*

We are working on a four vapor cell measurement to improve the limit on the permanent electric dipole moment (EDM) of ^{199}Hg. The measurement of a finite EDM would reveal a new source of CP violation beyond the standard model. Currently, the best limit on an atomic EDM is given by our previous measurement[1] using a two vapor cell setup, which gave a limit of $|d(^{199}\mathrm{Hg})| < 2.1 \times 10^{-28}\, e\,\mathrm{cm}$. Upgrades implemented in our current measurement, described in a previous report,[2] have enhanced our statistical sensitivity per unit time by a factor of 3.

We began taking data towards the new measurement during the past year. Data is taken under a variety of conditions, including the magnetic field direction, high voltage ramp rate, and the direction the probe wavelength is detuned off resonance. These conditions are changed according to a schedule based on factorial design principles, which ensures that the effects of these parameters are sampled evenly throughout the entire data set.

We have occasionally observed magnetic fields correlated with the electric field direction that create EDM-like signals. This leads to long delays as the source of the problem must be sought out. One problem found was that discharges were occurring between the high voltage (HV) cables and the cell-holding vessel, as the HV was ramped between ± 10 kV, creating magnetic fields large enough to orient possible residual ferromagnetic contaminants. The HV finishes ramping before the spin precession is probed, but magnetic fields from the ferromagnetic impurities would persist into the probe phase, leading to a signal that mimics an EDM. We found that switching to a different type of HV cable has led to the elimination of discharges to the vessel during the HV ramp, which should reduce the possibility of ferromagnetic materials leading to false signals.

During the past year we also made several improvements to our UV laser system. We use a semiconductor master oscillator-power amplifier laser operating at 1015 nm, which is then frequency quadrupled by two nonlinear crystal doubling stages, to access the 253.7 nm $6^1S_0 \rightarrow 6^3P_1$ transition of Hg. Power stability of the system had become an increasing problem requiring frequent realignment of the doubling cavity optics. The crystal for the first doubling stage ($KNbO_3$), which had been "bought off the shelf" for use at 1064 nm, was replaced with a crystal custom cut for 1015 nm. We had the second doubling stage crystal (BBO) repolished by the manufacturer to repair hygroscopic surface damage. We installed a HEPA filtration system over the entire laser system which has reduced the frequency of the need for optics cleaning from daily to monthly. Since these changes were made, the laser has required much less maintenance, and the power output from the semiconductor laser required to produce the level of UV light needed for the experiment has been reduced by 40%.

*Department of Physics, University of Washington, Seattle, WA 98195.
†Department of Physics, Princeton University, Princeton, NJ 08544.

[1]M. V. Romalis, W. C. Griffith, J. P. Jacobs and E. N. Fortson, Phys. Rev. Lett. **86**, 2505 (2001).
[2]CENPA Annual Report, University of Washington (2002) p. 6.

Torsion Balance Experiments

1.7 Sub-mm test of Newton's Inverse-Square Law

E. G. Adelberger, T. S. Cook, J. H. Gundlach, B. R. Heckel, C. D. Hoyle,* D. J. Kapner and H. E. Swanson

We have completed the analysis of our third successful measurement of Newton's Inverse Square Law (ISL). We use a torsion pendulum with 22-fold azimuthal symmetry which we operate as a driven harmonic oscillator. The drive for this oscillator is a similar mass distribution which rotates below the pendulum. We measure the pendulum twist angle in amplitude and phase at the 22*nd*, 44*th* and 66*th* harmonics of the frequency of rotation as a function of vertical and horizontal separation between the pendulum and drive mass. We compare these measurements to a detailed calculation of the expected Newtonian signal.[1] We see no deviation from the ISL and can set a limit of $90\mu m$ for the scale at which there is no new force or interaction with a strength comparable to gravity's. We have improved over our own previous result[2] by up to a factor of 100.

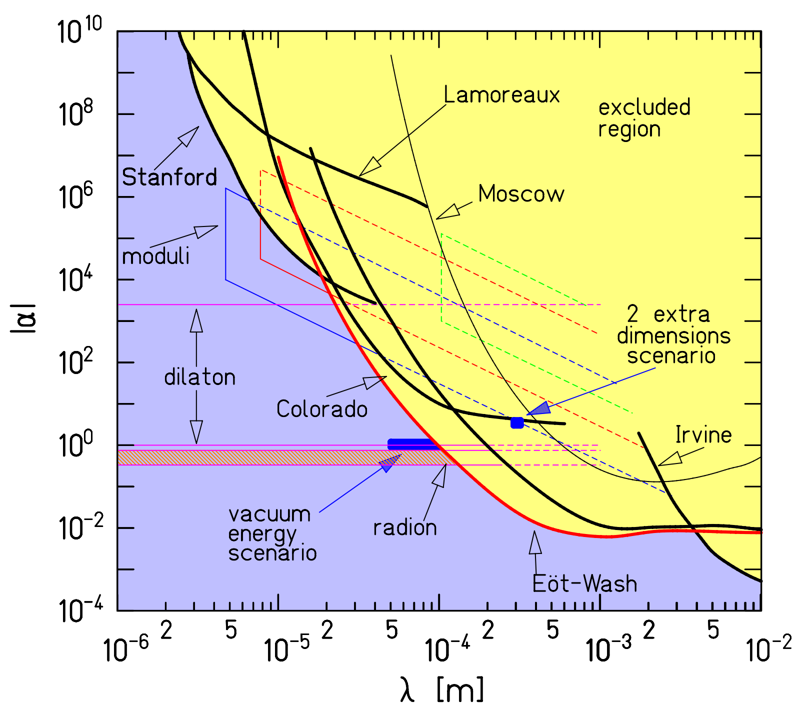

Figure 1.7-1. 95% confidence limits on the parameters α and λ, which characterize an addition to the Newtonian potential, $V_N = -\frac{Gm}{r}$, as $V = V_N(1+\alpha e^{\frac{-r}{\lambda}})$. The curve labeled "Eöt-Wash" is our new result, which runs parallel to our previous result.

*Presently at University of Trento, Trento, Italy.

[1] CENPA Annual Report, University of Washington (2002) p. 11.

[2] C. D. Hoyle *et al.*, Phys. Rev. Lett. **86**, 1418 (2001).

1.8 Spin pendulum update

T. S. Cook, E. G. Adelberger, B. R. Heckel, H. E. Swanson and M. White

The next generation spin pendulum has been designed and is currently in the final stages of assembly. The spin pendulum is a torsion balance that utilizes the magnetic properties of Alnico and SmCo to produce a spin-polarized test body.[1] By accurately measuring the affinity of the test body for a preferred direction in space (or lack thereof), the pendulum puts limits on possible simultaneous Lorentz and CPT symmetry violation as described by Colladay and Kostelecky.[2] Over the past year, a number of design improvements have been implemented to increase the overall sensitivity to such a symmetry violation.

Smaller - Lighter: The diameter of the pendulum has been reduced while maintaining the same active mass as previous versions. In the past, pendula were built with an aluminum harness to place rectangular magnets into an octagonal ring. For the new pendulum, the magnets are precision machined into trapezoidal wedges to form the octagonal ring. The maximum diameter of a ring has been reduced from 1.67" to just 1.04". This reduced geometry requires less inert mass to support the ring structures, lowers the torsion moment of the pendulum and, due to the decreased mass, allows the inclusion of a magnetic shield on the pendulum while still using a 30-μm diameter suspension fiber.

New Materials: We are now using Sm_2Co_{17} instead of $SmCo_5$ as the offset material to Alnico. The magnetization in Alnico comes entirely from electron spin alignment and is therefore the material responsible for providing the net polarization. The magnetization in SmCo comes largely from orbital contributions and serves to close the magnetic circuit without canceling the spin vector provided by the Alnico. Sm_2Co_{17} is able to sustain a larger magnetic field than $SmCo_5$ - 11,600 and 8,600 gauss respectively[3] - so the net polarization in the Alnico should be proportionately increased.

Improved Optics: The angular position of the pendulum is monitored with an auto-collimator that reflects a laser off a mirror attached to the pendulum. The Spin Pendulum experiments run in the old Eöt-Wash apparatus which is designed for a single reflection off the pendulum mirror. However, one can double the angular resolution by double reflection: reflecting the light to an auxiliary mirror and then back to the pendulum mirror before returning it to the auto-collimator. We are in the process of re-fitting the old Eöt-Wash apparatus to accommodate a double reflection system.

As may be expected, the attenuation of all magnetic "leakage" fields from the pendulum is essential to performing a precise measurement. A magnetic coupling between the pendulum and the Earth's field or any ambient laboratory fields could overwhelm a potential signal or even produce a false signal. To accurately ascertain the strength of our leakage fields, we have constructed a stepper motor driven turntable and data acquisition system to read data from a 3-axis hall probe as the pendulum is rotated. With this system we have been able to measure the fields at any given radius from the pendulum to less than 50 μG.

---

[1] M. G. Harris, Ph.D. thesis, University of Washington (1998).

[2] D. Colladay and V. A. Kostelecky, Phys. Rev. D **55**, 6760 (1997); *ibid.* **58**, 116002 (1998).

[3] www.magnetsales.com.

1.9 Eötwash data acquisition system development

H. E. Swanson

A critical element in all our systems has been a 16-bit ISA-bus multifunction data-acquisition board. Recently the manufacturer informed us that they would no longer be able to repair them. Readily available motherboards no longer even have sockets for these ISA boards. We had developed hardware device drivers to run under the Windows 95 operating system but they use an older VxD style architecture that is not supported in Windows 2000 or XP. Modifying this code for newer data acquisition boards would only help in the short term as we would not be able to upgrade the operating system beyond Windows 98. It will be increasingly difficult to maintain these systems.

The core software for our existing systems is a windows application developed in Visual C++ with a graphical user interface built using Lab Windows CVI. Each experiment has its own electronics for multiplexing up to 16 temperature sensors into one ADC channel and reading the angle of the source field. They each require a unique hardware driver to read in a data event. We are currently developing a prototype acquisition system with a modern PCI-bus multifunction board. It retains most of the existing code but requires changes in the way the hardware interface is accessed. We have two versions of this board: One with 64 analog input channels and the other with 16 channels. This is a more generic system because the additional input channels make the external multiplexer unnecessary, and the angle encoder is now monitored with an on-board pulse counter. The supplied hardware driver is also compatible with Windows XP. With the systems currently taking data, the maximum sustained data rate is 20Hz. The new system can achieve kilohertz rates when only ADC channels are read. If we require reading the angle for each event, the rate is considerably lower. Improving the performance in this later mode will probably require writing our own device driver.

Two systems are now running with the new multifunction boards and prototype code. One is used in measuring residual external fields of the new spin pendulum (see Section 1.8). The other will be the data-acquisition computer for the LISA project (see Section 1.12). Synchronous detectors and filters are implemented in software in this system so lock-in amplifiers are not needed to demodulate the autocollimator signals.

1.10 A new equivalence principle test

E. G. Adelberger, K. Choi, J. H. Gundlach, B. R. Heckel, D. J. Kapner and H. E. Swanson

We have constructed[1] a new rotating torsion balance to search for violations of the equivalence principle due to fundamentally new forces with Yukawa ranges greater than 1 m. The torsion balance consists of a composition-dipole containing titanium, beryllium, or aluminum test bodies. The pendulum is suspended inside a vacuum chamber and hanging from a constantly rotating turntable.

During the past year we have begun taking long data runs with the instrument. The statistical uncertainty is as expected at about 2 nrad in one day of data taking. We found a slowly varying systematic effect which is likely related to small rotation rate variations of the main turntable that rotates the instrument. We are now changing our data taking protocol to modulate the composition dipole orientation w.r.t. the turntable at a frequency (1 day^{-1}), which is high compared to the variation of the systematic effect. In addition we have equipped the turntable with extra temperature sensors and an additional set of tilt sensors.

We have reduced the clearly identifiable systematic sensitivities of our apparatus:

Gravity gradient effect: we measured the strength of the Q_{21}, Q_{31} gravity-gradient fields around the pendulum with special test bodies that have exaggerated gravity-gradient moments. The field were compensated with Q_{21}, Q_{31} gravity-gradient compensators masses so that their strength was about 0.13% and 6% the uncompensated strength, respectively. We noticed a small change in the Q_{21} field which is attributable to water (rain) in the nearby soil.

Tilt coupling: we eliminated the tilt of the turntable rotational axis by using an active leveling system.[2] With this system turned on, the tilt angle of the turntable is nearly unresolved in the sensor that is used by the feedback system. Since this sensor cannot be at the exact location of the pendulum a small effective tilt remains. From the local mass distribution we estimate this tilt to be 36 nrad, which causes a 0.6 nrad pendulum rotation.

Thermal coupling: the thermal shield around the vacuum chamber has constant-temperature water circulating through it. We modulated the temperature of this water at our normal signal frequency to measure the thermal feedthrough. The thermal feedthrough is 0.099 ± 0.008 nrad/mK, corresponding to 0.028 nrad the signal.

Magnetic coupling: We reduced the susceptibility of the apparatus to magnetic fields by installing a second μ-metal shield inside the vacuum chamber. The response of the pendulum to an externally applied field of 870 mG is 2.08 ± 2.15 nrad. The systematic uncertainty due to magnetic coupling is less than 0.05 nrad.

[1] CENPA Annual Report, University of Washington (2002) p. 10.
[2] CENPA Annual Report, University of Washington (2001) p. 4.

1.11 Development of an 'anapole pendulum'

E. G. Adelberger, T. S. Cook, B. R. Heckel, F. V. Marcoline and H. E. Swanson

We are currently developing an 'anapole pendulum' which will be used in a rotating torsion balance to make a photon mass measurement. If the photon field, A^{μ}, has a Dirac mass, m_{γ}, then there is an additional term in the electromagnetic energy density equal to $\frac{1}{2}m_{\gamma}^{2}A_{\mu}A^{\mu}$. Just as an external magnetic field will exert a torque on a magnetic dipole, an external photon field will exert a torque on a dipole magnetic vector potential (an anapole) towards the minimum photon field energy density configuration.

A toroidal current distribution produces a magnetic field confined within the toroid, and an anapole field external to the toroid. Previous experiments[1,2] have used wire-wrapped iron cores which require constant current supplied to the pendulum. Our active mass will consist of a single toroidal soft ferromagnet with a high permeability and magnetic remanence, giving a large anapole at low mass without needing to supply current to the pendulum.

We have constructed a simple setup to determine the hysteresis curve of our magnet. Early tests indicate that the magnetic properties are sufficient to allow a significant improvement on the current upper limit of the photon mass.

Initial design of the pendulum is complete, and we have begun manufacturing components. The pendulum is designed to maximize our sensitivity to a photon mass, while minimizing torques due to local gravity gradients and stray magnetic fields. The 70-gram pendulum will have magnetic shielding surrounding the magnet, and will be suspended from a 20-μm tungsten fiber. Annealing and final machining of the magnet is under way. Further tests on the completed magnet are needed to finalize the design. In particular, measurement of leakage fields (see Section 1.8) is needed to determine how much magnetic shielding we need on the pendulum body.

[1] R. Lakes, Phys. Rev. Lett. **80**, 1826 (1998).

[2] J. Luo, L.-C. Tu, Z.-K. Hu and E.-J. Luan, Phys. Rev. Lett. **90**, 081801 (2003).

1.12 Small force measurements for LISA

E. G. Adelberger, J. H. Gundlach, B. R. Heckel, C. Kurz, P. Searing and H. E. Swanson

To date gravitational waves have only been observed indirectly. NASA and ESA are planning jointly to build a space-based gravitational wave antenna, LISA,[1] which will have enough sensitivity to observe gravitational waves from various sources such as massive black-hole mergers or even from the early phases of the universe. The instrument will consist of three spacecraft placed at the corners of an equilateral triangle of 5,000,000-km arm length. This constellation will trail Earth on its orbit about the Sun by 20 days. A gravitational wave causes small variations in the arm lengths. Each arm length is measured to a precision of 20 pm using laser beams. The end of each laser beam path is defined by a cubical mass, freely floating inside the spacecraft called a gravitational reference sensor or proof mass. LISA's sensitivity is optimized in the frequency range from 10^{-4} to 1 Hz with a minimum detectable fractional length change of 10^{-23}. To achieve the proposed sensitivity of LISA any time-varying acceleration of the proof masses along the laser beam direction must be avoided. In particular spurious coupling of the proof masses to the spacecraft, which is servoed to follow the proof masses, must be avoided.[2] The nearest distance from the proof mass to its housing will be 2 to 4 mm. This close spacing raises concerns about forces acting between nearby surfaces. A known but little studied interaction is due to patch-effect potentials. We are currently building a specialized torsion-balance system to measure patch-effect forces between closely spaced surfaces. Our first setup will consist of a stepped torsion-pendulum body (Fig. 1.12-1) suspended parallel to a larger surface. The separation to the pendulum surface will be varied by modulating the position of the larger surface. To approach the sensitivity requirements for LISA the closest, we will use separations much closer than those in LISA. Our setup will also allow us to vary the electrostatic potential between the pendulum and the proof mass to simulate the effect of charging and of the electrostatic control of the proof masses in LISA. In addition to patch-effect forces our setup will be sensitive to other forces which may arise, for example due to residual gas.

We have assembled a stainless steel vacuum chamber and rebuilt an autocollimator system. A prototype translation device for the large plate was built. We chose a pneumatic actuator to avoid electrical currents near the pendulum plate. The dynamic range of this actuator is about 2 mm. We poured a 30 cm thick concrete base plate in a space that was freed by dismantling the cyclotron. A thermal enclosure was constructed. We have built a data acquisition system, which we are in the process of connecting to the instrument. In the next few months we will install a test pendulum to acquire first test data. The research is funded with a contract from NASA/GSFC.

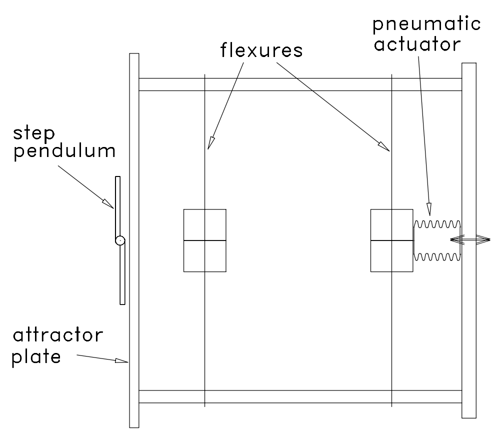

Figure 1.12-1. Schematic top view of step pendulum setup.

[1] http://lisa.jpl.nasa.gov/.

[2] B. L. Schumaker, Class. Quantum Grav. **20**, S239 (2003).

2 Neutrino Research

SNO

2.1 The Sudbury Neutrino Observatory

J. F. Amsbaugh, T. H. Burritt, G. A. Cox, P. J. Doe, C. A. Duba, J. A. Formaggio, G. C. Harper, K. M. Heeger,* M. A. Howe, K. K. S. Miknaitis, S. McGee, A. W. Myers, N. S. Oblath, J. L. Orrell, R. G. H. Robertson, M. W. E. Smith† and L. C. Stonehill

The Sudbury Neutrino Observatory (SNO) is a heavy water Čerenkov detector that was designed to study the flux, spectrum, and oscillation characteristics of ^{8}B neutrinos from the Sun. Previous solar neutrino experiments, able to detect primarily electron type neutrinos, have observed a deficit in the flux of solar neutrinos relative to the predictions of solar models. This discrepancy between the observed flux of electron type neutrinos and the expected flux is known as the Solar Neutrino Problem. The use of heavy water as a target medium in SNO allows sensitivity not only to electron neutrinos, but also to mu and tau neutrinos, through the neutral current (NC) reaction of neutrinos on deuterium. The three primary reactions through which we detect solar neutrinos are shown below,

$$\begin{aligned}
\nu_x + {}^2\mathrm{H} &\longrightarrow \nu_x + p + n \quad \text{Neutral Current (NC)} \\
\nu_e + {}^2\mathrm{H} &\longrightarrow p + p + e^- \quad \text{Charged Current (CC)} \\
\nu_x + e^- &\longrightarrow \nu_x + e^- \quad \text{Elastic Scattering (ES)}
\end{aligned} \tag{1}$$

where x denotes any of the three active neutrino flavors. A comparison of SNO's measured CC and NC rates has shown that solar electron neutrinos are oscillating into mu and tau neutrinos prior to reaching our detector. The flux of mu and tau neutrinos explains the previously observed deficit in solar electron type neutrinos. SNO's results over the past two years have thus provided strong evidence for the oscillation of solar neutrinos and solved the long-standing puzzle of the missing solar neutrinos.[1] The SNO experiment has been designed to maximize our confidence in the NC to CC comparison, and we have therefore incorporated several unique mechanisms for confirming and improving our measurement of the NC reaction rate. Since June 2001 we have been running SNO with ultra-pure salt (NaCl) added to the heavy water. Neutron capture on the salt provides an even more distinct signal than neutron capture in pure heavy water. We will soon deploy an array of discrete Neutral Current Detectors (NCDs), to provide an independent means of detecting the NC neutrons. As we continue to refine our measurement of the NC and CC rates, we will also be able to provide more stringent limits on the fundamental physics parameters that govern solar neutrino oscillations.

The University of Washington has played an active role in the analysis of the data from the first and second phases of the experiment, as well as in studying the day-night effect and solar anti-neutrinos. We are the primary institution responsible for the hardware, installation, and analysis for the NCD phase of the experiment, which will begin Summer 2003.

*Lawrence Berkeley National Laboratory, 1 Cyclotron Road, Berkeley, CA 94720.

†DASI, University of Chicago, South Pole.

[1] Q. R. Ahmad *et al.*, Phys. Rev. Lett. **89**, 011301 (2002).

2.2 Status and updates to the SNO data acquisition system

P. Harvey,* M. A. Howe, B. L. Wall and J. F. Wilkerson

Since the SNO DAQ system has been described extensively in past annual reports,[1] only a brief review of the most significant updates is provided here.

Last year a new 733-MHz G4 Macintosh was installed underground as the primary SNO DAQ computer. In addition, a new 622 PCI card was installed that uses an optical-fiber cable to communicate from the Mac to the VME Bit 3 controller. After the installation we began to see occasional VME exceptions occurring when shipping records to the event builder through the Sun dual port memory (dpm). These errors commonly stopped the execution of time slope calibration runs with an 'unable to create/access the Sun dpm' message printed to the SHaRC status log window. The errors also occurred occasionally at the start of a run during the shipment of the run record. This became known as the 'Sun dpm error problem' and was a serious issue because it was adversely affecting detector live time.

Because of the sporadic nature of the error, a special software test module was added to SHaRC to emulate an electronic calibration task running at a very high rate. All testing was done on the on-site above-ground test stand. Since it was unclear whether the problem was limited solely to the 622 PCI card, a 617 PCI card was also installed into the test-stand Mac. The test results were very sporadic. Sometimes a test would run for hundreds of thousands of cycles without a single Sun dpm error. At other times, 1% of the records shipped caused an error. The lowest rate was an over-night run that shipped 4.5 million records with only 16 errors. There was some speculation that the effect was temperature related, but experimentation with a heat gun was inconclusive. It was noted that although errors occurred using either PCI card, the error rate was in general 25 times higher when using the 622 PCI card.

Once it became possible to reproduce the error on a regular basis, it was possible to pinpoint the cause as either a VME adapter card bus grant starvation error or a PCI bus timeout during a read of the Sun dpm circular buffer control block. The error was never seen while pushing records into the circular buffer. It appears that the Sun dpm errors are entirely hardware related, but the actual root cause is not known at this time. The code that is currently installed underground has a work-around installed that re-reads the circular buffer control block three times before letting an exception propagate into a full-blown Sun dpm error. This solution was successful and the Sun dpm error has not reccurred.

There were also a number of minor software updates to streamline detector operations and to transmit detector parameters to remote sites for tracking detector operation over time.

---

*Queens's University, Kingston, Ontario, Canada K7L 3N6.

[1]Nuclear Physics Laboratory Annual Report, University of Washington (1997) pp. 20-23; (1998) pp. 18-20; (1999) pp. 16-18; (2000) p. 19; CENPA Annual Report (2001) p. 25; (2002) p. 26.

2.3 Energy and optical calibration of the Sudbury Neutrino Observatory

J. A. Formaggio and the SNO Collaboration

Part of the process of extracting the solar-neutrino flux and separating charged-current from neutral-current events involves knowing to great precision the energy and optical response of the SNO detector. The optical calibration of the SNO detector makes use of a dye laser with a fiber-optic cable connected to a diffuser ball. The laser provides pulsed radiation at 337 nm with a 600-ps pulse width and peak power of 150 kW. The laser pulses up to 45 Hz and can be used directly or as a pump for several dye lasers that provide wavelengths in the range of 360-700 nm. The optical calibration process results in the determination of attenuation and scattering coefficients for the heavy water, light water, and acrylic. In combination with a detailed Monte Carlo that simulates the Čerenkov photon production from electrons, SNO is able to extract the energy response of the detector.

The energy response is verified via the employment of a series of calibration sources. The main source that tests the energy response is ^{16}N. The ^{16}N is produced via (n,p) on the oxygen in CO_2 gas and decays by a beta delayed 6.13-MeV (66%) or 7.12-MeV (4.8%) gamma ray with 7.13-s half-life. The ^{16}N provides a check of the energy response of the detector as a function of both time and position.

In addition to ^{16}N, SNO also uses a ^{8}Li β source and a tagged ^{252}Cf neutron source to further test the energy response of the detector. The ^{8}Li β source has an end-point energy of 13 MeV, allowing one to test the energy scale above what is probed by ^{16}N. The tagged neutron source, on the other hand, tests SNO's sensitivity to neutrons directly.

Fig. 2.3-1 shows how well the Monte Carlo tracks the energy response of the detector for ^{8}Li calibration sources. The combination of laser, radioactive, and tagged sources allow one to limit the energy uncertainty of the SNO detector to approximately $\pm 1.25\%$ for the duration of the salt phase. This systematic error is similar to what has been measured in the D_2O phase of the SNO experiment.

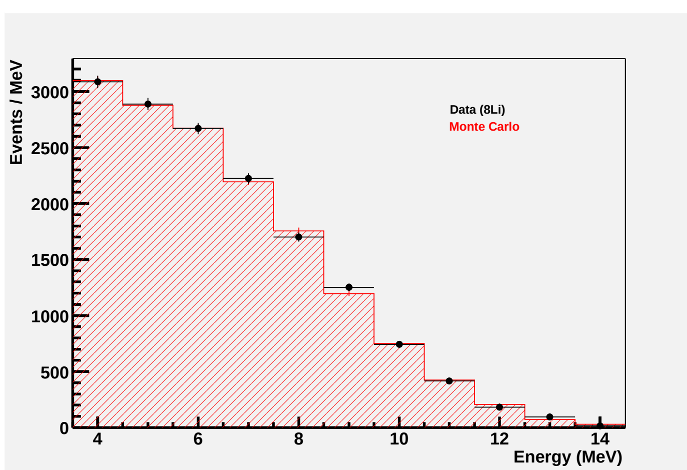

Figure 2.3-1. Energy profile for data (black points) and Monte Carlo (red) for ^{8}Li tagged β decays.

2.4 Selection of the neutrino analysis data set for the Salt Phase of SNO

S. McGee and J. L. Orrell

The Sudbury Neutrino Observatory (SNO) collaboration has recently decided upon the period of data taking to be used in the first results from the salt phase of the experiment. During the previous year Orrell was chairperson of the run selection committee composed of graduate students and post-doctoral fellows from SNO member institutions, individuals who have spent a significant amount of time on location at the experiment learning the details and peculiarities of the day-to-day data taking. This on-site experience makes the members of this committee valuable resources as adjudicators of exactly when the SNO detector is in an optimum solar neutrino data taking configuration.

Data selection during the salt phase of the SNO experiment consists of three main tasks. First, a simple near-line computer analysis package analyzes all runs and identifies which runs are of the neutrino type, that have the correct number of photomultiplier tubes on-line, and are over 30 minutes long. Second, a data integrity computer analysis package analyzes those runs identified by the first step, and tests that each run has the correct data structureand the expected average data rate, and that no electronics failures occur during the run. Third, for *each and every* run, two members of the run selection committee independently read the operations reports to verify that there were no unusual circumstances during the run and that no neutrino runs were missed by the computer analysis packages due to operator error in setting the run type.

The results of over a year of bi-weekly meetings of the run selection committee produced the a selected data set with characteristics given in Table 2.4-1. Salt phase data taking has continued past 10/10/2002 and the run selection committee continues to add to the salt phase data set.

Expected Salt Phase Data Set

Data taking period	7/26/2001 $\rightarrow$ 10/10/2002
Total calendar days	441
Number of selected runs	697
Total days of selected data	258.8
Total livetime fraction	58.7 %

Table 2.4-1. The characteristics of the data set expected to be used for the first reported results from the salt phase of the SNO experiment.

2.5 Distinguishing muon spallation types in SNO

J. A. Formaggio, K. K. S. Miknaitis, J. L. Orrell and J. F. Wilkerson

As reported in last year's report,[1] the Sudbury Neutrino Observatory (SNO) is sensitive to the spallation products from high energy cosmic ray muons passing through the detector. It was demonstrated that the dominant spallation products were neutrons. These initial studies also showed there was a broad range of muon-follower multiplicities. Muon-follower multiplicity is defined as the number of candidate physics events that follow within 0.5 seconds of a muon. The observed high-multiplicity muons suggested sub-dividing the muons into two classes: (1) real and virtual photo-induced spallation and (2) "other processes" including deep inelastic scattering, muon decay, muon capture, or pion production.[2]

Inspection of the 10 highest multiplicity sets of events revealed high energy Čerenkov rings following within 5 microseconds after the initiating muon. During this short period of time following the passage of a high-energy muon, the SNO detector continuously retriggers due to both residual light in the detector and the electronics relaxation response to the large charge deposition in the photomultiplier tubes from the muon's initial Čerenkov signal.

An algorithm was developed to search the events following a muon for Gaussian-distributed photomultiplier-tube trigger times above a constant background of photomultiplier-tube "noise" triggers. The goal of this algorithm was to distinguish high-multiplicity muons without relying upon the high-multiplicity signature. The results of this work are shown in Fig. 2.5-1. The "all muons" histogram is scaled by a factor of 100 for clarity and shows both high- and low-multiplicity muons in the data sample. The "clean muons" histogram demonstrates that the algorithm successfully distinguishes and removes high-multiplicity muons. It is expected that this separation will allow us to study and characterize a distributed sample of photo-induced spallation neutrons.

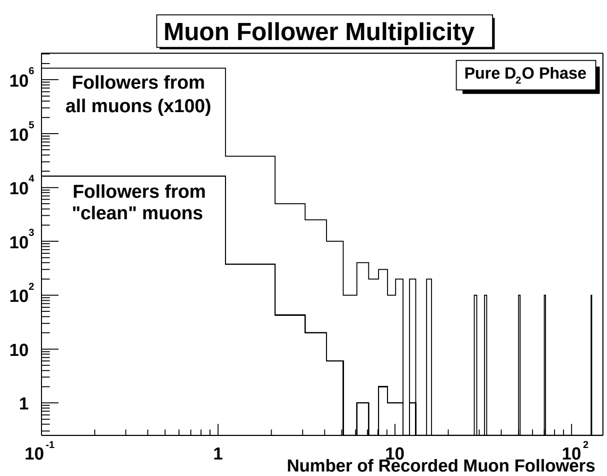

Figure 2.5-1. The number of candidate events recorded within 0.5 seconds of a muon.

[1]CENPA Annual Report, University of Washington (2002) p. 18.
[2]Y.-F. Wang *et al.*, Phys. Rev. D **64**, 013012 (2001).

2.6 Electron antineutrino detection at the Sudbury Neutrino Observatory

J. L. Orrell and J. F. Wilkerson

The charged-current weak interaction of electron antineutrinos on deuterons,

$$\bar{\nu}_e + d \;=\; e^+ + n + n \qquad Q = -4.03 \qquad (\overline{CC})$$

produces a positron, e^+, and two neutrons, n. Each of these three products can potentially produce a signal that will trigger the Sudbury Neutrino Observatory (SNO) detector. This coincidence of detection events provides a unique signature of electron-antineutrino interactions in the SNO detector. Observing or limiting the flux of electron antineutrinos addresses several hypothetical antineutrino production mechanisms. Specifically, if neutrinos are Majorana particles, then a fraction of the electron neutrinos produced in the Sun's core may experience resonant spin-flavor transitions in the Sun's magnetic field, producing electron antineutrinos. There is also a speculative hypothesis of a Geo-nuclear reactor located at the center of the Earth. We are pursuing a line of research that demonstrates a robust, low energy, and large fiducial volume analysis of the SNO data set for the measurement or limiting of the flux of electron antineutrinos.

The demonstration of the low energy and large fiducial volume analysis relies on spallation neutrons produced by muons in the SNO detector (see Section 2.5). The left hand of Fig. 2.6-1 clearly shows the spallation neutron signal that follows within a half second of the muon. For comparison, the right hand plot shows the half second preceding the muon. The plots are energy-measure versus the reconstruction radius relative to the entire detector volume.

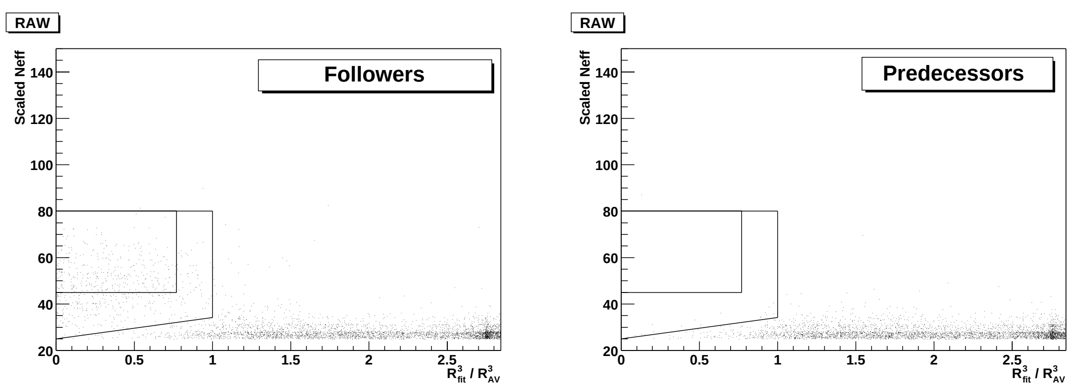

Figure 2.6-1. Neutron-like events following and preceding within half a second of a muon. This neutron signal mimics the expected electron antineutrino coincidence. The x-axis is volume with 1 equal to the entire D_2O volume. The y-axis is an energy measure.

The small rectangle represents the neutron measurement window reported in SNO's solar neutrino analysis.[1,2] The larger region is the proposed analysis region for an electron antineutrino analysis using the SNO data set. We are currently determining the backgrounds expected inside this analysis window.

[1] Q. R. Ahmad *et al.*, Phys. Rev. Lett. **89**, 011301 (2002).
[2] Q. R. Ahmad *et al.*, Phys. Rev. Lett. **89**, 011302 (2002).

2.7 Reactor antineutrinos at the Sudbury Neutrino Observatory

J. L. Orrell

The Sudbury Neutrino Observatory (SNO) is capable of detecting electron antineutrinos, $\bar{\nu}_e$, through weak interactions with deuterons contained in the heavy water of the SNO experiment:

$$\begin{aligned} \bar{\nu}_e + d &= e^+ + n + n & Q &= -4.03 & (\overline{CC}) \\ \bar{\nu}_e + d &= \bar{\nu}_e + p + n & Q &= -2.23 & (\overline{NC}) \end{aligned}$$

Commercial, electric power generating, nuclear reactors generate approximately 2×10^{17} $\bar{\nu}_e$/s per MW of thermal power, with energies from 1 - 10 MeV. The reactor $\bar{\nu}_e$ flux from distant North American nuclear reactors induces several $\overline{CC}$ and $\overline{NC}$ interactions per year. These interactions are a small background to the solar neutrino interactions SNO is designed to measure (see Section 2.1). Furthermore, measurements that attempt to place limits on the *total* $\bar{\nu}_e$ flux at SNO *are* restricted by the reactor induced $\bar{\nu}_e$ signal (see Section 2.6).

A new and more comprehensive calculation of the $\overline{CC}$ and $\overline{NC}$ interaction rate at SNO has taken into account (on a monthly basis[1]) the true reactor power levels convolved with SNO's actual data taking periods. The reactor $\bar{\nu}_e$ spectrum is determined by a weighted sum of the individual $\bar{\nu}_e$ spectra from the fission products of ^{235}U, ^{238}U, ^{239}Pu, and ^{241}Pu. The total flux is determined from the monthly power output of all nuclear reactors within 700 km of the SNO experiment. The total $\overline{CC}$ and $\overline{NC}$ interaction rates for each month are calculated including the suppression effect due to neutrino oscillations. The neutrino oscillation portion of the calculation used world data,[2] best-fit values for the neutrino mixing parameters $\sin^2 2\theta = 0.83$ and $\Delta m^2 = 5.5 \times 10^{-5}$ eV^2. The total number of $\overline{CC}$ and $\overline{NC}$ interactions was further weighted by the fraction of time that SNO was recording experimental data during each month. Table 2.7-1 shows the results of this calculation.

Phase of experiment	Total # $\overline{CC}$	Total # $\overline{NC}$	Detector live # $\overline{CC}$	Detector live # $\overline{NC}$
Pure D_2O	1.65	7.24	0.89	3.90
Salt	1.41	6.22	0.73	3.24

Table 2.7-1. Calculated number of $\overline{CC}$ and $\overline{NC}$ interactions in the SNO detector during each phase of the SNO experiment. Neutrino oscillations are included with $\sin^2 2\theta = 0.83$ and $\Delta m^2 = 5.5 \times 10^{-5}$ eV^2.

[1] Thank you to the US Nuclear Regulatory Commission and Chalk River Laboratory for providing the historical monthly power output for all North American nuclear reactors.

[2] G. L. Fogli *et al.*, Phys. Rev. D **66**, 053010 (2002).

2.8 The day-night asymmetry measurement in the salt phase of SNO

K. K. S. Miknaitis and the SNO Collaboration

Solar-neutrino oscillations are governed by two parameters, Δm^2, which quantifies the mass difference between the neutrino states that participate in solar-neutrino oscillations, and $\tan^2\theta$, which quantifies the strength of the mixing between states. A combined fit of SNO's solar neutrino results along with other neutrino experiments, notably the first results from KamLAND, has narrowed down the allowed values of these parameters to a single region of the formerly large parameter space. This region, known as the Large Mixing Angle (LMA) solution, includes values in the vicinity of $\Delta m^2 \sim 10^{-4}$ and $\tan^2\theta \sim 0.4$.

Solar neutrino oscillations governed by LMA parameters involve matter enhanced oscillations in the sun (the MSW effect). Beyond the flavor-changing effects of the oscillation phenomenon, the MSW effect has two additional possible signatures. First, it can result in a distortion of the energy spectrum measured in an experiment like SNO relative to the original solar-neutrino spectrum. Second, the same matter effects that enhance oscillation in the sun can potentially alter the flavor content of the solar neutrino "beam" as it passes through the earth. This latter effect would produce a difference between the rate of electron-type neutrinos detected by SNO during the day and during the night, when solar neutrinos have to pass through the earth to reach our detector.

For our first measurement of a potential day-night asymmetry in the electron-type neutrinos detected by SNO, we constructed an asymmetry parameter

$$A = 2\frac{\Phi_N - \Phi_D}{\Phi_N + \Phi_D} \tag{1}$$

where Φ_N and Φ_D are the night and day neutrino fluxes, respectively. Neutrino oscillation parameters in the LMA region predict asymmetry values between 0% and around 8%.

The day-night asymmetry measurement, if non-zero, could provide direct evidence for the MSW effect. However, even if the day-night asymmetry is too small to be able to make a significant non-zero measurement, this parameter can still limit the LMA parameters to a more restrictive region of the parameter space. In the LMA region, the day-night effect is primarily sensitive to differences in Δm^2.

In the first phase of SNO we measured $A = 7.0 \pm 4.9(\text{stat.}) \pm 1.3(\text{syst.})\%$. This measurement was statistically limited, so future measurements will combine the data from multiple phases to improve the statistical sensitivity. We have undertaken a thorough study of the covariances between systematics between the pure D_2O phase and the salt phase in order to be able to perform this joint measurement. We are also laying the groundwork for possible improvements to the measurement, including studying the day-night effect as a function of the zenith angle, or the amount of the earth's matter that the neutrinos traverse en route to SNO. Precise measurements of the detector "live" time for day and night have been completed for the salt phase, and studies of the variation of systematic effects day and night are in progress.

2.9 SNO signal extraction in the salt phase

K. K. S. Miknaitis and the SNO Collaboration

The exceptional opportunity afforded to SNO to make solar-neutrino measurements using heavy water as a neutrino target is so unique that the experiment was designed to include several complementary detection techniques, to ensure robust results that will be worthy of an honored place in the history of nuclear and particle physics. During the first phase of the experiment, our measurements of the charged current (CC) and neutral current (NC) reactions between neutrinos and deuterium provided an answer to the long-standing solar neutrino problem. We now move on to the next two phases of the experiment, designed especially to fine tune, check, and improve our measurement of the NC reaction, which will be SNO's most significant lasting contribution to physics.

Since May 2001 we have been in the second phase of the experiment, in which ultra-pure salt (NaCl) has been added to the D_2O in the detector. This phase will be followed by a third phase involving the deployment of discrete neutral current detectors into the heavy water volume. Both of these additions to the detector are meant to increase sensitivity to the specific signature of the NC reaction, neutrons:

$$\text{NC Reaction:} \qquad \nu + \mathrm{d} \longrightarrow \nu + \mathrm{p} + \mathrm{n} \tag{1}$$

In pure heavy water, the neutrons capture on deuterium nuclei, producing a 6.25-MeV gamma. The neutron-capture event distribution in energy was characterized by a broad peak centered on the gamma energy and a radial distribution that fell off near the boundary of the detector, as the neutrons would scatter outside the heavy water volume and be captured on other materials. With the addition of salt to the detector, neutrons can also capture on ^{35}Cl. This reaction has a higher cross section, and the gamma cascade emitted has a higher energy (8.6 MeV). The higher cross section means that neutrons will capture more quickly after they are produced, flattening the distinct radial profile that was characteristic of neutron events in the first phase. In addition, while electron events yield a clear Čerenkov pattern of light, the gamma cascade creates a more diffuse pattern. We can parameterize the different degree of isotropy of the light produced in physics events.

Although the different types of event (CC, ES, and NC) all have different distributions in our measurable parameters, we cannot tell the difference between them on an event-by-event basis. Instead, we use detailed models of the physics and of our detector to create probability distribution functions (PDFs) describing the event types. We then do a statistical separation of the signals by performing a maximum likelihood fit of our entire data set to these PDFs, to extract the most likely amplitudes of the different signal contributions.

To incorporate the differences between salt and the pure heavy-water phase, we have developed signal extraction software in C++ that is capable of performing such statistical fits to any number of input PDFs with adjustable acceptance regions. This allows us not only to include isotropy distributions in the fits, but to study the features of the signal extraction depending on how many input PDFs are used and what acceptance windows in energy and volume are defined.

SNO Neutral Current Detectors (NCDs)

2.10 NCD data analysis

G. A. Cox, P. J. Doe, A. L. Hallin, S. McGee, R. G. H. Robertson, L. C. Stonehill and J. F. Wilkerson

The NCD's data acquisition system, Section 2.13, has limited analysis and detector monitoring capabilities. However, the NCDDAQ does produce custom formatted data files for off–line analysis. In order to analyze our data we have employed the ROOT analysis framework developed at CERN.[1] A set of NCD event structures, which contain all information about an event in our system, have been created and our data files have been converted into ROOT readable files based upon these event structures.

The first major analysis completed with the ROOT-based tools was determining which NCD's should be deployed in the reduced array (see Section 2.11). The analysis was done on measurements made by our Shaper/ADC cards,[2] which produce an energy spectrum of the events in our detectors. The critical selection criteria were the existence of a neutron peak with good resolution, and low count rate above the neutron peak, most of which are attributable to alphas from intrinsic radioactivity in the counter. We also selected counters that had similar gas gains. The goal was to select the working NCD's with the lowest levels of intrinsic radioactivity.

NCDDAQ also records the pulse shape of events with two digitizing oscilloscopes. Due to a change in our data structure, our previous set of pulse shape analysis tools,[3] known as Analyst, have become obsolete. The source code from Analyst is being ported into our ROOT–based analysis tools. Once constructed, work can resume on analysis projects such as the "Water Wall" study to measure the thermal and fast neutron fluxes from the rock walls at SNO.[4] Pulse shape analysis begins with the extraction of the real pulse shape from our logarithmically amplified signal. The logarithmic amplifiers are characterized by $V_{out} = a \cdot log(1 - V_{in}/b) + c$, where a, b, and c must be determined for each amplifier. Extraction of these parameters is done with a χ^2–squared minimization routine on the output signal generated from an known input. This has been done on a preliminary level, and automated calibration routines are under construction. The typical pulse shape analysis calculates the energy of the pulse and the amount of time it takes the pulse to reach 90% of its peak value. In the risetime vs. energy space, ∼50% of the captured neutrons fall in a region known as the "background free region" A pulse shape fitting routine is being developed to distinguish neutron events from alphas in the NCD's. It is based on semi–analytic functions that describe the expected NCD signals from alphas and neutrons. The goal is to reject alphas without sacrificing ∼50% of the neutrons, as in the risetime vs. energy method.

---

[1] http://root.cern.ch.

[2] CENPA Annual Report 2001, University of Washington, p. 32.

[3] CENPA Annual Report 2001, University of Washington, p. 31.

[4] CENPA Annual Report 2002, University of Washington, p. 27.

2.11 NCD array optimization

G. A. Cox, P. J. Doe, J. Formaggio, A. L. Hallin, J. Manor, J. L. Orrell,
R. G. H. Robertson, L. C. Stonehill and J. F. Wilkerson

The neutral-current detector (NCD) phase at SNO was designed to provide an independent measurement of the neutral-current neutrino flux from the sun. The ^{3}He filled detectors used for the NCD phase are ideal for this measurement, as they are uniquely sensitive to neutrons produced from the neutral-current reaction $\nu_x + d \to n + p$. The NCD Phase at SNO was initially proposed and constructed prior to knowledge of the exact mechanism responsible for the suppressed neutrino flux from the sun. This assumption considered that solar neutrino experiments prior to SNO were measuring the full non–sterile neutrino flux, rather than just $\sim$1/3 of the flux predicted by the standard solar model (SSM). In order to have enough statistics in a reasonable amount of time, 96 NCD strings, totaling 770 m in length, were built. However, since the time construction began, SSM–independent measurements have verified that the SSM is an accurate model and that neutrino oscillation is seen as the most likely mechanism for the suppressed flux. A reassessment of the NCD array and the number of detectors to be deployed was made.

Installation of the NCDs will impact SNO mainly in two ways. First, it will provide an independent measurement of the neutral current (NC) interaction flux. Second, it will obscure light produced by the charged current (CC) and electron scattering (ES) interactions that take place in the D_2O. This effectively increases the energy threshold of the CC interactions that SNO's PMTs can measure, increasing the uncertainty in the CC flux. In general, measurements that depend mostly upon the PMTs at SNO will favor fewer NCDs installed, and those that depend mostly upon the NC flux will favor more NCDs. However, the NCDs will absorb neutrons that would otherwise produce a background to the CC measurement. Thus, for measurements that depend upon the CC interaction, installation of some of the NCDs is desirable. Monte Carlo simulations were done to quantify the effect of installing various percentages of the full NCD array.

Overall, there were 11 physics topics that were considered: CC flux, NC flux, CC Day/Night sensitivity, NC Day/Night sensitivity, seasonal flux variations, supernovae, anti-neutrinos, MSW parameters, "hep" neutrinos, sterile neutrinos, and CC spectral distortions. Most of the science addressed by the NCDs optimized in one of two ways:

1. Minimize the amount of light occultation induced by the presence of counters in the array. Light occultation decreases the resolution of charged and neutral current signals, while increasing the amount of background that falls in the fiducial volume.

2. Maximize the number of neutrons capture in the array. Measurements that are sensitive to neutron statistics (such as anti-neutrinos and supernovas) fall in this latter category.

The final recommendation after the Monte Carlo study was to install $45 \pm 5\%$ of the array. After considering different configurations of installing the NCD array into SNO, it was decided that, using the centrally located strings, 50% of the array was to be installed.

2.12 Determination of Z-position for hits in the NCD array

J. V. Germani,* S. McGee, R. G. H. Robertson, L. C. Stonehill and J. F. Wilkerson

Determination of the z-position of an event in the NCD array will assist in the characterization of backgrounds in the acrylic vessel (AV) and in the NCD's as well. Other background exclusions could be made by correlating reconstructed PMT events with hits in the NCDs. Also, a determination of the neutral current signal efficiency per fiducial volume would be possible.

Knowledge of the z-position of hits could also be used to monitor the health of the segmented NCD strings before and after deployment. The success of NCD connections made over the neck of the AV during deployment could be easily checked with a neutron source positioned in close proximity to upper and lower sections of the string. Also, knowing the position of high voltage discharges allows for prompt diagnoses of potentially damaging breakdowns.

A z-position determination is possible because the open-ended configuration of the NCD allows for pulse-reflection timing. This is enhanced by the addition of a 30 ns delay line at the bottom of each string. Upon arrival of the charge at the anode, the pulse is split in two. One proceeds directly to the DAQ while its mirror image heads to the bottom of the string before being reflected back. Taking the propagation speed of the pulse in the NCD to be c, the range of separation of the initial and reflected pulse in a 10-m long string is 60 ns for an event at the bottom of the string and 126 ns for an event near the top.

The thermalization distance for neutrons in the D_2O is roughly 1.5 m. Therefore, the desired resolution for a z-position measurement would be on the order of 1 m. This is also equivalent to the resolution of the x and y position since the NCD strings will be placed in a 2D square lattice with 1 m spacing.

Previous studies of z-position algorithms showed good resolution, $\sigma_z = 0.75$ m, for about a third of the data. The shape of the NCD pulse varies with the orientation of the track of the charged particles with respect to the wire. Previous method's efficiencies dropped considerably as the track moved from the optimal parallel orientation.[1]

Currently under study is the use of cepstrum coefficients. The cepstrum (an anagram of spectrum) is the inverse Fourier transform of the log of the Fourier transform. Similar to the standard Fourier transform whose coefficients represent the strengths of wavelengths present in a waveform, this rather convoluted-sounding procedure results in coefficients that represent the strengths of phase differences between like wavelengths. This is precisely what is needed in discerning the separation of two similar waveforms.

Using generic waveforms to simulate pulses in the NCDs, preliminary results indicate that the desired resolution is possible over a range of pulse shapes.

---

*Presently at Philips Ultrasound, Philips Medical Systems 22100 Bothell Everett Highway Bothell, WA 98021-8431.

[1] J. V. Germani, internal document.

2.13 Data acquisition for SNO's neutral current detectors

G. A. Cox, M. A. Howe, B. L. Wall and J. F. Wilkerson

Within the last year, the data acquisition system for the neutral current detectors (NCD-DAQ) at SNO has been updated to a version closer to our final goal. The description of the NCDDAQ from previous CENPA Annual Reports still sufficiently describes our system,[1,2,3] although implementation of the embedded CPU (eCPU) and Global Trigger Identification (GTID) components has yet to be completed. The major updates were the data acquisition from hardware routines, event packaging, definition of our data output stream,[4] and the implementation of hardware mapping that eliminates the recording of unnecessary data. Other updates include the development of a pulse generator controller for electronics calibration, as well as the usual minor bug fixes. Most major enhancements were completed by the summer of 2002 and data acquisition has been nearly continuous throughout the year (Fig. 2.13-1).

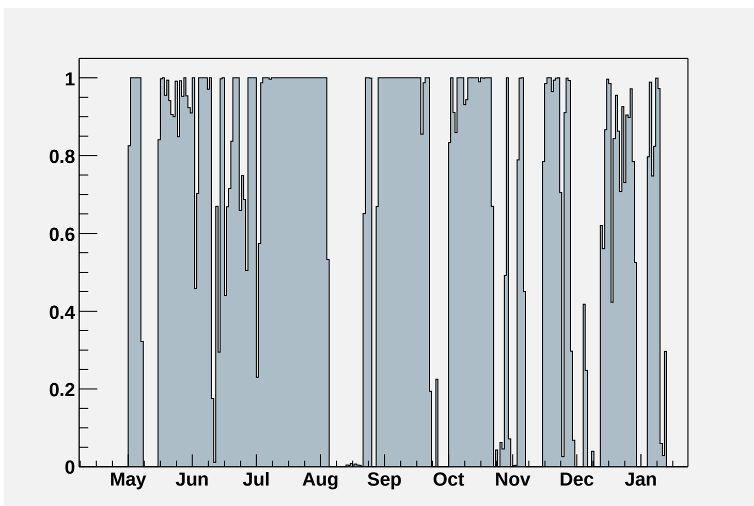

Figure 2.13-1. NCDDAQ livetime between May 2002 and Feb 2003.

The major causes for the periods of down–time in our system have been the installation of DAQ related hardware, the shutdown of the INCO mine, and two shipments of NCDs. We also experienced data storage issues that have been resolved.

The data is transferred to CENPA via FTP and stored on local disks and onto DVD as backup. Our normal data acquisition rate (excluding calibration data where a neutron source was present) has ranged from 1.5 MB to 6 MB per hour. This was dependent upon the number of detectors connected to the system and the implementation of some software. The data rate will be reduced significantly in the near future by using a packed data structure.

[1]CENPA Annual Report, University of Washington, (2002) p. 29.
[2]CENPA Annual Report, University of Washington, (2001) p. 32.
[3]CENPA Annual Report, University of Washington, (2001) p. 34.
[4]G. A. Cox, "A Description of the NCD Data Packets Dispatched from NCDDAQ," unpublished.

2.14 NCD underground status

T. H. Burritt, G. A. Cox, P. J. Doe, C. A. Duba, S. McGee, A. W. Myers, R. G. H. Robertson, L. C. Stonehill, T. D. Van Wechel and J. F. Wilkerson

The NCD array and associated electronics are nearly complete. Gas fill was completed in April, 2002 and the last two shipments of NCD's were delivered to SNO in May and November of 2002. Also delivered in the November shipment was enough hardware to allow data acquisition on all 96 channels. In February, 2003 the readout cables that will connect the deployed NCD's to the preamplifiers were delivered to SNO, after having passed rigorous microdischarge testing.[1] Also in that shipment was the pulser distribution system, which allows remote calibration of the electronics. The only piece of NCD data acquisition hardware that remains to be installed at SNO is the global trigger identification(GTID) board.

A period of data acquisition from the entire NCD array between November and February exercised the complete data acquisition system. There were 95 NCD strings hooked into 12 shaper/ADC cards, 8 multiplexer boxes, and two digitizing scopes. There were problems with the ribbon cables that connect the multiplexers to their controller boards, so for about the first month of this period only shaper data was being acquired. Not only did this period of intensive data acquisition help with debugging the electronics hardware, it also produced data that was vital for selecting which NCD's should be deployed in the reduced array.

The NCD pre-deployment welding began in February and, despite setbacks, was completed in early April, 2003. The 40 NCD strings that will be deployed are currently producing data that will be analyzed to detect any problems with the welded NCD's before deployment. In addition, data is being taken from some spare NCDs and unwelded cables, so replacement with well-characterized spares is possible in case problems are detected with the welded strings. Preparations for deployment are well underway and on schedule for deployment in September, 2003. The cables which will be used for the final system have been identified, labeled, and cleaned, and will be installed in the final cable tray soon. Final locations for NCD electronics have been identified and necessary SNO reviews have been completed.

[1] CENPA Annual Report, University of Washington (2002) p. 31.

2.15 NCD deployment equipment progress and training

J. F. Amsbaugh, M. Anaya,* J. Banar,* T. A. Burritt, P. J. Doe, G. C. Harper,
J. Heise,* G. Sillman,† J. Wilhelmy,* M. Williams† and J. Wouters*

The development of the equipment needed to deploy the neutral current detectors (NCDs) into the heavy water acrylic vessel (AV) of the Sudbury Neutrino Detector (SNO) is complete. The deployment is expected to occur in the fall of 2003. A previous progress report[1] mentioned completion of the gantry crane, the neckview camera system and equipment leaching tests. The next effort is to train the personnel who will install the deployment equipment at SNO and to train the personnel who will deploy the NCDs. The equipment has been installed at the Los Alamos National Laboratory (LANL) test pool as a training exercise by the installation team. The NCD deployment teams will have their training at LANL in May 2003 on this equipment. At some time before the deployment a final activity review will be done and just before deployment a failsafe review will have to be done.

The equipment installed at the LANL test pool is what will be used at SNO for deployment, configured for the shallower depth of the test pool. It consist of a Remote Operated Vehicle (ROV),[2] mounting plate, global and neck view cameras, NCD hauldown system, laser welding fixture, and various gloves, viewports, and manipulators. Many of the components can by moved around as needed during deployment. The NCD laser welding fixture is the only major component that is mocked up at the test pool as it is currently being used for the pre-deployment welding of NCDs at SNO.

The deployment training uses mock NCDs of the correct diameter and shorter in length. Also available are larger diameter mockups with buoyancies closer to the real NCDs. NCD laser welding experience was obtained by the team participation in the Pre-deployment welding. The trainees will hauldown NCDs, mockup NCD welds, deploy the NCD with the ROV (a small submersible) to an attachment point, and manipulate the readout cables. The ROV pilots will practice in small tight places just like the situation at SNO. Many of the differences between the setup at LANL and SNO will be emphasized. The equipment will be disassembled and shipped to SNO at the end of this training.

---

*Los Alamos National Laboratory, Los Alamos, NM 87545.
†Oxford University, Oxford, England.
[1] CENPA Annual Report, University of Washington (2002) p. 35.
[2] Deep Ocean Engineering, San Leandro, CA 94577.

2.16 Progress of the underground NCD welding prior to deployment

J. F. Amsbaugh, J. Banar,* T. A. Burritt, G. A. Cox, P. J. Doe, D. Earle,†
J. A. Formaggio, J. Heise,* A. Krimins,‡ I. T. Lawson,§ B. Morissette,†
R. W. Ollerhead,§ S. McGee, L. C. Stonehill and B. L. Wall

We have completed construction and testing of the laser welding equipment needed for neutral current detector (NCD) deployment in the Sudbury Neutrino Observatory (SNO) detector. The NCD welding occurs in two stages. First the so called pre–deployment welding in which individual NCD detectors are joined into the largest segments that will fit into the room above the SNO detector. The NCD anchors and readout cable ends are also welded to the segments during pre–deployment. The goal is to minimize the time the SNO detector is off for the second stage of welding, NCD deployment. During the NCD deployment these segments are welded together over the SNO detector into complete strings as they are inserted. The NCDs are scheduled to be deployed in fall 2003.

In last year's report,[1] an activity review was outlined. The review panel has finished its work. Equipment documentation, safety reports, assembly procedures, welding procedures, electrical inspection, and manpower schedules were finalized and approved. A test concerning the electrical interference (EMI) of the laser welder on the SNO detector and the water group's monitoring system was done, with no effects seen. The pre–deployment welding is currently underway.

It was estimated that pre–deployment welding would take about three months for the full 96 string array. Since then the array was optimized given the now known solar flux. Only 40 strings will be deployed requiring a total of 150 pre–deployment welds plus a few spares. As of 4 April 2003, 88 welds have been finished. Three were bad and one was possibly bad due to a procedural mishap. One of these four has been cut apart, reflared, and successfully rewelded. The second is being cut apart at this writing with the rest to follow soon.

The predeployment welding has had to overcome a series of mishaps, failures and interruptions. Shifts have been curtailed or canceled due to seismic activity, blasting, cage safety concerns and weather. Two gripping cuffs were damaged by improper use, the rotation motor shaft was sheared off, its drive shorted out, and the laser focus depth follower bearing seized. The previously reliable welding laser's control module failed and the replacement module was bad or incompatible requiring a field service technician. The laser was recalibrated and it was discovered the laser had been delivering 1.5 the rated power. This required developing new laser weld settings. All these have been finished and we have continued production the first two weeks of April. The lessons we have learned by these experiences will be applied to the NCD deployment.

*Los Alamos National Laboratory, Los Alamos, NM 87545.
†Sudbury Neutrino Observatory, Lively, Ontario, Canada P3Y 1M3.
‡Queens University, Kingston, Ontario, Canada K7L 3N6.
§University of Guelph, Guelph, Ontario, Canada N1G 2W1.
[1] CENPA Annual Report, University of Washington (2002) p. 34.

Neutrino Detectors

Double Beta Decay

2.17 Majorana update: construction, evaluation, simulation

P. J. Doe, V. M. Gehman, K. Kazkaz, R. G. H. Robertson and J. F. Wilkerson

The University of Washington continues its involvement initiated last year[1] in the Majorana collaboration.[2] The goal of the experiment is to determine the Majorana nature of the electron neutrino (*i.e.*, if the electron neutrino is its own antiparticle) and to measure the effective Majorana mass of the electron neutrino, $\langle m_\nu \rangle$. We propose to accomplish this goal by measuring the rate of neutrinoless double-beta ($0\nu\beta\beta$) decay of ^{76}Ge.

The full Majorana experiment will utilize a total of 500 kg of segmented germanium crystals isotopically enriched to 85% ^{76}Ge, which will act as both source mass and detector mass. Each crystal will weigh ∼2 kg and the crystals will be situated in a close-pack configuration. The segmentation geometry and final packing configuration are currently under evaluation. Majorana will have a sensitivity to the $0\nu\beta\beta$ decay halflife of 4.2×10^{27} years, corresponding[3] to a $\langle m_\nu \rangle$ of 20-70 meV. The Majorana experiment proposal is in the last editing stages.

Majorana has two testbed experiments, the Segmented Enriched Germanium Assembly (SEGA) and the Multi-Element Germanium Array (MEGA). SEGA utilizes a single segmented enriched crystal, and MEGA is an array of unsegmented, unenriched crystals in a close-pack configuration. These experiments will provide direction for the construction and analysis techniques used in the full Majorana experiment, but also have physics goals independent of Majorana. This past January the University of Washington was involved in evaluation of the SEGA crystal at the Triangle Universities Nuclear Laboratory, and has also been participating over the past year in ongoing construction of MEGA at Pacific Northwest National Laboratory. SEGA and MEGA will both be installed in the Waste Isolation Pilot Plant in Carlsbad, NM in the fall of 2003.

There are two major projects underway at CENPA that contribute to SEGA, MEGA, and Majorana. One project is the determination of which preamps will best suit the needs of the experiments. Our criteria for the preamp evaluations include restrictions on response time, resolution, noise, exponential decay of the collected charge, and heat dissipation. The other project is the construction of Geant4 models of SEGA and MEGA to provide Monte Carlo data. The simulations will provide a cross-check on the reliability of the Geant4 physics processes as well as provide a measure on the effect of radioactive contamination of the surrounding environment and construction materials.

---

[1] CENPA Annual Report, University of Washington (2002) p.43.

[2] http://majorana.pnl.gov.

[3] The spread in mass for a single halflife value comes from uncertainties in the nuclear matrix elements.

2.18 Electron-capture branch of ^{100}Mo and the efficiency of MOON

I. Ahmad,[*] J. Äystö,[†] P. Dendooven,[†] A. García, J. Huikari,[†] A. Jokinen,[†] I. Leikola,[†] F. Naab,[‡] H. Pentilä,[†] S. Rinta-Antila,[†] J. Szerypo[†] and S. Triambak

Recently Ejiri *et al.*[1] proposed to use ^{100}Mo as a solar neutrino detector. Neutrinos would undergo the reaction: $\nu + {}^{100}\mathrm{Mo} \rightarrow e^- + {}^{100}\mathrm{Tc}$, and ^{100}Tc would decay with a half-life of 15.8 s emitting another e^-. The signature for a neutrino absorption would be two electrons, providing a way to obtain clean signals. We have performed a first run on an experiment to measure the matrix element for the EC decay of ^{100}Tc, which determines the neutrino absorption cross section on ^{100}Mo.

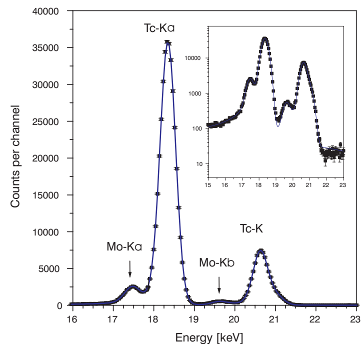

Figure 2.18-1. X-ray spectrum from our preliminary data taken at Jyväskylä.

A previous experiment[2] measured the ^{100}Tc EC branch to be $(1.8 \pm 0.9) \times 10^{-5}$ from which one obtains $B(\mathrm{GT}; {}^{100}\mathrm{Mo} \rightarrow {}^{100}\mathrm{Tc}) = 0.66 \pm 0.33$, nominally quite large, but still consistent with zero at 5% c.l. The present experiment was undertaken to produce a more significant result by using a separated beam of ^{100}Tc. This would reduce backgrounds that hindered a more accurate measurement in the previous experiment.

The present experiment was performed using the IGISOL[3] facility at the University of Jyväskylä. As shown in Fig. 2.18-1, the production of separated ^{100}Tc was very successful. shows our x-ray spectrum. The Mo x rays are the signature for the EC capture. We are presently analyzing the data and waiting to get more time at Jyväskylä to finish the data taking.

[*]Argonne National Laboratory, 9700 S. Cass Ave. Argonne, IL 60439.
[†]University of Jyväskylä, Jyväskylä, Finland.
[‡]Department of Physics, Notre Dame University, Notre Dame, IN 46556.
[1]H. Ejiri *et al.*, Phys. Rev. Lett. **85**, 2917 (2000).
[2]A. García *et al.*, Phys. Rev. C **51**, 439 (1995).
[3]J. Äystö, Nucl. Phys. A **693**, 477 (2001).

KATRIN

2.19 Characterizing silicon detectors for KATRIN

P. J. Doe, T. Gadfort, J. A. Formaggio, G. C. Harper, M. A. Howe, S. McGee, R. G. H. Robertson, J. F. Wilkerson and the KATRIN collaborators

The goal of KATRIN[1](Karlsruhe TRItium Neutrino Experiment) is to measure electron energies from tritium beta decay with a mass sensitivity of 0.35 eV. A deviation at the endpoint of the electron energy spectrum will be an indication of a neutrino mass. The experiment consists mainly of a gaseous T_2 source, a 10-m diameter retarding-field magnetic-electrostatic analyzer, and a large (approximately 10-cm diameter) silicon detector. A schematic of the project is shown in Fig. 2.19-1.

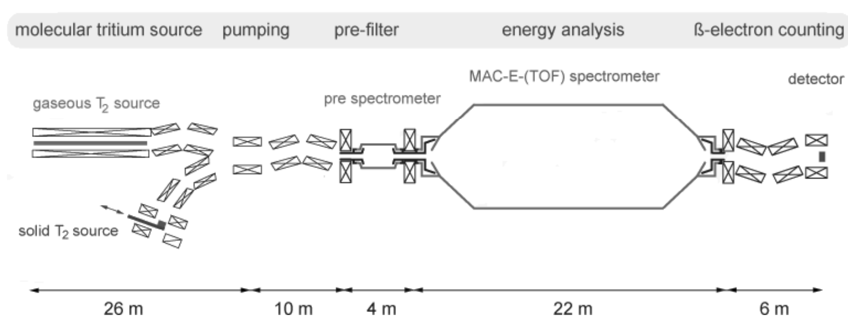

Figure 2.19-1. KATRIN Layout.

The UW group has taken up the task of characterizing and providing detectors, electronics and data acquisition for the KATRIN experiment. As part of this task, we have constructed an electron gun that produces 20 keV electrons incident on a particular detector surface (see Section 7.1). We also want to simulate the conditions of the KATRIN detector region as closely as possible. Thus, our detectors should reside in a high vacuum as well as be cooled to increase energy resolution. To meet these requirements, our detectors will be in contact with a Peltier device that will lower the surface temperature by 30 °C. Also, the electron gun will be attached to an oil free vacuum pump that will lower the internal pressure to 10^{-6} mbar. We plan to measure the uniformity of the detection layer, the effective detection region, the dead layer, and the back-scattering properties of various detectors. Proper characterizing of detectors is crucial to the KATRIN experiment since a neutrino mass measurement depends on stable, high-resolution, low-background recording of the energies of electrons arriving at the focal plane.

[1]KATRIN Letter of Intent, A. Osipowicz *et al.*, arXiv:hep-ex/0109033.

3 Nuclear Astrophysics

3.1 ^{7}Be(p,γ)^{8}B

E. G. Adelberger, A. R. Junghans* E. C. Mohrmann, P. N. Peplowski, K. A. Snover, H. E. Swanson and TRIUMF Collaborators†

Our Phase II measurement[1] of $S_{17}(0)$, the astrophysical S-factor for the ^{7}Be(p,γ)^{8}B reaction, is nearly completed. The measurement was made with a metallic ^{7}Be target[2] of 340 mCi initial activity and was carried out in a manner similar to the Phase I measurement.[3] Several improvements over the previous measurement were incorporated to further reduce systematic uncertainties.

Our Phase I solid angle measurements utilized the ^{7}Li(d,p)^{8}B reaction to determine the ratio of the counting rates in a "near" α-detector (used to make our ^{7}Be(p,γ)^{8}B measurements) and a "far" α-detector, whose solid angle we precisely determined from geometrical measurements. This method required a sizeable calculated correction for the portion of the continuous α-spectra from ^{8}B decay that lies below the experimental threshold.

We eliminated this use of the ^{7}Li(d,p)^{8}B reaction by making a ^{148}Gd α-source on a backing of identical design to that used for the ^{7}Be target, and using it to determine the solid angle ratio of the α-detectors. As before, this was done using the ratio of counting rates in the "near" and "far" detectors. In addition, the near detector was mounted on a translation stage which aided in the solid angle determination, as well as allowing optimization of the target to detector distance.

A small area "thin" Si α-detector ($\sim$150 mm^2, 20 μm thick) was used in addition to the large area ($\sim$450 mm^2, $\sim$30 μm thick) "thick" detector used previously. The thin detector had a lower background from gamma rays from the target radioactivity, enabling the use of a lower threshold for the detected α-particles. This resulted in a smaller correction for the fraction of the α-spectrum from ^{8}B decay below the experimental threshold.

Measurements of the ^{7}Be(p,γ)^{8}B cross section were made over the range of energies from $\bar{E}_{cm}$ = 116 to 1754 keV. Backscattering rate calculations were made (see Section 3.2) and compared to measured data in order to determine the target composition. Knowledge of the target composition was important for determining the energy loss of the proton beam in the target, which becomes especially important at low E_p where the cross section varies rapidly with energy.

Our Phase II determination of $S_{17}(0)$ is in good agreement with our earlier result.[3] Our new results are currently being finalized for publication.

---

*Presently at F. Z. Rossendorf Institut fuer Kern-und-Hadronenphysik, Dresden, Germany.

†L. Buchmann, S. Park and A. Zyuzin, TRIUMF, Vancouver, BC, Canada.

[1] CENPA Annual Report, University of Washington (2002) p. 47.

[2] A. Zyuzin *et al.*, Nucl. Instrum. Methods B **187**, 264 (2002).

[3] A. R. Junghans *et al.*, Phys. Rev. Lett. **88**, 041101-1 (2002); see also CENPA Annual Report, University of Washington (2001) p. 4.

3.2 Target composition analysis for ^{7}Be(p,γ)^{8}Be S-factor measurement

A. R. Junghans,* E. C. Mohrmann, P. N. Peplowski and K. A. Snover

In order to properly interpret the experimentally measured cross-sections for the ^{7}Be(p,γ)^{8}B reaction, it is necessary to understand the beam energy loss within the target. Uncertainty in the deduced S-Factors $S_{17}(E)$ due to uncertain target composition is largest at low energies where the cross-section is highly energy dependent. This region is important for the extrapolation to $S_{17}(0)$. In order to determine the beam energy loss, the target composition must be known.

The energy thickness of the target (ΔE_{target}) and the energy loss due to the ^{7}Be in the target (ΔE_{7Be}) must be measured and used to determine the target composition. ΔE_{target} was determined by measuring the narrow 1378-keV resonance in the ^{7}Be(α,γ)^{11}C reaction. The width of this resonance can be directly attributed to the energy thickness of the target. ΔE_{7Be} was determined from target activity measurements. The energy loss due to contaminants is $\Delta E_{cont} = \Delta E_{target}$ - ΔE_{7Be}.

TRIM[1] calculations were made with several possible target stoichiometries that account for ΔE_{cont}. The ^{8}B backscattering probability for the various target compositions was calculated and compared to the experimentally measured values. It is displayed in Fig. 3.2-1.

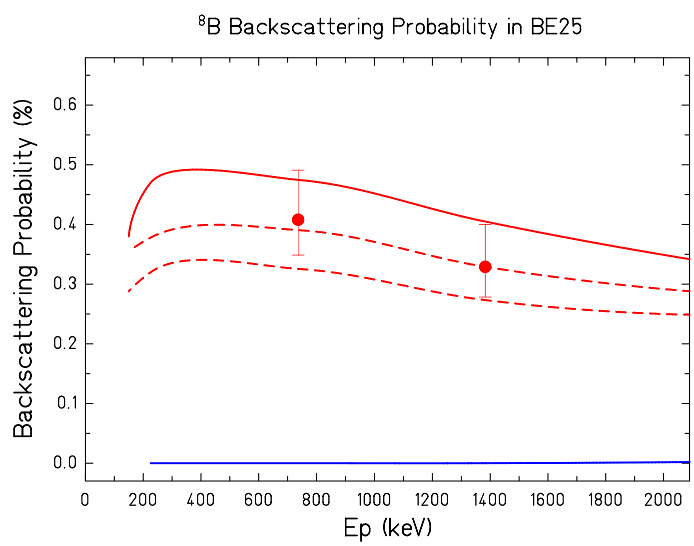

Figure 3.2-1. ^{8}B backscattering probability for different target compositions compared to the experimentally measured backscattering probability. Target compositions are, from top to bottom, ^{7}Be:C:Mo = 63:0:37 (solid curve), 58:8:34 (dashed curve), 57:13:30 (dashed curve), and 35:65:0 (solid curve).

The best fit target composition of ^{7}Be:C:Mo=58:8:34 is within 1σ of pure Mo contamination, which was used in the final data analysis.

*Presently at F. Z. Rossendorf Institut fuer Kern- und Hadronenphysik, Dresden, Germany.
[1] TRIM Version 2000.40, J. F. Ziegler, www.srim.org.

3.3 Search for the ^{8}B(2^+) $\rightarrow$ ^{8}Be(0^+) ground state transition

M. K. Bacrania, D. W. Storm, R. G. H. Robertson, M. W. Gohl* and S. Uehara

We are searching for the ^{8}B(2^+) $\rightarrow$ ^{8}Be(0^+) ground state transition. The decay of ^{8}B takes place primarily through the allowed $2^+ \rightarrow 2^+$ transition to the 3 MeV broad excited state in ^{8}Be, with an endpoint energy of approximately 14 MeV. It is also possible for ^{8}B to decay to the ground state of ^{8}Be, through a second forbidden transition ($2^+ \rightarrow 0^+$) with an endpoint of approximately 17 MeV. This second forbidden decay is predicted to have an extremely small branching ratio, and it has never been experimentally measured. The astrophysical significance of this transition is discussed elsewhere.[1]

We are able to produce beams of 15 MeV ^{8}B using the CENPA Tandem van de Graaff accelerator (see Section 8.3). The ^{8}B is implanted into a 500μm Si PiN detector. The resulting ^{8}B decay ($t_{1/2}$ = 770ms) produces a β^+, and the prompt decay of ^{8}Be produces a pair of α particles. The β^+ particle is detected via a scintillation counter, and is used as a coincidence trigger which virtually eliminates beam and electronics backgrounds. For ^{8}Be excitation energies below 7 MeV, both α particles come to rest inside the Si detector. A decay via the $2^+ \rightarrow 2^+$ branch results in a broad α energy spectrum centered around 3 MeV, and a decay via the $2^+ \rightarrow 0^+$ branch will result in a spectral line centered at 92 keV.

In 2002, we built and tested the ^{3}He gas cell system, and conducted beam tests in order to determine backgrounds due to scattered and degraded ^{6}Li and ^{3}He from the ^{8}B production region. A potentially large background source is scattering from the beam regulation slits in the image region beamline. To eliminate this background, we operate the Tandem in GVM regulation mode, with the regulating slits fully retracted out of the beamline. We have reduced our singles background rate to approximately 1 kHz. Our ^{8}B implantation rate is approximately 6 Hz, and our detection efficiency is approximately 40%.

We have had three data-taking runs to date, and are presently analyzing the data from these runs. We have accumulated approximately 3×10^5 coincidence-tagged ^{8}B decays. In the first run we had relatively poor energy resolution (FWHM = 30 keV for 88 keV photons), and also observed a significant beam-independent background in the region of the $2^+ \rightarrow 0^+$ transition. In the second and third runs, our resolution has been improved by the addition of a Peltier cooling system for the Si detector (FWHM = 20 keV for 81 keV photons), and by more extensive radiation and RF shielding.

*Presently at Justus-Liebig-Universität Gießen, Germany.

[1]CENPA Annual Report, University of Washington (2002) p. 49.

3.4 Is e^+e^- pair emission important in the determination of the ^{3}He + ^{4}He S-factor?

A. E. Hurd and K. A. Snover

The astrophysical S-factor $S_{34}(0)$ for ^{3}He+^{4}He fusion is very important for determining the production rate of neutrinos from the decay of ^{7}Be and ^{8}B in the sun. Experimental determinations of $S_{34}(0)$ have been made by two methods - detection of the capture γ-rays, and detection of the residual ^{7}Be activity. The relatively large uncertainty in the recommended value of $S_{34}(0)$ stems from an apparent difference in the results of these two methods, with the activation experiments yielding a somewhat larger mean value than the capture γ-ray experiments.[1] While the statistics in these comparisons are suggestive, but not compelling, this apparent difference has led to the question of whether there might be some other capture reaction mechanism that could explain it, such as $E0$ pair emission. At low bombarding energies, the capture reaction takes place at large radial distances, and hence processes such as $E0$ pair emission should be enhanced.

The dominant reaction mechanism for ^{3}He+^{4}He fusion at low energies is direct $E1$ photon emission. Since the operators for $E0$ and $E2$ transitions, $O_{E0} = \sum_i (e_i/e) r_i^2$ and $O_{E2} = \sum_i (e_i/e) r_i^2 Y_{2m}(\Omega_i)$, have the same radial dependence (in the long wavelength limit), $E0$ direct capture amplitudes for specific partial wave transitions may be numerically related to the corresponding $E2$ direct capture amplitudes. At low bombarding energies, this leads to a simple relation between the cross sections for $E0$ pair emission and $E2$ photon emission. For a transition energy of several MeV in ^{3}He+^{4}He $\rightarrow ^7$Be, the result is a cross section ratio $\sigma_{E0}/\sigma_{E2} \sim 2 \times 10^{-4}$. The magnitude of this ratio is easy to understand: $E2$ (real) and $E0$ (virtual) photons have the same degree of forbiddenness, while pair emission brings an extra power of α, the fine structure constant, as well as a smaller phase space factor. Direct capture calculations show $\sigma_{total} \sim \sigma_{E1} \sim 400\sigma_{E2}$ at these energies. Hence $\sigma_{E0} \sim 10^{-6}\sigma_{total}$ and is completely negligible. Sum rule arguments show that $E0$ pair emission by any other mechanism, such as resonance emission, must also be negligible.

In general, all electromagnetic multipole transitions may occur by pair emission. An $E0$ transition is distinguished from other multipole transitions by the absence of single photon emission rather than the presence of pair emission. Pair emission is a weak function of multipole order, hence $E1$ pair emission is strongest in ^{3}He+^{4}He. Published pair emission coefficients show that $E1$ pair emission is of order 10^{-3} of $E1$ single photon emission at several MeV, so that e^+e^- pair emission of any multipolarity is negligible in ^{3}He+^{4}He radiative capture. Internal conversion is also negligible. Thus there cannot be significant contributions to the ^{3}He+^{4}He $\rightarrow ^7$Be capture cross section at low energies from electromagnetic emission processes other than single photon emission.[2]

[1] E. G. Adelberger *et al.*, Rev. Mod. Phys. **70**, 1265, (1998).
[2] K. A. Snover and A. E. Hurd, Phys. Rev. C, in press.

4 Nuclear Structure

4.1 Testing the isospin multiplet mass equation and its implications

P. Cheung, A. García, G. Hodges, H. Iwamoto, A. Sallaska and S. Triambak

The isospin multiplet mass equation (IMME) relates the masses of the members of an isospin multiplet: $M(T_z) = a + bT_z + cT_z{}^2$. Recently, a precise determination of the mass of ^{33}Ar led to the conclusion that an unexpectedly large cubic term was needed to fit the members of the lowest T=3/2 state in the A=33 system.[1] Later we found out that the problem originated in an incorrect determination of the mass of the lowest T=3/2 state in ^{33}Cl. Using the more recent measurements of both ^{33}Ar and ^{33}Cl we found excellent agreement with the parabola.[2] We are presently setting up an experiment to determine the mass of the lowest T=2 state in ^{32}S whose uncertainty is claimed to be ± 3 keV.[3] There is a paper presented at a conference claiming an uncertainty of ± 0.4 keV with no published details on how the small uncertainty was achieved.[4] We aim to determine the energy of this state with ± 0.1 keV uncertainty. As a result, the T=2 multiplet in the A=32 system would constitute the most accurately known quintuplet and it would be interesting to show that the IMME holds to this level of accuracy. On the other hand, we want to pursue measurements in the beta decay of ^{32}Ar (both of the electron-neutrino correlation and of the $\log ft$ for the $0^+ \rightarrow 0^+$ decay) for which the IMME may help determining the Q value for the decay.

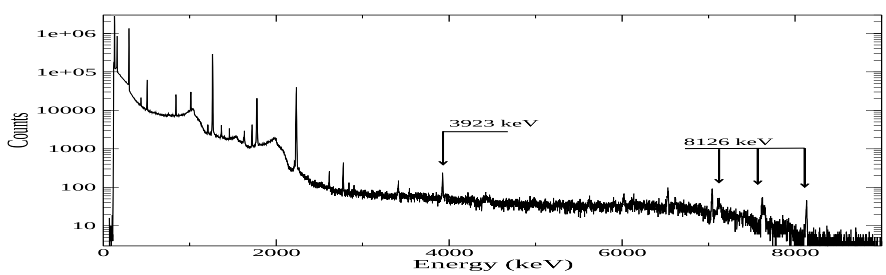

Figure 4.1-1. Gamma ray spectrum from ^{31}P(p,γ) at the T=2 resonance. The arrows indicate gammas from the decay of the T=2 state.

Using the sputter ion source, we produced an implanted ^{31}P target with a thickness of approximately 4 keV, measured using the ^{31}P(p,γ) reaction to produce the narrow T=2 state. Fig. 4.1-1 shows a γ spectrum taken at the T=2 resonance. We have performed Monte Carlo simulations that calculate Doppler effects on the gammas keeping in mind the energy losses, detector resolution, detector angle with respect to the beam and the gamma-ray angular correlations to help us understand potential problems. To reduce our systematic uncertainties we shall check for Doppler effects in two oppositely placed Ge detectors.

[1] F. Herfurth *et al.*, Phys. Rev. Lett. **87**, 142501-1 (2001).
[2] M. C. Pyle *et al.*, Phys. Rev. Lett. **88**, 122501-1 (2002).
[3] G. Audi and A. H. Wapstra, Nucl. Phys. A **595**, 409 (1995).
[4] M. S. Antony, A. Huck, G. Klotz, A. Knipper, C. Miehé and G. Walter, in *Proceedings of the International Conference on Nuclear Physics*, Lawrence Berkeley Laboratory, Berkeley, CA, Vol. 1 (1980).

4.2 Low-temperature measurement of the giant dipole resonance width

D. Bazin,* J. R. Beene,* Y. Blumenthal,* M. J. Chromik,* M. Halbert,* P. Heckman,* J. F. Liang,* E. C. Mohrmann, T. Nakamura,* A. Navin,* B. M. Sherrill,* K. A. Snover, M. Thoennessen,* E. Tryggestad* and R. L. Varner*

We have made a new determination of the width of the Giant Dipole Resonance in the inelastic scattering of ^{17}O particles from ^{120}Sn at 80 MeV/u.[1] The experiment was carried out at the National Superconducting Cyclotron Laboratory at Michigan State University. The inelastically scattered ^{17}O particles were detected at forward angles in the S800 spectrometer, and the γ rays were detected in the ORNL - Texas A&M - MSU BaF_2 array in coincidence with the S800. γ-ray spectra were recorded for different inelasticities ranging from 20 to 90 MeV.

The spectrum of inelastically scattered ^{17}O particles in coincidence with all γ rays exhibits strong peaks corresponding to the opening of the 1n, 2n and 3n channels, up to 30 MeV of ^{17}O energy loss, suggesting a close correspondence between inelasticity and residual excitation energy over this range. This conclusion is also consistent with a recent inelastic α-scattering study. Accordingly, we performed a CASCADE analysis of the spectral shape measured for energy losses in the range 20 - 30 MeV, assuming equality between energy loss and residual (initial) excitation energy. The spectrum is fitted well by including a bremsstrahlung component and allowing the GDR strength, width and energy to vary. The result is a width $\Gamma = 4 \pm 1$ MeV for decays with a mean excitation energy following GDR decay of 9.7 MeV, corresponding to a mean (final-state) temperature of 1.0 MeV.

This result for the GDR width is comparable to the width of the GDR built on the ground state of similar mass nuclei, and is much narrower than the value calculated in the adiabatic shape fluctuation model. This new data confirms the trend suggested by other experiments in this mass region, in which the GDR width was found to be narrower than the model predictions for temperatures in the range $\sim$ 1.3 - 1.7 MeV, and shows clearly that the GDR width increases much more slowly with temperature than predicted by the model. Since pairing corrections should not be important at these temperatures, and shell effects are small for ^{117}Sn and nearby nuclides, this seems to be a clear failure of the adiabatic shape fluctuation model.

Deviations from the adiabatic approximation, which assumes that the time scale for shape fluctuations is long compared to the inverse frequency spread associated with the deformation broadening of the GDR, would result in a smaller GDR width; however, it would be surprising if such deviations occured only at low temperature. Attempts to explain the observed GDR widths by mechanisms other than deformation broadening also do not agree with the data. Hence we conclude that narrow GDR widths observed in Sn and nearby nuclides at low temperature are not understood.

---

*For current address, see reference 1.

[1] P. Heckman *et al.*, Phys. Lett. B **555**, 43 (2003).

5 Relativistic Heavy Ions

5.1 Introduction to event-structure analysis

T. A. Trainor

Event-structure analysis attempts to determine, by correlation analysis of the hadronic final state, the dynamics of heavy-ion collisions from first contact to kinetic decoupling. Emphasis is placed on the 'soft' p_t regime below 2 GeV/c, thought to be dominated by non-perturbative QCD. Although the soft p_t regime is emphasized, traditional high-p_t phenomena such as jet quenching are also a subject of study through their generalization *via* the fluctuation-dissipation theorem.

Fluctuations and correlations are intimately related and can be reduced to a common representation: the autocorrelation distribution. Charge-independent correlations are mainly sensitive to initial-state momentum transfers. Charge-dependent correlations are mainly sensitive to local measure conservation during hadronization. An element common to these two aspects is the presence of a dissipative (of partonic energy) and opaque (to hadrons) medium unique to heavy-ion collisions of sufficient energy and centrality. The centrality dependence of fluctuations and correlations is a key element in the study of this medium. The principal elements of the program are

- Centrality dependence of fluctuations and correlations
- Equivalence of fluctuations and correlations and their efficient representation
- Scale-dependent $\langle p_t \rangle$ fluctuations
- Scale-dependent number and net-charge fluctuations
- Charge-independent and -dependent joint number autocorrelations
- Hard and soft components of p-p collisions
- The role of dissipation in heavy-ion collisions
- The role of measure conservation during hadronization
- Stochastic multiple scattering as a correlation/fluctuation source

Scale dependence of fluctuations can be inverted to reveal net autocorrelations depending on difference variables. Net autocorrelations can also be determined directly as ratios of object and reference two-particle distributions. Centrality dependence of heavy-ion event structure should go asymptotically to p-p results for the most peripheral A-A collisions. Understanding of p-p collisions is in turn essential to determine what is unique (nonlinear) about heavy-ion collisions, beyond contributions from initial-state stochastic multiple scattering.

5.2 Mean-p_t fluctuations and minijet production in Hijing-1.37

Q. J. Liu and T. A. Trainor

Minijets (semi-hard parton scattering with momentum transfers of a few GeV/c) should be copiously produced in ultra-relativistic heavy-ion collisions at RHIC energies. A dissipative medium formed early in the collision could cause jets/minijets to lose energy through induced gluon radiation, a process known as jet quenching.[1] We used the Monte Carlo event generator Hijing-1.37[2] to study $\langle p_t \rangle$ fluctuations as a measure of dissipation properties of a colored medium. Three sets of Hijing-1.37 events were generated: Hijing default (jet quenching on), quenching switched off and jet/minijet production switched off, with impact parameter less than 3 fm (equivalent to top 5% most-central collisions). A graphical analysis of $\langle p_t \rangle$ fluctuations compares data distributions with a gamma distribution central-limit reference modeling independent particle emission. A difference between data and reference would imply non-statistical variations in collision dynamics (such as minijets).

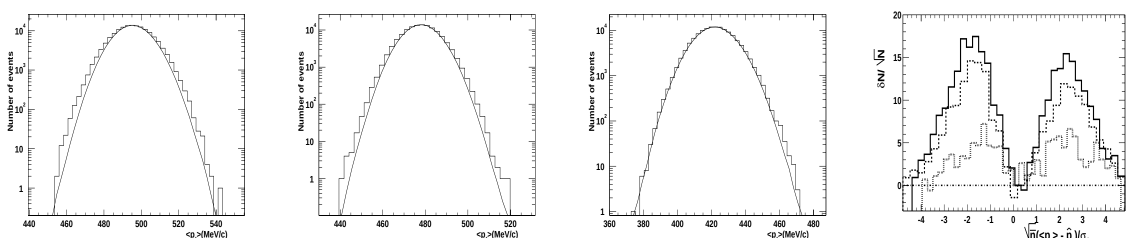

Figure 5.2-1. Distributions of event-wise $\langle p_t \rangle$ for Au-Au collisions at $\sqrt{s_{NN}} = 200$ GeV from Hijing-1.37 (histograms) compared with gamma distribution central-limit references (curves). The three left panels are jets-on quench-off, jets-on quench-on and jets-off. The right-most panel shows the differences between data and reference in the first three panels.

Frequency distributions of event-wise $\langle p_t \rangle$ for the three Hijing event types are shown in Fig. 5.2-1 as histograms with reference distributions plotted as curves. Histograms with minijets on (left two panels) deviate substantially from the reference, indicating that nonstatistical fluctuations are significant. Excess fluctuations in events with jets off (third panel) are substantially less. With these histograms it is not possible to detect a change with quenching on or off. A more differential approach plots the difference between data and reference (fourth panel). The dramatic increase from jets-off (lowest histogram) to jets-on is consistent with the qualitative difference in the left three panels. A significant difference with quenching on and off (upper two histograms) is also apparent. Thus, according to the Hijing model, $\langle p_t \rangle$ fluctuations are sensitive to jet quenching, revealing properties of a colored medium formed in heavy-ion collisions. The difference histograms are more sensitive to the effects of jet quenching and enable precision comparisons. Numerical analysis using a central-limit reference analogous to the gamma distribution to make variance comparisons would be even more precise. This graphical study shows that in the Hijing model, $\langle p_t \rangle$ fluctuations are sensitive to jet production *and* jet quenching, and that fluctuation analysis could serve as a probe of dissipation properties of a dense colored medium formed in heavy-ion collisions.

[1] X. N. Wang and M. Gyulassy, Phys. Rev. Lett. **68**, 1480 (1992).

[2] M. Gyulassy and X. N. Wang, Comp. Phys. Comm. **83**, 307 (1994).

5.3 Mean-p_t fluctuation scaling on (η, ϕ) in Au-Au collisions at $\sqrt{s_{NN}} = 200$ GeV

Q. J. Liu and T. A. Trainor

Heavy-ion fluctuation measurements probe event-wise variation of A-A collision dynamics which could arise from critical phenomena near the QCD phase boundary or from hard partonic scattering in the early collision, among other possibilities. We analyze $\langle p_t \rangle$ fluctuations in minimum-bias STAR data for Au-Au collisions at 200 GeV with a scale-dependent measure of excess p_t variance based on the central limit theorem. The variance difference factor $\Delta\sigma_{p_t\,n}$, an rms measure of excess p_t fluctuations, is defined by

$$\Delta\sigma^2_{p_t\,n}(\delta\eta, \delta\phi) \equiv 2\sigma_{\hat{p}_t}\,\Delta\sigma_{p_t\,n}(\delta\eta, \delta\phi) \equiv \overline{(p_t(\delta\eta, \delta\phi) - n(\delta\eta, \delta\phi)\,\hat{p}_t)^2/n(\delta\eta, \delta\phi)} - \sigma^2_{\hat{p}_t} \tag{1}$$

where $p_t(\delta\eta, \delta\phi)$ and $n(\delta\eta, \delta\phi)$ are bin-wise total p_t and charge multiplicity, and $\hat{p}_t$ and $\sigma^2_{\hat{p}_t}$ are the inclusive p_t distribution mean and variance respectively.

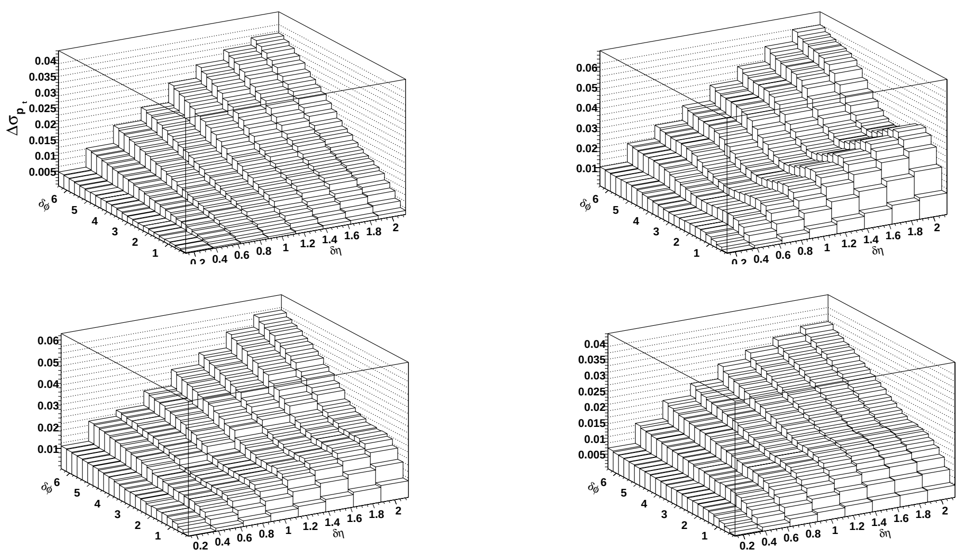

Figure 5.3-1. $\Delta\sigma_{p_t\,n}$ as a function of scale $(\delta\eta, \delta\phi)$ for three centrality bins. Upper left panel shows results for peripheral events (70-80% of σ_{tot}), upper right for mid-central event (30-40%), lower left for most-central events (0-5%). Lower right is from the Hijing MC for the top 5% most-central events.

In Fig. 5.3-1 we see that strong scale-dependent structure persists from peripheral to central collisions. These scaling distributions can be inverted (see Section 5.5) to obtain joint p_t autocorrelations on difference variables $(\eta_\Delta, \phi_\Delta)$ which reveal dominant monopole and quadrupole components plus a small-scale peak structure. The p_t quadrupole component is related to elliptic flow, a number correlation. To better understand the source of correlations we also analyzed Hijing Monte Carlo events where jets/minijets are modeled. Hijing data suggest that jets/minijets could be an ingredient of p_t correlations driving the observed mean-p_t fluctuation scaling in STAR data.

5.4 Scale dependence of net-charge fluctuations

D. J. Prindle and T. A. Trainor

Fluctuations of conserved quantities such as charge, strangeness and baryon number, have been studied in elementary collision systems.[1] The long-range correlations, correlations among particles far apart in rapidity, probe the initial interactions while short range correlations probe the late-stage fragmentation. The short-range correlations demonstrate that charge and strangeness are locally conserved during the fragmentation. With our much better statistics in STAR we can perform a much more detailed study of the dependence of net-charge fluctuation on the scale.

Our measure of net charge fluctuation is

$$\Delta\sigma^2_{N_\Delta}(\delta\eta,\delta\phi) = \overline{(\delta N_+(\delta\eta,\delta\phi) - \delta N_-(\delta\eta,\delta\phi))^2} / \overline{(N_+(\delta\eta,\delta\phi) + N_-(\delta\eta,\delta\phi))}$$

where $\delta N(\delta\eta,\delta\phi)$ is a deviation from the mean and $N_+(\delta\eta,\delta\phi)$ and $N_-(\delta\eta,\delta\phi)$ are the numbers of positive and negative charged particles measured within a bin the size of $\delta\eta$ by $\delta\phi$. Our bin sizes range from the detector acceptance, $\delta\eta = 2$ by $\delta\phi = 2\pi$ to $\delta\eta = 2/16$ by $\delta\phi = 2\pi/24$.

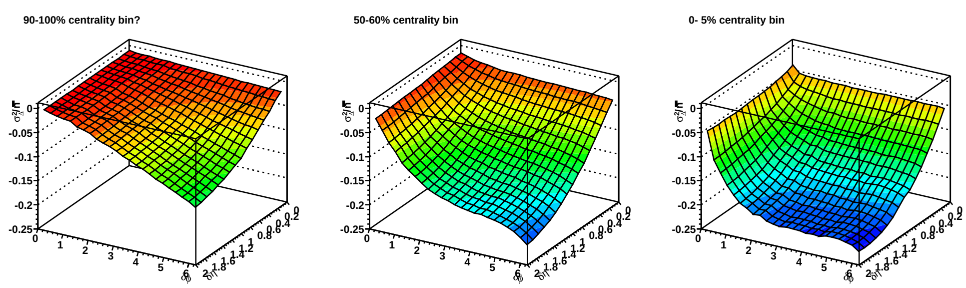

Figure 5.4-1. Net-charge fluctuations, $\Delta\sigma^2_{N_\Delta}$, as a function of scale for 200 GeV Au-Au collisions. The panels show data from peripheral, mid-peripheral and central collisions from left to right. The x and y axis are $\delta\phi$ and $\delta\eta$, the bin size of the measurement.

In heavy-ion collisions we have a broad range of impact parameters and we expect the mixture of physics processes will change from peripheral to central collisions. We separate events into centrality bins according to the total number of observed tracks. Our scale-dependent measurements of net-charge fluctuations are shown for peripheral, mid-peripheral and central collisions in Fig. 5.4-1. The shape changes from a linear decrease in $\Delta\sigma^2_{N_\Delta}$ with increasing scale for peripheral data to a sharp drop in $\Delta\sigma^2_{N_\Delta}$ at small scales for central data. The changing curvature indicates a dramatic change in the correlation lengths of charge-dependent correlations an (η,ϕ), as indicated in Section 5.6.

[1] H. Aihara *et al.*, Phys. Rev. Lett. **53**, 2199 (1984).

5.5 Relating fluctuations and correlations in heavy-ion collisions

T. A. Trainor

We can relate scale-dependent fluctuations of a measure $\mathcal{U}$ distributed on particles indexed with kinematic variable x in acceptance Δx binned at scale δx to two-particle correlations represented by net autocorrelation ΔA_2. A bin of size δx contains integrated measure $u(\delta x)$ and multiplicity $n(\delta x)$. The scale-dependent variance of u over a bin (and/or event) ensemble is defined by $\sigma_u^2(\delta x) = \overline{(u(\delta x) - \bar{u}(\delta x))^2}$. Scale variation of this variance is determined by two-particle correlations.

The per-particle variance difference across a scale interval is defined by

$$\Delta\sigma_u^2(\delta x_1, \delta x_2) \equiv \overline{(u(\delta x_2) - \bar{u}(\delta x_2))^2/n(\delta x_2)} - \overline{(u(\delta x_1) - \bar{u}(\delta x_1))^2/n(\delta x_1)}. \tag{1}$$

The rank-2 correlation integral, second moment and autocorrelation density are related by

$$C_2(u, \delta x) = M(\Delta x, \delta x)\,\overline{u^2(\delta x)} = \int_0^{\delta x} A_2(u, x_\Delta) dx_\Delta. \tag{2}$$

$\Delta C_2(u, \delta x) = C_{2,obj} - C_{2,ref} = \Sigma^2(u, \delta x)$ defines the last quantity as the total variance. If total variances are compared across a scale interval, the total variance difference is equal to an integral of the net autocorrelation on difference variable $x_\Delta \equiv x_1 - x_2$

$$\Delta\Sigma_u^2(\delta x_1, \delta x_2) = \Sigma_u^2(\delta x_2) - \Sigma_u^2(\delta x_1) = \int_{\delta x_1}^{\delta x_2} \Delta A_2(u, x_\Delta) dx_\Delta. \tag{3}$$

If $\bar{N}(\Delta x)$ is the mean total multiplicity in the acceptance then for a factorization reference $\Sigma_{u,ref}^2(\delta x_1, \delta x_2) = \bar{N}(\bar{N}-1)\bar{u}^2$ and

$$\begin{aligned} \Delta\sigma_u^2(\delta x_1, \delta x_2) &= \Delta\Sigma_u^2(\delta x_1, \delta x_2)/\bar{N} = (\bar{N}-1)\bar{u}^2\, \Delta\Sigma_u^2/\Sigma_{u,ref}^2 \\ &\simeq (\bar{N}-1)\bar{u}^2 \int_{\delta x_1}^{\delta x_2} \frac{\Delta A_2}{A_{2,ref}}(u, x_\Delta) dx_\Delta. \end{aligned} \tag{4}$$

We now consider measure $\mathcal{U}$ distributed on final-state charged hadrons detected in axial momentum space (η, ϕ) with larger scale $\delta x_2 \rightarrow (\delta\eta, \delta\phi)$ within acceptance $(\Delta\eta, \Delta\phi)$ and smaller scale $\delta x_1 \rightarrow (d\eta, d\phi)$ defined by a binning of difference variables

$$\begin{aligned} \Delta\sigma_u^2(\delta\eta, \delta\phi) &= (\bar{N}-1)\,\bar{u}^2 \int_{d\eta, d\phi}^{\delta\eta, \delta\phi} K(\eta_\Delta, \phi_\Delta)\, \frac{\Delta A_2}{A_{2,ref}}(u, \eta_\Delta, \phi_\Delta)\, d\eta_\Delta d\phi_\Delta \\ \Delta\sigma_u^2(m\, d\eta, n\, d\phi) &= \frac{(\bar{N}-1)\,\bar{u}^2}{M_\eta\, M_\phi} \sum_{k=1}^{m}\sum_{l=1}^{n} \left(1 - \frac{k-1/2}{m}\right)\left(1 - \frac{l-1/2}{n}\right) \frac{\Delta A_2}{A_{2,ref}}(k\, d\eta, l\, d\phi). \end{aligned} \tag{5}$$

The kernal K represents the binning process in the variance difference. The second line shows the discrete form of the integral used in a numerical analysis. This is a Volterra equation of the first kind, which can be inverted to obtain the net autocorrelation from a fluctuation scaling measurement. This equation has been applied to net-charge fluctuation scaling to obtain net autocorrelation densities on $(\eta_\Delta, \phi_\Delta)$ (see Section 5.6).

5.6 Determination of auto-correlation using net-charge fluctuations

D. J. Prindle and T. A. Trainor

In Section 5.4 we described our measurement of net charge fluctuation. The relationship with the underlying auto-correlation is discussed in Section 5.5. Inverting the Volterra equation is formally straight-forward but in practice very sensitive to measurement error. One way around this is to parameterize the auto-correlation and minimize the function

$$\chi^2 = \sum_k \sum_l (\Delta\sigma^2_{N_\Delta}(k,l) - \Delta\sigma^2_{N_\Delta}(a_1 ... a_n))^2 \tag{1}$$

where $\Delta\sigma^2_{N_\Delta}(a_1 ... a_n)$ is found by integrating a model function as auto-correlation. If one is confident in the form of the model function this is a good method.

When the form of the auto-correlation is unknown, one can require the auto-correlation to be "smooth". In this method we treat each bin of the auto-correlation as a free parameter but add a smoothing term to the χ^2. The additional term is

$$\lambda \sum_k \sum_l \left(\bar{N}\frac{\Delta A}{A}(k,l) - \overline{\bar{N}\frac{\Delta A}{A}(k,l)} \right)^2, \tag{2}$$

where λ is an arbitrary Lagrange multiplier and $\overline{\bar{N}\frac{\Delta A}{A}(k,l)}$ is the average value of the auto-correlation for bin (k,l) as determined by the nearest-neighbor bins. The resulting total χ^2 is small when $\lambda = 0$ (and there is no smoothing) and attains a maximum when λ is big (and the smoothing term is zero). When there are no fluctuations the auto-correlation is flat and this maximum χ^2 will be one per measurement point. When there are correlations a reasonable criterion for λ is to require the total χ^2 be one per measurement point. The advantage of this method is that the only assumption is the auto-correlation is smooth.

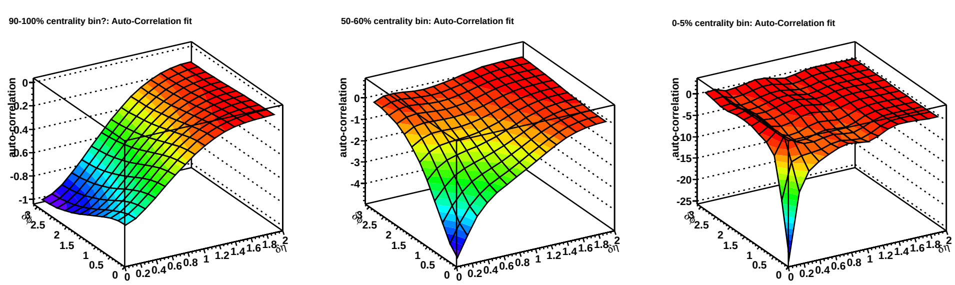

Figure 5.6-1. Auto-correlations derived from the data shown in section 4.2.2. The panels show data from peripheral, mid-peripheral and central collisions from left to right. The x and y axis are $\delta\phi$ and $\delta\eta$, the bin size of the measurement.

The auto-correlations for the three centrality classes used in the previous section are shown in Fig. 5.6-1. There is a strong evolution of the shape of the auto-correlation with centrality. For the most central data there is a very narrow peak at small scales. The ripple structure is an artifact of smoothing. We are examining ways to reduce this.

5.7 Centrality dependence of $\langle p_t \rangle$ fluctuations in Au-Au collisions

Q. J. Liu, J. G. Reid and T. A. Trainor

Significant nonstatistical fluctuations of $\langle p_t \rangle$ (event-wise mean transverse momentum) have been observed in 130- and 200-GeV Au-Au collisions at RHIC. Difference factor $\Delta\sigma_{p_t}$, an *rms* measure of nonstatistical fluctuations, indicates a 14% increase (50 MeV/c) relative to finite-number fluctuations for central Au-Au collisions. One source of information about the fluctuation mechanism is centrality dependence – variation with collision geometry from peripheral to central events. We observe a three-fold increase in $\Delta\sigma_{p_t}$ with centrality.

One mechanism that could produce excess fluctuations is binary collision processes (Cronin multiple scattering and minijet production) in the initial stages of the A-A collision. In a limiting case such binary collisions are a form of stochastic multiple scattering. To test this hypothesis we adopt centrality measure $\nu = 2\,N_{bin}/N_{part}$, the number of binary collisions per participant nucleon pair, which estimates the average path length of one nuclear constituent (nucleon or parton) in traversing the other nucleus. We also introduce an alternative fluctuation measure, $2/N_{part}\,\Delta\Sigma^2_{p_t}$, the total variance difference per participant pair. Whereas $\Delta\sigma_{p_t}$ is an *rms* difference measure per final-state hadron, $2/N_{part}\,\Delta\Sigma^2_{p_t}$ is a variance difference measure per initial-state participant, more suitable for testing the multiple-scattering hypothesis. The two are simply related as shown in Fig. 5.7-1.

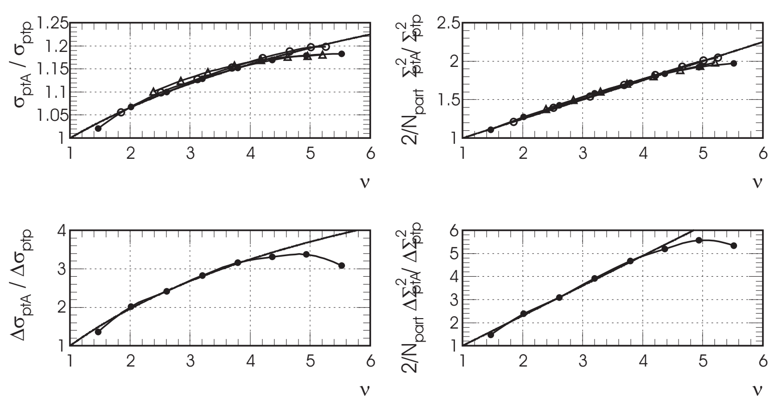

Figure 5.7-1. Centrality dependence of p_t and $\langle p_t \rangle$ variance measures.

We observe in Fig. 5.7-1 lower right panel that $2/N_{part}\,\Delta\Sigma^2_{p_t}$ increases linearly with ν for all but the most central A-A collisions, a linear variance increase consistent with stochastic multiple scattering and also with minijet production as the primary source of $\langle p_t \rangle$ fluctuations. Variation of $\Delta\sigma_{p_t}$ with ν is not linear (the curve in the lower left panel of Fig. 5.7-1 is consistent with the straight line in the lower right panel) because it is not the correct fluctuation measure for this hypothesis test. In the upper two panels is shown a similar situation for the *rms* width of the inclusive p_t distribution and the total p_t variance per participant pair, indicating that a significant fraction of p_t production also depends on multiple scattering. Deviations from linearity in the most central events can be interpreted as growth of a dense dissipative medium in the more central events. As indicated on the axis labels, fluctuation measures are normalized to results from p-p collisions where $\nu = 1$.

5.8 Charge-independent $p_t \otimes p_t$ correlations in Au-Au collisions at 130 GeV

A. Ishihara* and T. A. Trainor

Excess $\langle p_t \rangle$ fluctuations observed in Au-Au collisions (see Section 5.7) can be related to two-particle correlations in several ways. In this study, $p_t \otimes p_t$ correlations are determined as object/reference ratio distributions on $x_1 \otimes x_2$, with flattening variable $x(p_t) \equiv 1 - \exp(-(m_t - m_\pi)/0.4) \in [0,1]$, and fitted with 2D Lévy distributions. The fitting function for ratio densities is

$$R_{fit}(\Sigma_{p_t}, \Delta_{p_t}; T_0, n, n_\Sigma, n_\Delta) = \frac{\left(1 + \frac{\Sigma_{p_t}}{2nT_0}\right)^{2n}}{\left(1 + \frac{\Sigma_{p_t}}{2n_\Sigma T_0}\right)^{2n_\Sigma}} \cdot \frac{\left\{1 - \left(\frac{\Delta_{p_t}}{2nT_0 + \Sigma_{p_t}}\right)^2\right\}^n}{\left\{1 - \left(\frac{\Delta_{p_t}}{2n_\Delta T_0 + \Sigma_{p_t}}\right)^2\right\}^{n_\Delta}}, \tag{1}$$

where $\Sigma_{p_t} \equiv x_1 + x_2$, $\Delta_{p_t} \equiv x_1 - x_2$, T_0 is a temperature, $n \approx 12$ is a 1D fluctuation measure and n_Σ, n_Δ measure correlations of 'temperature' (local energy or p_t density) fluctuations in configuration space. If $n = n_\Sigma = n_\Delta$, temperature fluctuations are uncorrelated and there are no p_t correlations: the ratio distributions are flat. Otherwise, $1/n - 1/n_\Sigma$ and $1/n - 1/n_\Delta$ measure the curvatures of ratio distributions on sum and difference variables respectively, and hence the extent of spatial correlation of temperature fluctuations.

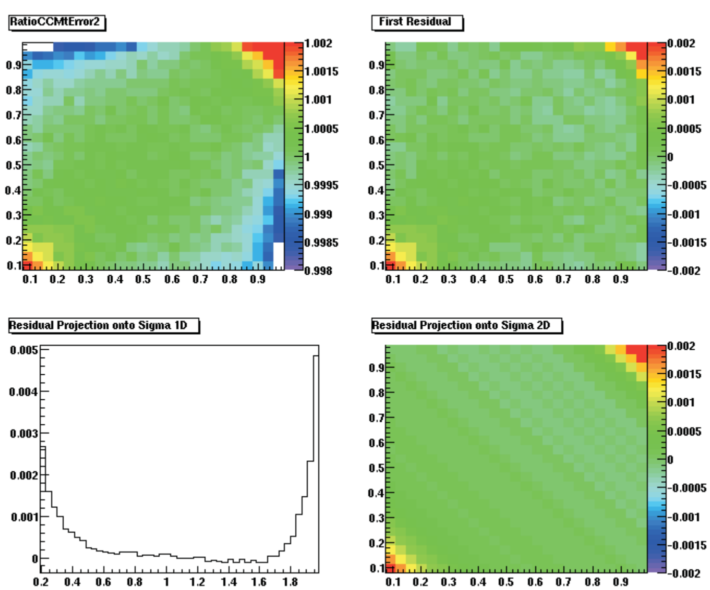

Figure 5.8-1. Two-particle p_t correlations for central Au-Au collisions at 130 GeV.

In Fig. 5.8-1 we show in the upper-left panel the ratio distribution from data for the most central Au-Au collisions. In the upper-right panel are the residuals from a fit with the model function above. Residuals depend only on the sum variable Σ_{p_t}. That 1D dependence is illustrated in the lower-left panel. Variation of sum and difference curvatures and 1D residuals with increasing centrality give information on the growth of a dissipative medium.

*Department of Physics, University of Texas at Austin, Austin, TX 78712.

5.9 Charge-dependent correlations in axial-momentum space

A. Ishihara* and T. A. Trainor

Two-particle correlations of charged hadrons on axial-momentum space (η, ϕ) can be measured separately for like-sign (LS) and unlike-sign (US) charge combinations as object/reference ratio distributions on difference variables $\eta_\Delta \equiv \eta_1 - \eta_2$, and similarly for ϕ_Δ. These distributions can then be combined in two linear combinations, of which the combination CD $\equiv$ LS - US measures correlations due to local charge conservation in the hadronization process. These ratio distributions measure the CD net autocorrelation in the form $\Delta A_2/A_{2,ref}$. The dominant feature of this distribution for heavy-ion collisions is a peak centered at the origin, with independent widths $\eta_{\Delta,0}, \phi_{\Delta,0}$, peak shape parameter b and amplitudes A_0 and A_1

$$R(\eta_\Delta, \phi_\Delta; A_0, A_1, x_0, y_0, b, n) = A_0 + A_1 / \left\{1 + [(\eta_\Delta/\eta_{\Delta,0})^2 + (\phi_\Delta/\phi_{\Delta,0})^2)]^{b/2}/n\right\}^n . \quad (1)$$

In Fig. 5.9-1 upper panels are shown 2D distributions ranging from most peripheral (left) to most central (right). The peak shape changes dramatically, from a wide Gaussian for peripheral events to a narrow exponential for the most central events. For more peripheral events than shown in this study the distribution goes asymptotically to that for p-p collisions, in which case the curvature on ϕ_Δ actually reverses sign.

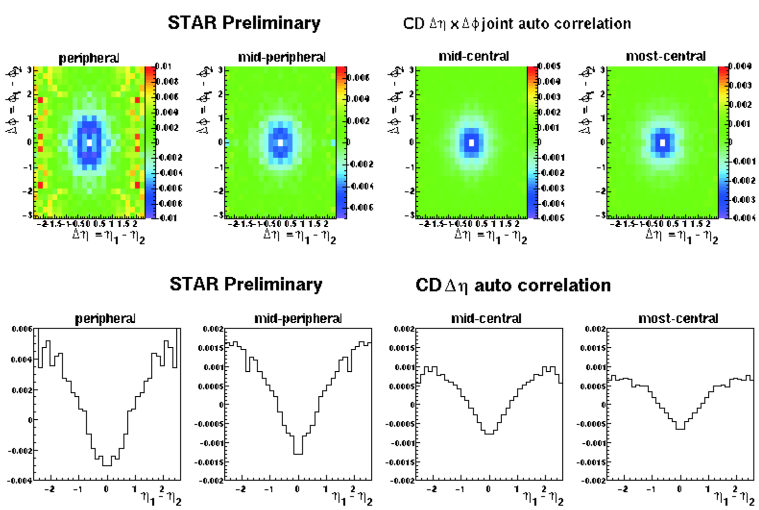

Figure 5.9-1. Centrality dependence of charge-dependent correlations in Au-Au collisions.

This direct measurement of net autocorrelations in the form $\Delta A_2(n, \eta\Delta, \phi_\Delta)/A_{2,ref}$ compares well to results from an inversion of scale-dependent net-charge fluctuation measurements (see Section 5.4). Such measurements tell us about local-measure conservation during the hadronization process and the environment of emerging hadrons, specifically the transparency to hadrons of any prehadronic medium. The centrality dependence of CD correlations, consistent with measure conservation in a 1D system for p-p collisions, suggests the growth of a hadron-opaque medium with increasing centrality in Au-Au collisions.

*Department of Physics, University of Texas at Austin, Austin, TX 78712.

5.10 Hard and soft scattering in p-p collisions

J. Gans* and T. A. Trainor

The mechanisms for p_t production in Au-Au collisions at RHIC are of considerable interest. These include thermal-hadron production, hydrodynamic flow and initial-state multiple scattering, including Cronin scattering and minijet production. A good understanding of p_t production in p-p collisions is required as a basis for studies in A-A. p-p collisions can be separated into soft collisions (no hard interaction), one hard scattering and more than one hard scattering. We want to identify these classes and study their characteristics separately. To do this we separate events into multiplicity ($|\eta| < 0.5$) classes in the range [1,16]. The inclusive p_t distribution for each class is then analyzed as shown in the left panel of Fig. 5.10-1.

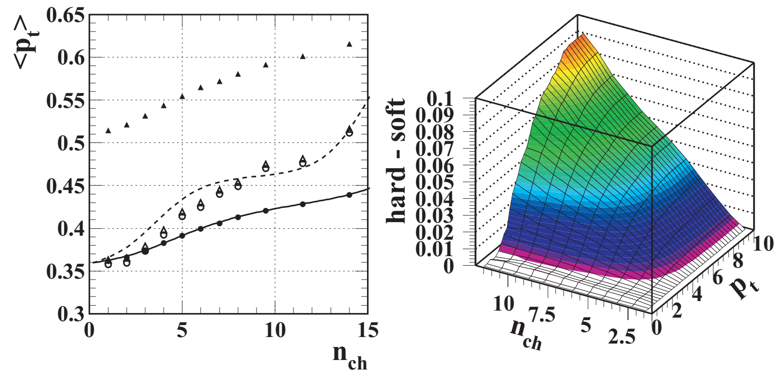

Figure 5.10-1. Left panel – inclusive mean p_t *vs* event multiplicity for p-p collisions. Right panel – soft component subtracted from p_t distributions for a range of event multiplicities.

Open symbols indicate $\langle p_t \rangle$ (inclusive mean p_t) obtained from a conventional 'power-law' or Lévy distribution fit. These values are biased because the Lévy distribution is not the proper model function for events with one or more hard scatterings. The solid dots are obtained from direct integration of p_t distributions extrapolated to zero p_t with a Lévy distribution describing soft collisions (which dominate events with $n_{ch} = 1$). Solid triangles indicate $\langle p_t \rangle$ from direct integration without extrapolation. Lévy fits tend to underestimate the low-p_t part of the distributions, biasing the $\langle p_t \rangle$ fit values toward the unextrapolated limit.

Soft p-p collisions have $\langle p_t \rangle \approx 0.36$ GeV/c, relatively independent of $\sqrt{s}$. The distribution of $\langle p_t \rangle$ on n_{ch} indicates that with increasing n_{ch} the admixture of single-hard-scattering events, with a $\langle p_t \rangle$ value near 0.47 GeV/c, increases. The two-state nature of the event population is emphasized by the dashed curve in the left panel, which describes the quantity $d\langle P_t \rangle / dn_{ch}$, the change in mean *total* p_t per additional hadron, and suggests the onset of a second hard scattering for large n_{ch}. The right panel shows the residuals when a Lévy distribution describing soft collisions is subtracted from the inclusive distributions *vs* n_{ch}, isolating the contribution from hard scattering rising above $p_t \approx 2$ GeV/c. The surface indicates a hard contribution increasing in amplitude with increasing fraction of hard collisions.

*Department of Physics, Yale University, New Haven, CT 06520.

5.11 Dimensionality of a strange attractor as a function of scale

J. G. Reid and T. A. Trainor

The fractal (capacity) dimension is one of the most fundamental properties of a strange attractor. It is a measure of the correlation structure of the attractor calculated by covering the attractor with a partition and counting the number of occupied partition elements. In the canonical formulation this dimension is calculated in the zero-scale limit of the partition element size, but we can expand this concept with a scale generalization:[1]

$$d_q = \lim_{e\to 0}\left[-\frac{S_q}{log(e/L)}\right] \Rightarrow d_q(e) = -\frac{\partial[S_q(e)]}{\partial[log(e/L)]}. \qquad (1)$$

The canonical dimension calculations made in the zero-scale limit are useful for characterizing the underlying mechanism behind the measured attractor, but strange attractors have interesting correlation content over a broad range of scale. It is this scale behavior that we want to characterize. Previously the dimension of such attractors has been calculated with varying partition size,[2] but only as steps toward the goal of obtaining the zero-scale limit dimension.

Here we present the dimension of a strange attractor explicitly as a function of the covering partition scale. The chaotic attractor we analyze occurs for the Hénon map ($x \mapsto a + by - x^2; y \mapsto x$) parameter values $a = 1.4$ and $b = 0.3$, and has been thoroughly investigated in the existing literature.[3] Scale-local dimension results are shown in Fig. 5.11-1.

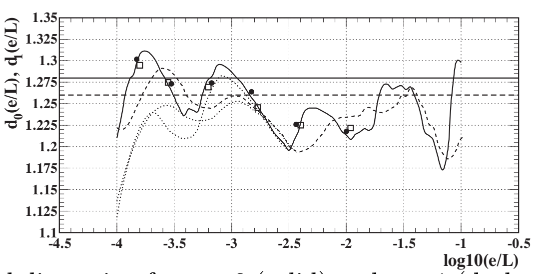

Figure 5.11-1. Scale-local dimension for $q = 0$ (solid) and $q = 1$ (dashed) over three decades from 10M map iterations. Dotted curves are for 1M map iterations showing void bin bias. Solid dots are local scale averaged d_i from Grassberger. Open boxes are comparable averages from our calculations. Horizontal lines correspond to canonical limit-based dimension results.

This rich, characteristic structure of the scaled dimension is another representation of the attractor's unique correlation structure. It is only logical that the scaled dimension of an attractor will have meaningful features over the same scale range as the correlation content of the attractor, independent of the specific points chosen to illuminate the attractor. This is a significant improvement upon the conventional approach that summarizes the dimension of a complex fractal object in a single number at the asymptotic small-scale limit.

[1] J. G. Reid and T. A. Trainor, submitted to J. Phys. A (2003) math-ph/0304010.
[2] P. Grassberger, Phys. Lett. A **97**, 224 (1983).
[3] B. R. Hunt, Nonlinearity **9**, 845 (1996).

5.12 Dimensionality of a strange attractor as a function of position

J. G. Reid and T. A. Trainor

Because scale-local dimension calculations rely on direct analysis of attractor points and not on zero-scale-limit extrapolations (see Section 5.11), it is trivial for us to calculate the dimension of an attractor as a function of position. By analyzing the dimension of the attractor points which fall into a particular region we can obtain a measure of the contribution to the dimension of the overall attractor from the points within that region.

An attractor constructed from one hundred million iterations (rejecting initial transients) of the Hénon map (with $a = 1.4$ and $b = 0.3$) was divided into ten x slices. These slices were then analyzed individually, without rescaling. The dimension of the points of the attractor falling in each x-slice was calculated as a function of scale, independent of the other attractor points. Because the different regions of the attractor have varying density and correlation structure, the number of points in each x-slice varies substantially, and thus the scale interval over which the dimension calculations are meaningful varies. Also, since each distribution represents a fraction of the actual attractor, the large-scale behavior is not meaningful. To avoid problems at the large- and small-scale regimes we consider the calculated dimension over a restricted scale interval ($-4.5 < \log(e/L) < -2.5$).

The average dimension over this scale interval is presented in Fig. 5.12-1 along with a calculation of the position-dependent dimension employing relationships between local Lyapunov exponents and zero-scale-limit dimension.[1]

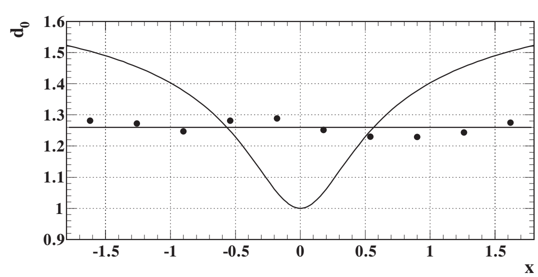

Figure 5.12-1. Dimension of a Hénon attractor as a function of x. The solid line shows analytical results derived using the Kaplan-Yorke conjecture (from Hunt), the solid circles show our results from numerical calculation of average scale-local dimension in the region near $\log(e/L) \sim -3$ for ten different x slices.

There is substantial disagreement between the expected dimension from the Kaplan-Yorke conjecture and our results for the average dimension in the $\log(e/L) \approx -3$ region. This should not be surprising; the analytical result relies on a canonical limit-based dimension formulation, whereas we calculate dimension in a finite scale interval. Further work needs to be done to understand the relation between scale-local and limit-based dimension and the roles they play in characterizing the correlation structure of complex distributions. Clearly the rich scale- and position-dependent dimension structure of this attractor cannot be simply described by the classical approach to dimension calculation.

[1] B. R. Hunt, Nonlinearity **9**, 845 (1996).

5.13 Overview of HBT physics at STAR

J. G. Cramer, J. M. S. Wu, J.-H. Yoon and the STAR HBT Physics Working Group*

The STAR HBT[1] Physics Working Group (HBT PWG), active membership about 20 physicists led by conveyors Sergei Panitkin and Michael Lisa, has made very significant progress in the past year in analyzing data from the first three years of operation of the STAR detector at RHIC. A paper reporting the initial HBT results for pion data at 130 GeV per nucleon from the first year of RHIC operation was published in Physical Review Letters.[2] Several additional papers about aspects of STAR HBT physics are in various stages of preparation. Analysis of RHIC Year-2 data at 200 GeV per nucleon and Year-3 data on d-Au and p-p collisions is in progress.

The impact of our initial STAR HBT results has been very strong. In particular, the relatively small increase in R_{long}, the longitudinal radius of the pion-emitting source, has called into question the conventional assumption of boost invariance, the approximation that the longitudinal source can be treated as infinitely long because of the kinematic cutoff arising from the gradient in longitudinal velocity along the source.

An even larger impact has come from the observation from the HBT analysis that the ratio $R_{out}/R_{side} \approx 1$ is inconsistent with essentially all of the theoretical models of Au + Au collisions that existed before initial RHIC operation. The large increase in source size and emission duration that most models predicted for the RHIC regime are not observed, so that in some sense the models have been falsified. In the theoretical community, this failure of model predictions has been named "The RHIC HBT Puzzle".

In the past year we at CENPA working in the HBT PWG have refined our estimates of the pion phase space density in Au + Au collisions at $\sqrt{S_{NN}} = 130$ GeV for 7 centrality intervals and 6 intervals of pair-average momentum. We have used these phase-space density estimates to obtain corresponding estimates of the pion entropy per particle as a function of centrality. These results have added even more puzzling facts to the investigation of RHIC collisions. Contrary to expectations of "universality,"[3] the pion phase-space density is observed to be rather large, roughly double the phase-space density observed in central collisions at the CERN SPS at $\sqrt{S_{NN}} = 17$ GeV. Moreover, the entropy per particle is found to decrease with increasing centrality and approach the value predicted for a Bose gas of pions in thermal equilibrium. This behavior is the opposite of that expected with the onset of a quark-gluon plasma phase, in which the opening of extra degrees of freedom should produce a strong increase in entropy with centrality.

In addition, we have collaborated with G. A. Miller of the UW Nuclear Theory Group on a full quantum mechanical optical-model-based treatment of opacity effects in the transport of pions through the collision fireball, as they affect the HBT observables. To our knowledge,

---

*See the HBT PWG web site at http://connery.star.bnl.gov/STAR/html/hbt_l.

[1]HBT is a widely used abbreviation for Hanbury-Brown Twiss interferometry.

[2]C. Adler *et al.*, Phys. Rev. Lett. **87**, 082301 (2001).

[3]D. Ferenc, U. Heinz, B. Tomášik, U. A. Wiedemann and J. G. Cramer, Phys. Lett. B **457**, 347 (1999).

this is the first application of quantum mechanical particle transport techniques to such phenomena. Preliminary results show promise of providing at least a partial explanation of the RHIC HBT Puzzle.

In parallel with these investigations, other members of the STAR HBT Physics Working Group have continued investigations of a number of other aspects of the physics of correlations and interferometry, including azimuthal HBT correlations, three-particle pion correlations, correlations of unlike particles, and the correlations of other identical particles including protons, charged and uncharged kaons, and other strange particles.

In summary, the STAR HBT Physics Working Group has made considerable progress in analyzing the data from the first three years of RHIC operation. The initial HBT analysis has presented several of theoretical puzzles that are now being addressed. We look forward in the coming year to further progress in data analysis and in theoretical understanding.

5.14 Pion phase space density and "Bump Volume"

J. G. Cramer, J. M. S. Wu and the STAR HBT Physics Working Group*

The average 6-dimensional phase space density $\langle f \rangle$ of pions emitted from an ultra-relativistic heavy ion collision is a Lorentz scalar that has the form:

$$\langle f \rangle = \left[\frac{1}{E_\pi}\right]\left[\frac{d^2N}{2\pi m_T dm_T dy}\right]\left[\frac{1}{\sqrt{\lambda}}\right][V_p] \quad \text{where} \quad V_P = \left[\frac{\lambda(\hbar c\sqrt{\pi})^3}{R_S\sqrt{R_O^2 R_L^2 - R_{OL}^4}}\right]. \tag{1}$$

Here the first term in brackets is the Jacobian that preserves Lorentz invariance, the second term is the pion momentum spectrum, and the third term corrects for the "purity" of the observed pions. The last term V_p is the momentum-space volume occupied by the three-dimensional Bose-Einstein "bump" $[C_2(q_O, q_S, q_L) - 1]$, where C_2 is the two-particle momentum-space correlation function.

Therefore, the phase space density $\langle f \rangle$ can in principle be obtained from STAR data on pion HBT observables and spectra. The principal problem with extracting the phase space density is to estimate accurately the momentum volume V_p under the Bose-Einstein enhancement "bump", in the presence of non-Gaussian correlation shapes, curvature at large q, and limited statistics. Last year we reported a preliminary analysis using Year 1 data for Au+Au at $\sqrt{S_{NN}} = 130$ GeV, employing the 3D correlation histograms generated for our Phys. Rev. Letter publication.[1] Subsequently, we have performed a reanalysis of the Year 1 data for seven centrality bins with several improvements in the analysis: (1) we use K_T rather than p_T binning, with 6 K_T bins vs. 3 p_T bins in the old analysis; (2) we combine π^+ and π^- correlation data for improved statistics; (3) we limit the vertex Z-position to ± 50 cm and bin the data in 21 z-bins, using only events in the same bin to do event mixing, (4) with the help of Dan Majestro of the HBT PWG, we also choose only events within $\pm 30^0$ of the same reaction plane for event mixing, and (5) we use the Bowler/Sinyukov/CERES procedure[2] for Coulomb correction. We note that this change in Coulomb correction procedure has lead to systematically smaller HBT λ values, larger radii, and smaller $\langle f \rangle$ values than those previous reported.

We have addressed the problem of extracting the momentum volume V_p by using and comparing several methods:
(Method 1) Perform a 3D–Gaussian fit to the histograms and calculate the momentum volume V_p from the HBT λ and radii.
(Method 2) Same as *(Method 1)*, but include a parabolic background under the Bose-Einstein bump to account for the large-Q curvature.
(Method 3) Analyze the 1D Q_{inv} correlation function by fitting it with a Gaussian using the Bowler/Sinyukov/CERES procedure, and calculate V_p using a procedure suggested by David Brown.
(Method 4) Same as *(Method 2)*, but use an exponential function instead of a Gaussian for

*See HBT PWG web site at http://connery.star.bnl.gov/STAR/html/hbt_l.

[1] C. Adler *et al.*, Phys. Rev. Lett. **87**, 082301 (2001).

[2] M. G. Bowler, Phys. Lett. **B** 270, 69 (1991).

the correlation shape.
(Method 5) Directly sum the correlation bump $[C(Q)-1]$ of the 3D histogram out to some cutoff Q_{cut}, and match this to the tail provided by the fit described in (1).
(Method 6) Directly sum the correlation bump $[C(Q_{inv})-1]Q_{inv}^2$ of the 1D histogram out to some cutoff radius, and match this to the exponential tail provided by the fit described in *(Method 4)*.

We find that, after the dust has settled, *Method 1* is the method of preference, with *Method 2* giving essentially the same results, and *Method 4* giving very similar results when it is stable. We find that with the data at hand, *Methods 5* and *6*, which directly sum the histogram, are not reliable because the choice of the matching Q_{cut} strongly determines the value of V_p obtained and there is no stability plateau within which a stable value of V_p can be extracted. From the point of view of such stability, the new analysis is worse than the previous analysis, which showed some stability against the Q_{cut} value.

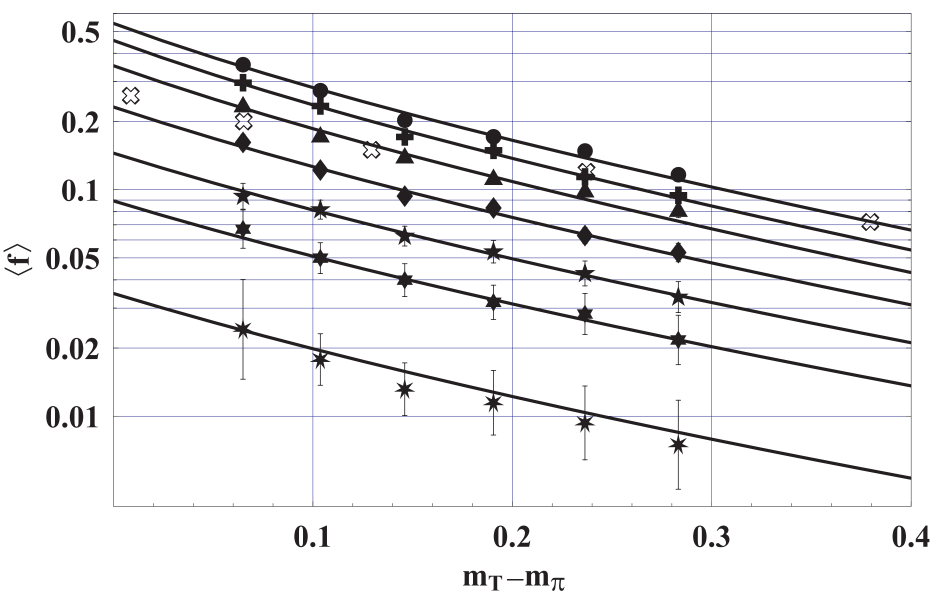

Figure 5.14-1. Pion Phase space density $\langle f \rangle$ vs. average pair momentum K_T for Au + Au collisions at $\sqrt{S_{NN}} = 130$ GeV in seven centrality bins (0-5% of total reaction cross section=circle, 5-10%=cross 10-20%=triangle, 20-30%=square, 30-40%=5-star, 40-50%=6-star and 50-80%=7-star). The $\times$ symbols are NA49 points, as described in the text. The solid curves are a global fit to the data using blue-shifted Bose-Einstein distributions, as discussed in the following article.

Fig. 5.14-1 shows the extracted values of $\langle f \rangle$ vs. K_T, for the seven centrality bins, with the highest points the most central. The error bars are statistical only, propagated from the uncertainties in fit parameters. The $\times$ symbols indicate phase space densities for Pb + Pb collisions at $\sqrt{S_{NN}} = 17$ GeV derived from NA49 data.[3] We note that there is significant systematic error associated with the method used for the extraction of V_p, and the values shown are probably on the low side.

[3] D. Ferenc, U. Heinz, B. Tomášik, U. A. Wiedemann and J. G. Cramer, Phys. Lett. **B** 457, 347 (1999).

5.15 Entropy at freeze-out in RHIC collisions

J. G. Cramer, J. M. S. Wu and the STAR HBT Physics Working Group*

The average pion phase space density $\langle f \rangle$, estimated by combining the pion-momentum spectrum and the HBT correlation function, can be used to estimate the entropy per particle (S_π/N) of the colliding system at freeze-out. The relation for converting $\langle f \rangle$ to entropy per particle is:

$$S_\pi/N = \frac{\int_0^\infty [(\langle f \rangle + 1)\log(\langle f \rangle + 1) - \langle f \rangle \log(\langle f \rangle)]\, p_T\, m_T\, dp_T}{\int_0^\infty \langle f \rangle\, p_T\, m_T\, dp_T} \tag{1}$$

To make use of this relation, we need the functional dependence of $\langle f \rangle$ with respect to p_T for all values of p_T. It is well known that the phase space density of a static Bose gas should be a Bose-Einstein distribution, and that such a distribution is blue-shifted for a system that experiences radial flow. Therefore, we have modeled the momentum dependence of $\langle f \rangle$ with a blue-shifted Bose-Einstein distribution of the form

$$\langle f \rangle = 1/\{\exp[\frac{m_T}{T_0}\cosh(\eta_T)\cosh(\eta_L) - \frac{p_T}{T_0}\sinh(\eta_T) - \frac{\mu_\pi}{T_0}] - 1\} \tag{2}$$

In this work we set the longitudinal-flow rapidity η_L and the pion chemical potential μ_π to zero. Further, we assume that the radial-flow rapidity $\eta_T = \alpha \tanh^{-1}(\frac{p_T}{m_T})$ where α is a constant of proportionality. We assume that the parameters T_0 and α can be described as second order polynomials with respect to participant number, and we perform a simultaneous global fit to $\langle f \rangle$ at all values of K_T and centrality. The results of these fits have been shown as the solid curves in Fig. 5.14-1 of the preceding article.

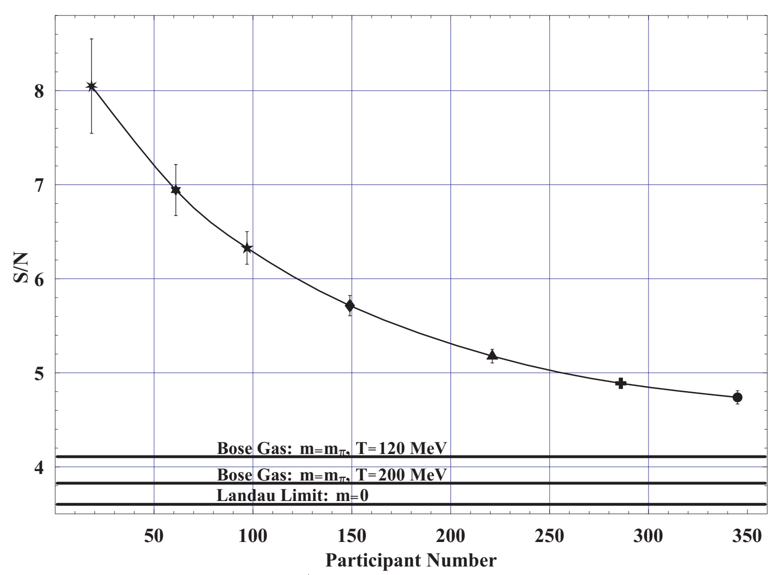

Figure 5.15-1. Entropy per particle S_π/N vs. participant number for Au + Au collisions at $\sqrt{S_{NN}} = 130$ GeV. The solid curve is a spline fit to guide the eye. Error bars are statisitical only. Horizontal lines are Bose gas thermal estimates of S_π/N.

*See the HBT PWG web site at http://connery.star.bnl.gov/STAR/html/hbt_l.

We then use these blue shifted Bose-Einstein fits to perform the integrals of Eq. 1 to obtain the entropy per particle S_π/N for each centrality. These are shown in Fig. 5.15-1. The horizontal lines represent Bose-gas thermal estimates of the entropy per particle for a massive ($m = m_\pi$) or a massless ($m = 0$) Bose gas with $\eta_L = \eta_T = \mu_\pi = 0$. The horizontal variable is the number of participant nucleons for each centrality bin, as estimated using the Glauber model, and is a good measure of centrality. The systematic error of S/N in Fig. 5.15-1 depends on the momentum-dependence modeling and is estimated to be about 20%.

Thus, the entropy per particle S_π/N is found to drop with increasing centrality and that S_π/N for the most central collisions approaches the entropy for a static non-flowing Bose gas with a temperature of 120 MeV. This suggests that in central collisions the system starts with a very low entropy process, and that even the entropy production in the subsequent evolutionary stages of the process are not sufficient to raise the entropy significantly above the thermal gas level. On the other hand, a quark-gluon plasma, because of the large increase in degrees of freedom in the plasma phase, is expected to be a process that generates large entropy.

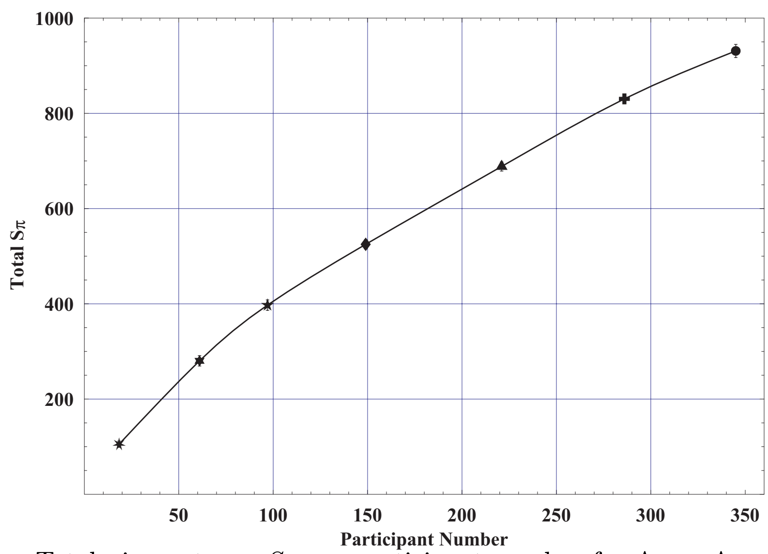

Figure 5.15-2. Total pion entropy S_π vs. participant number for Au + Au collisions at $\sqrt{S_{NN}} = 130$ GeV. The solid curve is a spline fit to guide the eye. Error bars are statistical only. The systematic error depends on the fitting procedures and is estimated to be about 20%.

It is also of interest to estimate the total entropy of the system. We can do this by integrating the pion spectrum over momentum to obtain an estimate of the total pion number N. Multiplying this by the entropy per particle gives the total pion entropy S_π of the system. This entropy is shown in Fig. 5.15-2. We see that the total pion entropy S_π monotonically increases with centrality and participant number, but presumably does so more slowly than the pion multiplicity.

5.16 Opacity effects in Bose-Einstein correlation radii at RHIC

J. G. Cramer, G. A. Miller,* J. M. S. Wu and J. - H. Yoon

In relativistic heavy ion collisions it is usually assumed that the pion source resulting from the collision is cylindrically symmetric around the beam axis and is transparent to emitted pions. This means that the detector should receive particles from all kinematically-allowed regions of the source. In particular, this leads to the prediction that the radius parameter towards the detector, R_O, is larger than the corresponding radius perpendicular to the detector, R_S, for particles of zero rapidity. To a good approximation, these radii are related by the equation $R_O^2 = R_S^2 + \beta_0^2 \delta\tau^2$. Here $\delta\tau$ is the duration of pion emission, $\beta_0 = p_T/m_T$ is the pion velocity in the direction of the detector, p_T is the transverse momentum of the pions, and $m_T = \sqrt{p_T^2 + m_\pi^2}$ is their transverse mass.

Experimentally these HBT radius parameters are extracted from the two-particle momentum correlation functions, and it is found[1] that for Au+Au collisions at RHIC, R_O is approximately equal to R_S. Moreover, it is observed[2] that at higher values of the average pion pair momentum $K_T = \frac{p_1+p_2}{2}$, R_O may actually be smaller than R_S. These observations contradict the theoretical expectations above, and they have been taken as an indication that the emission duration may be extremely short, i.e. that the source freezes out quite suddenly, even in the presence of pion-emitting resonances and transit-time effects.

To avoid this rather implausible scenario, Heiselberg and Vischer[3] have proposed that the source should not be assumed to be transparent to pions, but rather should be treated as opaque. Their preliminary study, as well as a more detailed study by Tomasik and Heinz,[4] showed that an opaque source would indeed lead naturally to R_O smaller than R_S for plausible emission durations. However, both of these studies used the high-energy limit and the semi-classical (eikonal) approximation. This procedure cannot be justified for low-energy pions with momenta of a few hundred MeV, as are used in the experimental correlation studies. Indeed, neither calculation could produce $R_O = R_S$ at $K_T = 0$, thus violating a basic symmetry theorem: at zero momentum one cannot distinguish the momentum differences q_O and q_S or define *any* directions in the transverse plane, so all direction-dependent observables must be equal.

The work reported here attempts to properly treat the effects of opacity by describing the system quantum mechanically. We solve the quantum mechanical wave equations for the pions in an opaque medium, using a relativistic optical model approach. These calculations are presently in a very preliminary form, but we can already state some of the results. We find that at $K_T = 0$, $R_O = R_S$ as required. We find also that at larger momenta R_O can be less than R_S, that there are saturation effects, and we predict some K_T dependence for R_O. The latter results are seen in the data but cannot be accommodated by references 3 and 4.

*Department of Physics, University of Washington, Seattle, 98195.

[1] C. Adler, *et al.*, Phys. Rev. Lett. **87**, 082301 (2001).
[2] K. Adcox, *et al.*, Phys. Rev. Lett. **88**, 192302 (2002)
[3] H. Heiselberg and A. P. Vischer, nucl-th/9609022.
[4] B. Tomasik and U. Heinz, nucl-th/9805016.

5.17 Testing the Bowler-Sinyukov-CERES Coulomb-correction procedure with same- vs. opposite-charge pion correlations

J. G. Cramer, J. M. S. Wu and the STAR HBT Physics Working Group*

The Bowler-Sinyukov-CERES (BSC) procedure[1] is a relatively new technique for analyzing HBT correlation functions in the presence of Coulomb effects. It accurately accounts for the fraction of correlated particles that participate in the Bose-Einstein and Coulomb correlations. The HBT analysis described in previous articles above (see Section 5.13) uses this technique. The BSC method involves fitting an uncorrected identical-particle HBT correlation function (Signal/Background) with a function of the form:

$$C_2^{identical}(\vec{q}) = A_0\{1 + \lambda[K_{Cou}(R_{Cou}, q_{inv})(1 + F_{Source}(\vec{R}, \vec{q})/\lambda) - 1]\} \qquad (1)$$

were A_0 is the overall normalization factor, λ is the fraction of pairs that participate in the Bose-Einstein enhancement and in the Coulomb interaction, $K_{Cou}(R_{Cou}, q_{inv})$ is the Coulomb correlation of like-sign particles for an incoherent source of radius R_{Cou} emitting a pion pair with invariant momentum difference q_{inv}, and $F_{Source}(\vec{R}, \vec{q})$ is the momentum-space Fourier transform of the autocorrelation function of the pion source. For 3D analysis, F_{Source} is assumed to have the Gaussian form $F_{Source}(\vec{R}, \vec{q}) = \exp[-(R_O q_O/\hbar c)^2 - (R_S q_S/\hbar c)^2 - (R_L q_L/\hbar c)^2]$. For 1D analysis, it is assumed to have the form $\exp[-(R_{inv} q_{inv}/\hbar c)^2]$.

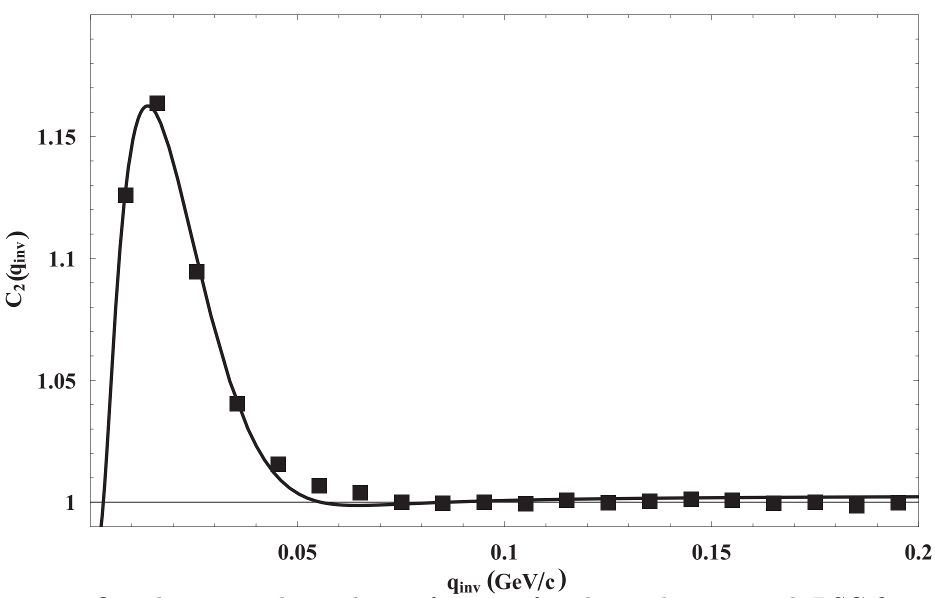

Figure 5.17-1. One-dimensional correlation function for identical pions, with BSC fit to the data. Fit parameters are given in the text.

The BSC procedure is based on two assumptions: (a) that the participant fraction λ is the *same* for the Bose-Einstein enhancement (which arises from symmetrization of overall wave function) and for the Coulomb correlation (which arises from the long-range action of

*See HBT PWG web site at http://connery.star.bnl.gov/STAR/html/hbt_l.

[1]M. G. Bowler, Phys. Lett. B **270**, 69 (1991).

the Coulomb force), and (b) that the background for non-participating pion pairs has the *same* shape and momentum dependence as that of participating pion pairs. We note that each of these assumptions is perhaps questionable.

Here we investigate the BSC procedure for identical- and opposite-sign pion correlations in events with a centrality of 0-5% of the total cross section and with a z-axis position between -55 cm and $+55$ cm binned in 10-cm intervals for event mixing. Event mixing was done with only other events that were within 15 degrees of having the same reaction plane as the event of interest. For the example shown here, we select pairs with a K_T range between 0.125 GeV/c and 0.175 GeV/c. To improve statistics, we add the signal and background for $\pi^+\pi^+$ and $\pi^-\pi^-$ correlations. Fig. 5.17-1 shows a 1D q_{inv} plot of the identical-pion correlation function, along with the fit of the form of Eq. (1) using $R_{Cou} = 5.0$ fm. The fit parameters are $R_{inv} = 7.54$ fm and $\lambda = 0.356$.

One consequence of the BSC procedure is that, neglecting other interactions (e.g. strong-interaction resonances in the $\pi^+\pi^-$ system, which should slightly damp the correlation function), the form for $\pi^+\pi^-$ correlations is predicted to have the form:

$$C_2^{opposite}(q_{inv}) = A_1(1 + \lambda[K^*_{Cou}(R_{Cou}, q_{inv}) - 1]) \tag{2}$$

where A_1 is the overall normalization factor for this system (not necessarily the same as A_0), λ is the same fraction of participant pairs as in Eq. (1), and $K^*_{Cou}(R_{Cou}, q_{inv})$ is the Coulomb correlation of opposite-sign particles, using the same radius and general form as that used for $K_{Cou}(R_{Cou}, q_{inv})$ in Eq. (1). Thus we have a testable prediction of the validity of the BSC procedure.

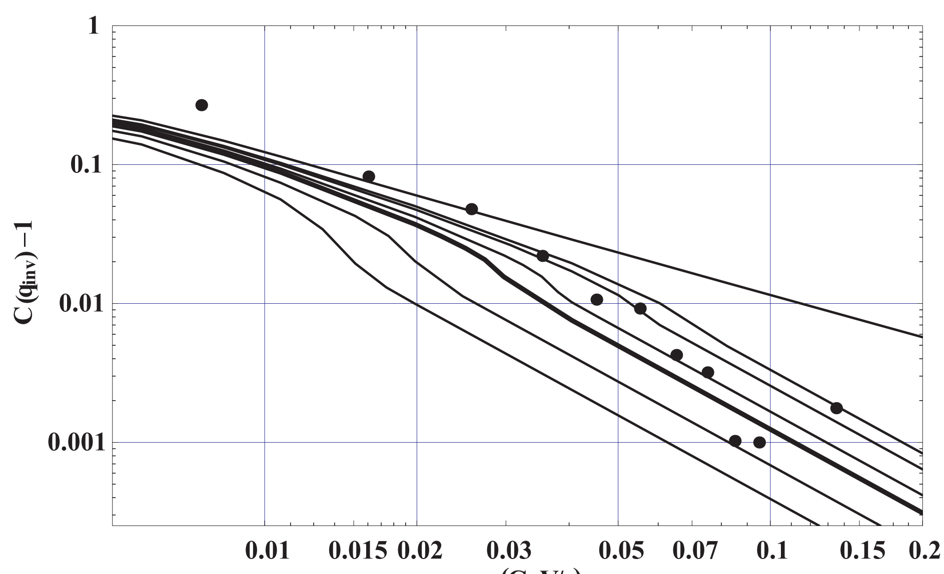

Figure 5.17-2. One-dimensional $\pi^+\pi^-$ correlation function, along with BSC predictions for $\lambda = 0.356$ and $R_{Cou} = 5.0$ fm (thick line) along with $R_{Cou} = 0$, 3.0 fm, 3.8 fm, 7.0 fm, 11.0 fm, and 16.0 fm predictions, (thin lines, highest to lowest, respectively).

Fig. 5.17-2 shows a 1D q_{inv} plot of the $\pi^+\pi^-$ correlation function, along with the BSC predictions from Eq. (2). To emphasize the difference between the data and prediction, we plot $[C_2^{\pi^+\pi^-}(q_{inv})-1]$ vs q_{inv} on a log-log plot. Here the thick line is the BSC prediction with $\lambda = 0.356$ and $R_{Cou} = 5$ fm,, while the other lines, from highest to lowest, represent similar predictions with $R_{Cou} = 0$, 3.0 fm, 3.8 fm, 7.0 fm, 11.0 fm, and 16.0 fm, respectively. We see that no matter what radius is used, the data and Coulomb curves have somewhat different shapes, and the fits are not good.

Fig. 5.17-3 again shows the $\pi^+\pi^-$ correlation function, but with BSC predictions for varying values of λ. Here the thick line is the BSC prediction with $R_{Cou} = 5$ fm and $\lambda = 0.356$, while the other lines, from highest to lowest, represent similar predictions with $\lambda = 1.0$, 0.9, 0.8, 0.7, 0.6, 0.5, and 0.4, respectively. We see that a value of about $\lambda = 0.6$ gives a fairly good account of the data.

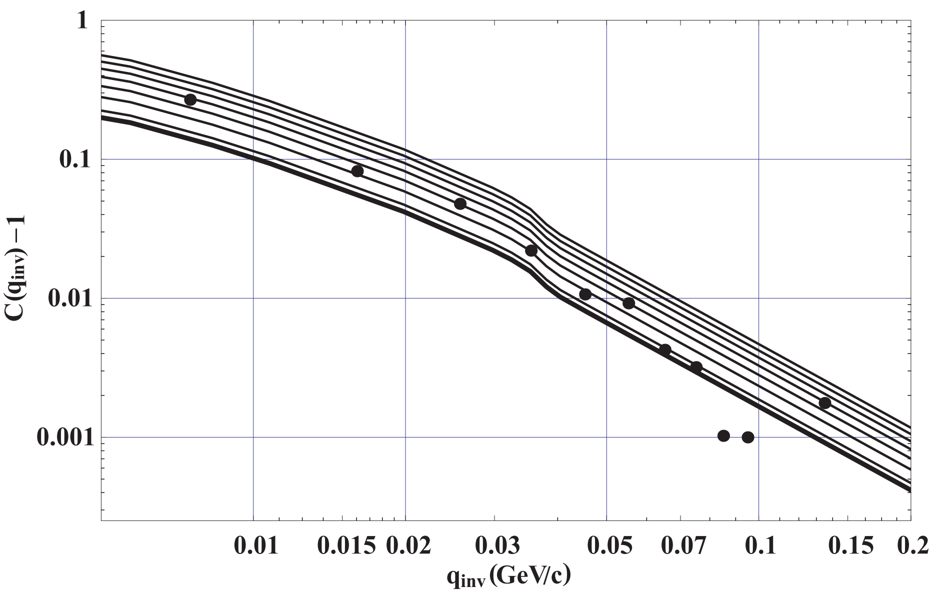

Figure 5.17-3. One-dimensional $\pi^+\pi^-$ correlation function, along with BSC predictions for $R_{Cou} = 5.0$ fm and $\lambda = 0.356$, (thick line) along with $\lambda = 1.0$, 0.9, 0.8, 0.7, 0.6, 0.5, and 0.4 predictions, (thin lines, highest to lowest, respectively).

Thus, we see that the BSC procedure appears to be inconsistent with the data. There is a definite indication that the assumption that the same λ parameter can describe the pairs participating in Bose-Einstein symmetrization as those participating in the Coulomb interaction is incorrect, and that there are more of the latter. From the STAR data analyzed, the indication is that $\lambda_{BE} \approx 0.36$ while $\lambda_{Cou} \approx 0.5$ to 0.6. As pointed out earlier, Eq. (2), which is compared with the $\pi^+\pi^-$ correlation function, does not include the effect of strong-interaction effects on the $\pi^+\pi^-$ system. For a source on the order of 5 fm, such effects are not large, but they can contribute to the difference in λ values discussed here. We estimate however, based on recent calculations of this effect using the code of R. Lednicky, that the enhancement due to the strong interaction would at most increase the λ value from 0.36 to about 0.46, so the strong interaction in itself does not appear to be large enough to explain the effect shown in Fig. 5.17-2 and Fig. 5.17-3.

5.18 Particle identification in STAR TPC

H. Bichsel and Y. Fisyak*

Studies of the physical processes in the STAR Time-Projection-Chamber (TPC) have been continued. Results have been presented in three STAR Notes,[1,2,3] and at the Quark Matter 2002 meeting.[4]

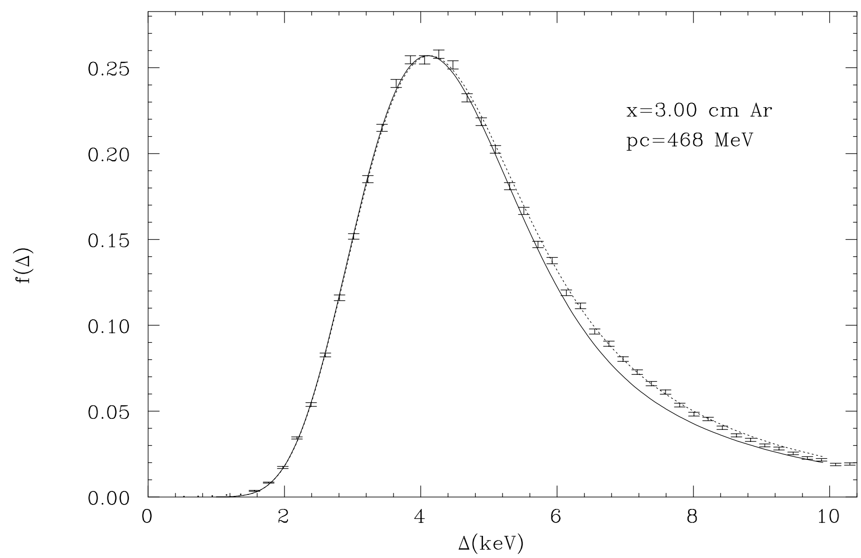

Figure 5.18-1. Comparison of an experimental Landau function with a function calculated for pions (solid line). The dotted line includes 6% electrons with the same momentum in the calculation.

These theoretical calculations in general agree with experimental measurements, as shown in Fig. 5.18-1. In particular, the dependence of the ratio of most probable energy loss to segment length is confirmed to depend on segment length. The calculations also permit us to elucidate various problems in the operation of the TPC, such as non-linearity of the gas gain in the proportional counters. This work has led to a modification of STAR's dE/dx calibration procedure resulting in an improvement in STAR's dE/dx resolution from 8.2% to 6.5%.[5]

---

*Brookhaven National Laboratory, Upton, NY 11973.

[1] Comparison of Bethe-Bloch and Bichsel functions, H. Bichsel, STAR Note SN 0439 (March 2002).

[2] Calculated and experimental Landau spectra in a TPC, H. Bichsel, STAR Note SN 0440 (June 2002).

[3] Resolution in particle identification with TPCs, Hans Bichsel, STAR Note SN 0441 (November 2002).

[4] Theory of Particle Identification (PID) for TPCs, Hans Bichsel, Poster presented at *Quark Matter 2002*, Nantes, Frances July (2002).

[5] http://www.star.bnl.gov/STAR/comp/meet/CM200302/Status-of-the-dE-March-2003.ppt.

6 Molecular Clusters

6.1 Attempt to produce dianions of Mg_2S_3

R. Vandenbosch

Boldyrev and Simons[1] have predicted on the basis of quantum chemical calculations that Mg_2S_3 is the smallest linear stable (to loss of an electron) dianion. The dianion is predicted to be bent with alternating Mg and S atoms. I am attempting to produce this dianion using the fragmentation technique reported previously for the production of the C_9 dianion.[2] The $RbMg_2S_3$ anion is produced by sputtering a compressed mixture of elemental S and Mg powder with Rb ions. The mass spectrum of anions produced by this sputtering is very complex, both chemically and isotopically. The natural Rb, Mg, and S used all have several isotopes. We select the most abundant isotopic species $^{85}Rb^{24}Mg_2{}^{32}S_3$ with A=229 and accelerate it to 72 keV. The accelerated ion then passes through a hydrogen gas fragmentation cell. The fragmented anions are analyzed with an electrostatic deflector.

The fragment electric rigidity spectrum is also quite complex. The most prolific anion is the Mg_2S_3 anion. Other fragments are typically more than an order of magnitude weaker in intensity. Anionic species observed include A=32 (S), A=56 (MgS), A=64 S_2, A=80 (Mg_2S), A=88 (MgS_2), A=96 (S_3), A=112 (Mg_2S_2), and A=120 (MgS_3). A weaker peak at A=75 is not expected but may be Mg_2Al from the aluminum pellet holding the Mg/S powder mix. The presence of S_2 indicates that not all of the $RbMg_2S_3$ parent has alternate Mg and S atoms.

The dianion of Mg_2S_3 is expected to appear at a mass-to-charge ratio of 144/2=72. A very weak peak is seen at this ratio. Confirmation of the presence of a dianion can be obtained by examining the pulse height distribution of ions at this mass-to-charge ratio with that of singly charged ions with mass numbers near 72. Since the energy of the ions resulting from fragmentation of energetic ions by the light hydrogen gas is proportional to the mass of the fragment, doubly charged fragments of mass 144 will have twice the energy of mass 72 fragments. The channeltron ion detectors produce signals roughly proportional to the fragment energy, although with a very broad spread in signal magnitude for a given energy. In our previous fragmentation study it was shown that the presence of dianions could be demonstrated by studying the dependence of the fragment yield on pulse height discriminator setting. This has been attempted in the present study but the results obtained so far are statistically inconclusive. Further work is planned.

---

[1] A. I. Boldyrev and J. Simons, J. Chem. Phys. **98**, 4745 (1993).

[2] R. Vandenbosch, D. I. Will, C. Cooper, B. Henry and J. F. Liang, Chem. Phys. Lett. **274**, 112 (1997).

7 Electronics, Computing, and Detector Infrastructure

7.1 Electron gun for profiling silicon detectors for KATRIN

P. J. Doe, T. Gadfort, G. C. Harper and R. G. H. Robertson

A monoenergetic electron source is being developed to profile the electron backscattering with respect to incident angle of the large area (18mm by 18mm) silicon detectors[1] to be used in the KATRIN experiment. The test setup, shown in Fig. 7.1-1, consists of an electron gun, an einzel lens, a UHV X-Y translator, an oil-free pumping system,[2] and the associated stand, diagnostics, power supplies, and sample chamber. The sample chamber has two rotational manipulators, one each for the device under test (DUT) and a backscattering detector. It also has a vacuum diagnostic tee and a full complement of power and signal feedthroughs.

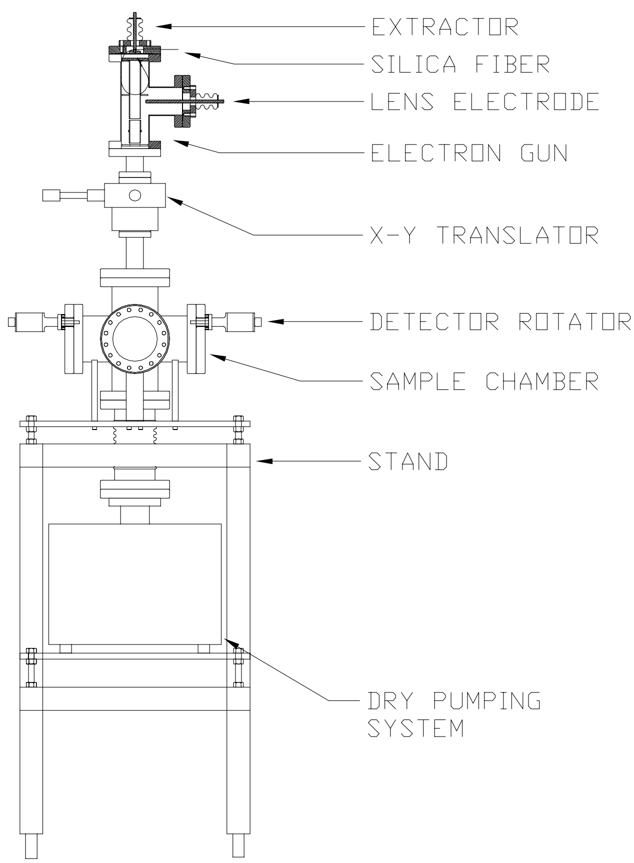

Figure 7.1-1. KATRIN monoenergetic electron gun and test stand.

The gun will produce low energy (of order 1 eV) electrons by UV photoemission from a stainless steel surface. A UV grade silica fiber and hypodermic needle collimator will direct

[1]Hamamatsu Photonics, Hamamatsu City, Japan.
[2]Varian Vacuum Products, Lexington, MA 02421

photons from a mercury arc UV lamp onto a 1 mm diameter spot on the emission surface. The electrons will be accelerated through a potential that can be varied up to -30 kV. The electron beam will be focused to a 1 mm diameter spot on the DUT 0.6 m from the emission surface by an einzel lens operating at about half of the accelerating potential. It will be possible to scan the beam across the DUT in both transverse axes with an X-Y translator stage having a range of ± 1.25 cm in each axis. The DUT may be rotated to any angle up to $\pm 60^\circ$ with respect to the longitudinal axis. Another silicon detector will be able to collect the backscattered electrons at an angle that may be varied $\pm 120^\circ$ with respect to the longitudinal axis.

Precision, low-ripple power supplies will be used for the electron extraction and focusing to ensure low energy spread and focus stability in the electron beam. The desired particle rate is of order 1000 Hz which we expect to be able to regulate by altering the UV lamp intensity. The DUT will be cooled by a peltier thermo-electric device[3] to approximately 30° C below ambient temperature. Two E-type chromel-constantan thermocouples will be used to measure the temperatures of the DUT and the peltier cold plate.

Electrostatic and beam transport studies of the gun and beam optics have been done using the ion optics program SIMION.[4] All of the required parts have been procured and 95% of these items have been delivered. The pump stand has been completed and the internal components of the sample chamber are presently under construction in our instrument shop. Testing of the vacuum system is presently underway.

[3]MelCor Corp., Trenton, NJ 08648.
[4]SIMION 3D, version 6.0, David A. Dahl, Idaho National Engineering Lab., Idaho Falls, Idaho 83415

7.2 Nanopore DNA sequencing

T. Butler and J. H. Gundlach

The development of novel, rapid DNA sequencing methods is very desirable. We have initiated a research effort to explore one of these alternative sequencing methods. The method we are exploring, nanopore sequencing, was first demonstrated in 1996.[1] It is illustrated in Fig. 7.2-1. A single, nanometer scale pore connects two small volumes of electrolytic buffer solution. The pore is formed by the self-assembly of the bacterial protein α-hemolysin in an artificial lipid bilayer. An applied potential induces a measurable ionic current through the pore. Single-stranded DNA molecules are introduced into the cathode volume and, because DNA becomes negatively charged in solution, they are driven through the pore into the anode volume. The limiting diameter of the pore[2] is 1.5 nm, slightly larger than the cross-sectional diameter of single-stranded DNA. The DNA significantly obstructs the ionic current during translocation. In addition, the small diameter of the pore necessitates that the DNA molecule's nucleotides pass through the pore sequentially. Information is obtained by analyzing the obstruction of the ionic current due to the presence of the DNA in the pore (see Fig. 7.2-1).

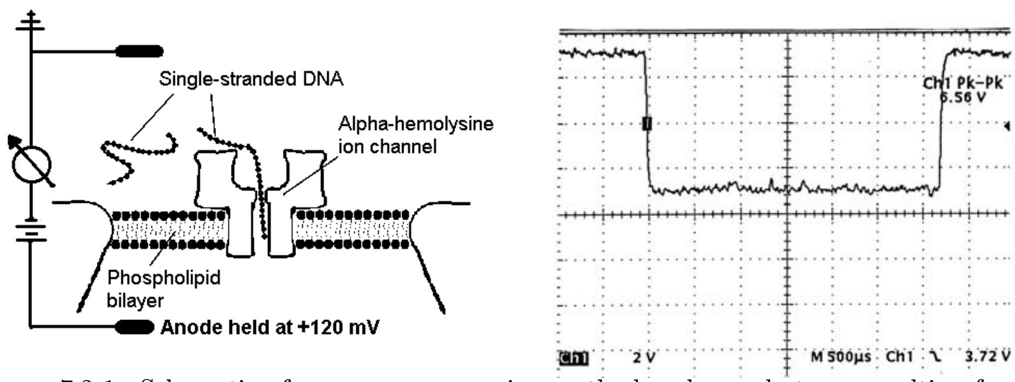

Figure 7.2-1. Schematic of nanopore sequencing method and sample trace resulting from translocation event.

We have built a functional nanopore apparatus. We fabricated a vibration isolation table, aluminum and teflon support devices and 25 μm apertures in teflon tubing for the apparatus. A patch clamp amplifier on loan to us from Bertil Hille (UW Biophysics Department), a 60X dissecting microscope and a digital storage oscilloscope round out the equipment for our preliminary apparatus. With the help of a three day visit to the lab of David Deamer and Mark Akeson at UC Santa Cruz, we have gained proficiency with the procedure for the production of stable nanopores. We have observed events characteristic of DNA translocation through the pore for two types of single-stranded DNA; a 390-nucleotide long adenine homopolymer and a 20-nucleotide long heteropolymer. Observed differences in the current recordings for the two polymers indicate that our preliminary apparatus is at least sensitive to gross details of the structure of individual molecules. The work has been funded by an NSF IGERT fellowship and a University of Washington Royalty Research Fund grant.

[1] J. J. Kasianowicz *et al.*, *Proc. Natl. Acad. Sci. USA* **93**, 13770 (1996).

[2] L. Song, *et al.*, Science **274**, 1859 (1996).

7.3 Electronic equipment

G. C. Harper, A. W. Myers and T. D. Van Wechel

Along with the normal maintenance and repair of the Laboratory's electronic equipment, projects undertaken by the electronics shop included the following:

1. The APOLLO Command Module (ACM) was designed and constructed for the Astrophysics department for use in the APOLLO (the Apache Point Observatory Lunar Laser-ranging Operation) experiment. The functions of the ACM have been implemented as a custom CAMAC module based on Altera MAX 7000AE programmable logic devices (PLDs). Specifically, an EPM7256AE chip is used to provide the CAMAC dataway interface and house the module's command set. An EPM7512AE chip is clocked at 50 MHz, and produces the state logic that drives the APDs, the laser, and selects STOP pulses for the TDC. For more details see http://www.astro.washington.edu/tmurphy/apollo/acm.html.

2. A VME based 100-MHz latched clock board was designed and constructed for the emiT experiment to provide timing information. Two Altera PLDs are used. An EPM9320RC208-20 chip is used to provide the 32-bit VME interface. An EPF10K10TC144-3 is used for the 56-bit 100-MHz counter and five individually latched 56-bit registers. Four of the latched registers are latched by TTL inputs and one register is latched by a software command. Each register has an Inhibit output that is asserted when the register has been latched. Once latched the register cannot be latched again until after it has been read and the Inhibit signal returns to logic zero.

3. All of the electronics for the emiT experiment were completed and shipped to NIST.

4. The SNO NCD pulser distribution system has been designed and constructed. It provides individually switched test-pulse signals for each of the SNO NCD preamps.

5. A fiber-optic transmitter was constructed to provide a signal to the SNO data-acquisition system when the laser welder is active.

6. Development work has started on a new preamplifier design for the SNO NCDs. The new preamplifier will have a much wider bandwidth and lower input noise than the present NCD preamplifiers. This is necessary to provide improved position resolution.

7. We constructed additional scope isolator boards, summing junction boards, approximately 70 double-shielded coaxial cables and various other cables for the SNO Underground cool-down electronics and data-acquisition system. This system was installed and tested this year for 96 neutral-current detector channels.

8. We are presently constructing 12 shaper adc boards, linear VME power supplies and other electronics for use in the KATRIN data-acquisition system. Design work has begun for electronics required in later stages of the KATRIN experiment.

7.4 PC based data acquisition system using JAM

H. E. Swanson

JAM, an open source data acquisition application authored at Yale University, is now being used at CENPA. Our data acquisition system consists of a PC running Windows XP Pro, a PCI CAMAC crate controller interface, the JAM program, and CAMAC.net an application which emulates their standalone VME based data acquisition computer. Fig. 7.4-1 describes the architecture of this application which was written in Microsoft's C#.net language. Classes are shown in boxes and individual threads of operation in ovals.

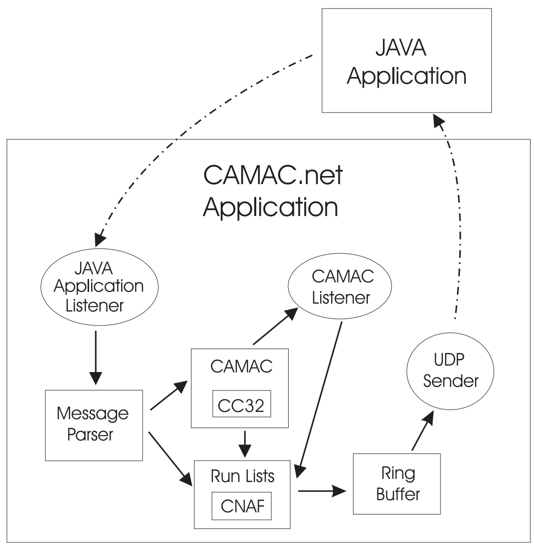

Figure 7.4-1. CAMAC.net application architecture.

The main method creates ring buffers to hold the data, initializes the CAMAC interface, starts the JAVA Application Listener thread and waits for further commands from JAM through this listener. The CNAF class is the most atomic as each of its objects represents a command function for a particular channel and module. The methods of the CAMAC class control the operation of the hardware interface. As JAM's On-Line setup loads the experimenters Sort class it signals the Message Parser to create run lists of CNAF objects from the CAMAC commands. Beginning acquisition starts the CAMAC Listener thread and enables the hardware interrupts. At each interrupt this listener commands CNAF objects in the run list to access the hardware interface and append their results to the ring buffer. When full the buffer starts a UDP Sender thread to send the data. The dot-dash curves show internet communication between the processes. Both JAM (shown as the JAVA Application) and our application are configured to use the Local Host as their IP address. No modifications to JAM's source code are required; it runs right out of the Jar. On a 1.6 GHz Pentium 4 computer with 8 ADC channels per event, the system saturates at about a 5 kHz event rate.

7.5 Status of an advanced object oriented real-time data acquistion system

M. A. Howe, F. McGirt,* J. Wouters* and J. F. Wilkerson

The Object oriented Real-time Control and Acquisition (Orca) software development effort has been described in past CENPA Annual Reports,[1] so only a brief overview is provided here. The goal of the Orca project is to produce a software application tool kit that can be used for quickly building flexible data acquisition systems. Since abandoning Linux in November of last year and adopting MacOS X as a development platform, progress has been rapid and continuous. Fig. 7.5-1 shows Orca in action.

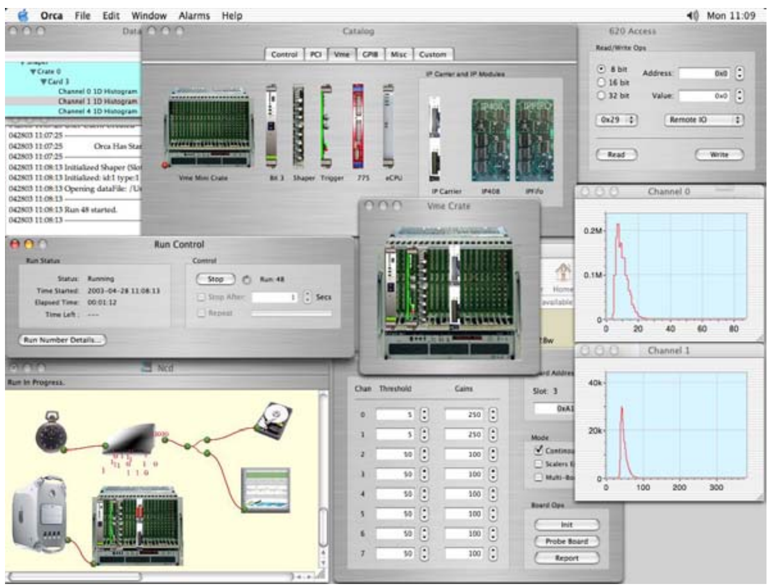

Figure 7.5-1. Orca taking NCD shaper data.

We now have working drivers for supporting the entire family of SBS PCI to VME adapters. Supported VME cards include the NCD/emiT shaper ADC, CAEN 775 TDC, CAEN 862 QDC, NCD/emiT 100MHz latched clock, and several IP modules, such as the IP408. A commercially obtained Ethernet to GPIB driver is being used to develop modules to support Tektronix digital scopes and HP Pulser hardware. Custom NCD hardware modules for the Multiplexer interface and Multiplexer Boxes have also been developed. A CAMAC driver has been developed and tested but, as of yet, no CAMAC cards are supported. In addition, modules have been developed that represent VME crates, data files, monitoring, data taking, and run control.

Using these modules a generic experiment can easily be set up to take event data from any of the supported cards.

*Los Alamos National Laboratory, Los Alamos, NM 87545.

[1]CENPA Annual Report, University of Washington (2001) p. 83; (2002) p. 81.

7.6 Laboratory computer systems

M. A. Howe, R. J. Seymour and J. F. Wilkerson

This year's newest "trend" has been the installation of dual-boot PCs on people's desktops. Instead of only Microsoft Windows, almost all of the new or replacement desktop systems have been set up with both Windows XP Pro and Red Hat Linux v7.3.

As happens with Linux, some PC motherboards are not well supported, so the hunt for cost-effective versus "works with Linux" occasionally hits snags. An example of a problem system is the Asus A7N266-VM. A nice Windows performer, a main-line motherboard manufacturer, but folding in the Linux drivers for the Nvidia chipsets is a problem. We have since "standardized" (while available) on a Matsonic MS9158E, as a component of 2.4 and 2.53 GHz Pentium 4 systems we are acquiring for $600.

Falling prices have also allowed continual "invisible" infrastructure improvements, such as the replacement of some network "hubs" with "switches", thereby doubling the effective bandwidth of the existing installed cabling by allowing full duplex operation and isolating many systems from competition for a shared link.

The SNO NCD group has installed a half-terabyte of shared large disks on some of their OS-X Macintoshes in the form of casually plugged-in 250 gigabyte external Firewire drives. These are shared with Linux systems located across the laboratory. That is just one example of the type of traffic growth spurts we experience.

Our firewall's attack logs are monitored daily. Any probes sourced from within the University of Washington's networks are forwarded to the campus network security office for action.

Our computing and analysis facility consists of:

- A mix of "generic" RedHat v7.3 Linux systems
- Twin dual-processor DEC/Compaq/HP Unix AlpherServer 4000s
- Five VMS/Vaxes and two VMS Alphas for email and "legacy" computing.
- The Ultra-Relativistic Heavy Ion group's Hewlett Packard Unix systems.
- The SNO and emiT groups rely upon Macintosh systems.
- Our Sun Sparcstation 20 and a pair of SunBlade 100 workstations serve CADENCE circuit design, analysis and layout duties.
- An MBD-11 and VMS VAXstation 3200 is the Lab's primary data acquisition system.
- A VAXstation is the Linac and Vacuum systems' control and display system.
- We have finally started taking data with the JAM acquisition and analysis system (see Section 7.4).
- Although not directly used by Lab personnel, we provide co-location services for the Institute for Nuclear Theory and the Physics Nuclear Theory group in the form of two VMS VAXstation 3200s. The Astronomy Department has located a 64-processor Xeon-based Beowulf cluster in our machine room.

8 Accelerator and Ion Sources

8.1 Van de Graaff accelerator operations and development

J. F. Amsbaugh, G. C. Harper, A. W. Myers, P. N. Peplowski, T. D. Van Wechel and D. I. Will

The tandem was entered 19 times this year. The ion species was changed during eight of the openings. The #3 accelerator tube was changed during three of the openings. The tube voltage gradient was changed eight times. The terminal ion source (TIS) canal was changed twice. Two different pelletron chain links were repaired during two of the openings. The internal components of the TIS were all replaced once during a routine servicing. One opening each was required to make repairs to a leak in one of the steerer feedthroughs, an idler, the TIS extraction supply, the terminal computer, and the TIS oscillator. One opening was used to install a parallel gas bottle tee to increase the available run time using protons. The TIS was removed and the foil stripper was installed during one opening. The accelerator tubes and stripper box were aligned during one opening.

Difficulty tuning the beam prompted us to check the alignment which we had not done since the earthquake of 28 February, 2001. Our survey showed that the optical target in the analyzing magnet was displaced 5 mm from the tandem line. Also, the accelerator tubes were no longer straight in the tank. Our conclusions led us to move the high energy end of the tandem 1.5 mm north and 0.75 mm up and to move the low energy end of the tandem 1.5 mm south. This brought the accelerator and analyzing magnet back onto the same line. The accelerator tubes and all other beam optics components were put onto the new line. The accelerator beam is now easy to tune and the object and image diagnostics indicate that the beam is well centered.

The tandem has begun producing x-rays in bursts when the terminal is raised above 6.5 MV. The x-rays can be substantially reduced by shorting two adjacent column planes somewhere in the tube #1 region with the shorting boat. The tank must be entered to pinpoint the location of the emitting plane and then further studies of this problem must be done.

During the 12 months from April 1, 2002 to March 31, 2003 the tandem pellet chains operated 1545 hours, the SpIS 758 hours, and the DEIS 62 hours. Additional statistics of accelerator operations are given in Table 8.1-1.

ACTIVITY SCHEDULED	**DAYS SCHEDULED**	**PERCENT of AVAILABLE TIME**
Molecular research, deck ion sources only	41	11
Nuclear physics research, deck ion sources	27	7
Nuclear physics research, terminal ion source	68	19
Subtotal, molecular or nuclear physics research	136	37
Machine development, maintenance, or crew training	81	22
Grand total	217	59

Table 8.1-1. Tandem Accelerator Operations April 1, 2002 to March 31, 2003.

8.2 Injector deck and ion sources

G. C. Harper and D. I. Will

A vacuum leak developed on the injector deck side of the deck accelerator tube. The seal in that region was disassembled, cleaned, and reassembled. The gridded lens was examined and found to be intact at the same time.

A molecular physics experiment required use of rubidium in the cesium oven of the modified 860i sputter ion source (SpIS).[1,2] Also see Section 6.1. Despite use of higher oven temperatures, repeated Rb blockages occurred. A redesigned oven and delivery tube assembly with 1/4 inch OD stainless steel tube and 1/4 inch VCR (Swagelok TM) fittings works well. A copper shell (part of the heater assembly) surrounds exposed parts of the delivery system maintaining tube and fitting temperatures above regulated oven temperature (as demonstrated with additional thermocouples).

The airlock for the SpIS cathode probe had screw caps electrically insulated with silicone rubber and consequently could not be easily disassembled for regular cleaning. Redesign of the acrylic air-lock insulator and associated flanges with long 1/4-20 nylon screws passing through clearance holes in that acrylic now allows rapid disassembly and reassembly for routine cleaning.

The direct-extraction ion source (DEIS) was put back into operation this year after being idle during the last reporting period. The DEIS was used in beam transport tests for a 3.5 MeV $^{1}H^{+}$ beam and for crew training. A spark during operation of the 860 SpIS punctured two of the DEIS HV cables. These have since been replaced.

The terminal ion source (TIS) was used for the $^{7}Be(p,\gamma)^{8}B$, $^{7}Li(d,p)^{8}Li$, and $^{6}Li(^{3}He,n)^{8}B$ experiments during this reporting period. The ions used were $^{1}H^{+}$ at terminal voltages from 0.16 MV to 1.5 MV, $^{2}H^{+}$ at terminal voltages from 0.77 MV to 1.4 MV, $^{3}He^{+}$ at a terminal voltages from 5.0 MV to 6.0 MV, and $^{4}He^{+}$ at a terminal voltage of 1.37 MV. The TIS was used in 68 of the 95 days scheduled for nuclear physics research this period. The internal components of the source were replaced once during routine servicing. The extractor supply and the RF oscillator supply were each repaired once.

[1] CENPA Annual Report, University of Washington (2002) p. 80.
[2] CENPA Annual Report, University of Washington (2001) p. 82.

8.3 A ^{8}B beam at the Tandem

M. K. Bacrania and D. W. Storm

We have developed the first radioactive beam at the UW Tandem. In order to be able to detect the ground-state decay of ^{8}B, in which the daughter ^{8}Be decays into two alpha particles with a total of 92 keV, it is necessary to implant the ^{8}B in the detector. (See Section 3.3 for a description of the experiment.) We realized that the Tandem switching magnet and beam transport can be used as a separator for radioactive ions created in a reaction. The object for the switching magnet is the tandem analyzing-magnet image, and our detector is placed just down stream of the center of the 24" scattering chamber on the 30° right beam line. We first tried making ^{8}B with the ^{6}Li(^{3}He,^{8}B)n reaction. However, this reaction requires the neutron to go backwards to make ^{8}B going at 0° into the narrow acceptance of the switching magnet, while the neutron angular distribution[1] is forward peaked. Consequently, we built a gas cell which is placed at the image of the Tandem analysing magnet, and we use a 24-MeV ^{6}Li beam (6 MeV in the cm) which produces ^{8}B of about 15.5 MeV at 0°. Detailed studies of the beam-line optics using Turtle[2] indicate that tuning a monoenergetic beam of 7.44 MeV ^{6}Li^{3+} through a small aperture in the chamber requires beamline settings that are optimum for the radioactive beam, with its relatively large energy and angle spreads. The system accepts approximately $\pm 3\%$ energy spread and ± 5 mr horizontally by ± 8 mr vertically. The energy and angle are correlated because the dispersion of the switching magnet is not canceled completely at the detector.

The gas cell is 28 mm in diameter with 2.5-μm Havar[3] windows and is filled with about 0.7 atmospheres of ^{3}He. With this configuration the energy spread of the outgoing ^{8}B is 10%, so a larger or higher pressure cell would be of no value. At those energies both B and Li are fully stripped. The magnetic rigidity of the 24-MeV ^{6}Li^{3+} is 1.8 times that of the ^{8}B^{5+}. The gas cell will run indefinitely with 600 nA of Li beam, and has survived short periods of over 1 μA. Backgrounds can be measured by filling the cell with ^{4}He.

It is necessary to take great care to operate with the least amount of material that can degrade the beam. We run with the image slits open to 0.7 inches and use the generating-volt-meter control to stabilize the Tandem terminal voltage. The beam is focused and steered carefully to avoid hitting any limiting apertures in the beam line after the analyzing magnet. The Li beam is stopped in a cup placed in the switching magnet, but only about half the current present at the location of the gas cell is measured in this cup. Presumably the rest is lost in the entrance to the switching magnet and against the poles because of multiple scattering in the gas cell windows. The detector itself has an 17-mm lead aperture in front of an annular scintillator with a 19-mm aperture. Another lead aperture of 15-mm diameter is 60-cm upstream of the detector, and this intercepts most of the ^{8}B which would otherwise hit the detector aperture. With this aperture system, we typically operate at a singles rate, predominantly degraded ^{6}Li, of 800 s^{-1} while tagging about two ^{8}B s^{-1} in our detector.

[1] P. van der Merwe, W. R. McMurray and I. J. Van Heerden, Nucl. Phys. A **103**, 474 (1967).
[2] PSI Graphic Turtle Framework by U. Rohrer based on a CERN-SLAC-FERMILAB version by K. L. Brown *et al.*; http://people.web.psi.ch/rohrer_u/turtle.htm.
[3] Hamilton Precision Metals, 1780 Rohrerstown Rd. Lancaster, PA 17601.

9 The Career Development Organization: A Student Organization

T. V. Bullard,* T. Butler, V. M. Gehman, K. Kazkaz, J. L. Orrell and L. C. Stonehill

The Career Development Organization (CDO)[1] for Physicists and Astronomers at the University of Washington is a student organization composed of physics and astronomy graduate students. The mission of the CDO is to facilitate the career advancement of physics and astronomy students by organizing career oriented seminars and workshops, providing access to career information specific to our field and hosting an annual Networking Day where students present their work to potential employers. In 2003 the CDO will begin its fourth year of career oriented programs.

CENPA boasts having three of the four CDO Presidents as student researchers – clearly demonstrating the motivation, versatility, and leadership which is typical of the graduate students that CENPA attracts. During 2002 there six were CENPA graduate students who were active contributers to the programs the CDO undertook. CDO's seminars included:

- Science Presentations to Employers Outside the Field: A How-To Guide
- The Grant-Machine Workshop: How Grants Work
- Life as a Physicist: Learning to Balance Academics and Life

Additionally, one of us (T. Butler) has initiated an outreach educational program designed to connect UW graduate students with high-school science teachers. Students develop an outline of a presentation geared toward high-school students and then teachers can arrange to have the students visit their class rooms.

The Second Annual UW Physics Networking Day took place on January 30, 2003. The Networking Day is the CDO's largest event during the year. The Networking Day brings representatives from industry and national laboratories to the University of Washington to interact with physics and astronomy students. The Second Annual Networking Day grew from the first and hosted 25 employer representatives and 30 student presenters. Students presented their work in both oral and poster formats. While the Networking Day is designed primarily to help students initiate and build contacts, only three months later the Networking Day has already borne the fruit of two job offers to participating students from participating employers. The Career Development Organization will continue make concrete contributions to the career advancement of the UW graduate students it serves and it is expected that CENPA graduate students will continue to have a large participation in and impact on the future CDO programs.

*Department of Physics, University of Washington, Seattle, WA 98195.

[1] http://students.washington.edu/cdophys.

10 CENPA Personnel

10.1 Faculty

Eric G. Adelberger	Professor	
Hans Bichsel	Affiliate Professor	
John G. Cramer	Professor	
Peter J. Doe	Research Professor	
Steven R. Elliott[1]	Research Assistant Professor	
George W. Farwell[2]		
Alejandro Garcia	Professor	
Jens H. Gundlach	Research Associate Professor	
Askel Hallin	Visiting Scientist	
Isaac Halpern	Professor Emeritus	
Blayne R. Heckel	Professor	
Arnd R. Junghans[3]	Research Assistant Professor	
R. G. Hamish Robertson	Professor;	Scientific Director
Kurt A. Snover	Research Professor	
Derek W. Storm	Research Professor;	Executive Director
Thomas A. Trainor	Research Professor	
Robert Vandenbosch	Professor Emeritus	
William G. Weitkamp	Professor Emeritus	
John F. Wilkerson	Professor	
Jin Hee Yoon	Visiting Scientist	

10.2 Postdoctoral Research Associates

Manojeet Bhattacharya[4]
Cristina Bordeanu
Joseph Formaggio
Ryuta Hazama[5]
Qingjun Liu
Sean McGee
Jeffrey Reid
Stephan Schlamminger

[1]Los Alamos National Laboratory, Los Alamos, NM 87545.
[2]Deceased, April 2003.
[3]Presently at F. Z. Rossendorf Institut fuer Kern- und Hadronenphysik, Dresden, Germany.
[4]Left May 2002.
[5]Presently at Kishimoto laboratory, Department of Physics, Osaka University Osaka 560-0043, Japan.

10.3 Predoctoral Research Associates

Minesh Bacrania
Theresa Bullard [1]
Thomas Butler
Ki-Young Choi
Ted Cook
G. Adam Cox
Charles Duba
Thomas Gadfort
Victor Gehman
William Clark Griffith
Karsten Heeger[2]
Dan Kapner
Kareem Kazkaz
Jeffrey Manor
Frank Marcoline
Kathryn Miknaitis
Erik Mohrmann
Hans Pieter Mumm
Noah Oblath
John Orrell
Anne Sallaska
Miles Smith[3]
Laura Stonehill
Smarajit Triambak
Jackson Wu

10.4 Research Experience for Undergraduates participants

George Gehring[4]
Chiara Losh[5]
Paul Searing[6]

[1]Department of Physics, University of Washington, Seattle, WA 98195.
[2]Lawrence Berkeley Laboratory, 1 Cyclotron Rd., Berkeley, CA 97420.
[3]DASI, University of Chicago, South Pole.
[4]Department of Physics, Juniata College, Huntington, PA 16652.
[5]Department of Physics and Astronomy, Arizona State University, Tempe, AZ 85287.
[6]Department of Physics, Cornell College, Mt Vernon, IA 52314.

10.5 Professional staff

The professional staff are listed with a description of their recent major efforts.

John F. Amsbaugh	Research Engineer	NCD deployment system
Tom H. Burritt	Research Engineer	Construction of SNO NCD's
Gregory C. Harper	Research Engineer	Electronic and mechanical design Accelerator upgrades and operation
Mark A. Howe	Research Engineer	Software for DAQ, control systems
Jeffrey Porter[1]	Visiting Staff	STAR-Data analysis
Duncan J. Prindle, Ph.D.	Research Scientist	Heavy Ion software
Richard J. Seymour	Computer Systems Manager	
H. Erik Swanson, Ph.D.	Research Physicist	Precision experimental equipment
Timothy D. Van Wechel	Electronics Engineer	Analog and digital electronic design
Brandon Wall	Research Scientist/ Engineer Assistant	SNO Operations
Douglas I. Will	Research Engineer	Cryogenics, Ion sources

10.6 Technical staff

James Elms	Instrument Maker
David Hyde	Instrument Maker
Allan Myers	Electronics Technician
Hendrik Simons	Instrument Maker, Shop Supervisor

10.7 Administrative staff

Barbara J. Fulton	Administrator
Kate J. Higgins	Fiscal Specialist

[1]Supported by Brookhaven National Laboratory, Upton, NY 11973.

10.8 Part Time Staff

Jesse Angle
Rogan Carr
Douglas Gabler
Matthias Gohl[1]
Araz Hamian[1]
Gregory Hodges
Robert Kyle
Christy McKinley
Bryan Munro
Patrick Peplowski
Derek Viita[1]
Matthew White
Ryan Bressler[1]
Stephanie Downey[1]
Evan Goetz
Mikel Grezner[1]
Danny Hinojosa
Karthik Jeyabalan
Mara Lemagie
Quinn Minor
Adam Oliver
Ehren Reich[1]
Mark Wehrenberg
Jonathan Will

[1] Left during 2002.

11 Publications

Published papers:

"Double beta decay," S. R. Elliott and P. Vogel, Ann. Rev. Nucl Part. Sci. **52**, 115 (2002).

"Shell effects and pairing correlations in fission investigated with radioactive beams," J. Benlliure, A. R. Junghans and K.-H. Schmidt, Eur. Phys. J A **13**, 93 (2002).

"Solar neutrino flux measurements by the Soviet-American gallium experiment (SAGE) for half the 22-year solar cycle," J. N. Abdurashitov and the SAGE Collaborators (including J. F. Wilkerson), J. Exp. Theor. Phys. **95**, 181 (2002).

"Comment on evidence for neutrinoless double beta decay," C. E. Aalseth and the SNO Collaborators (including P. J. Doe, S. R. Elliott, R. G. H. Robertson and J. F. Wilkerson), Mod. Phys. Lett. A **17**, 22, 1475 (2002).

"Lead percholate as a neutrino detection medium," L. C. Stonehill, M. K. Bacrania, P. J. Doe, S. R. Elliott, C. E. Paul and D. I. Will, Nucl. Instrum. Methods A **492**, 43 (2002).

"A prototype system for detecting the radio-frequency pulse associated with cosmic ray air showers," K. Green, J. L. Rosner, D. A. Suprun and J. F. Wilkerson, Nucl. Instrum. Methods in Phys. Res. A **498**, 256 (2003).

"A zero-to-few hundred eV proton beam for calibrations of neutron β decay experiments," F. Naab, L. O. Lamm, W. Zech, A. Garcia and H. P. Mumm, Nucl. Instrum. Methods in Phys. Res. B, **197**, 278 (2002).

"Isotope production comparision at ISOLDE with 1 and 1.4 GeV protons," U. Georg and the ISOLDE Collaborators (including A. R. Junghans), Nucl. Phys. A **701**, 137c (2002).

"Solar neutrino results and present status," V. V. Gorbachev *et al.*, Phys. Atomic Nucl. **65**, 2156 (2002).

"Cascade and anti-cascade+ production in central Pb+Pb collisions at 158-GeV/c per nucleon, S. V. Afanasiev and the NA49 Collaborators (including H. Bichsel, J. G. Cramer, Q. J. Liu, D. J. Prindle, J. G. Reid, T. A. Trainor and J. M. S. Wu), Phys. Lett. B **538**, 275 (2002) [hep-ex/0202037].

"Low temperature measurement of the giant dipole resonance width," P. Heckman, D. Bazin, J. R. Beene, Y. Blumenfeld, M,J. Chromik, M. L. Halbert, J. F. Liang, E. Mohrmann, T. Nakamura, A. Navin, B. M. Sherrill, K. A. Snover, M. Thoennessen, E. Tryggestad and R. L. Varner, Phys. Lett. B **555**, 43 (2003).

"Shell corrections in stopping power," H. Bichsel, Phys. Rev. A **65**, 052709 (2002).

"Reanalyses of α+α scattering and β-delayed α spectra from ^{8}Li and ^{8}B decays," M. Bhattacharya and E. G. Adelberger, Phys. Rev. C. **65**, 055502 (2002).

"Elliptic flow from two- and four-particle correlations in Au + Au collisions at $\sqrt{s_{NN}} = 130$ GeV," C. Adler and the STAR Collaborators (including H. Bichsel, J. G. Cramer, Q. J. Liu, D. J. Prindle, J. G. Reid, T. A. Trainor and J. M. S. Wu), Phys. Rev. C **66**, 034904 (2002), [nucl-ex/0206001].

"Energy dependence of pion and kaon production in central Pb + Pb collisions," S. V. Afanasiev and the NA49 Collaborators including (H. Bichsel, J. G. Cramer, Q. J. Liu, D. J. Prindle, J. G. Reid, T. A. Trainor and J. M. S. Wu), Phys. Rev. C **66**, 054902 (2002) [nucl-ex/0205002].

"K*(892)^0 production in relativistic heavy ion collisions at $\sqrt{s_{NN}} = 130$ GeV," C. Adler and the STAR Collaborators (including H. Bichsel, J. G. Cramer, Q. J. Liu, D. J. Prindle, J. G. Reid, T. A. Trainor and J. M. S. Wu), Phys. Rev. C **66**, 061901(R) (2002), [nucl-ex/0205015].

"Constraining the leading weak axial two-body current by SNO and Super-K," J. -W. Chen, K. M. Heeger and R. G. H. Robertson, Phys. Rev. C **67**, 025801 (2003) [nucl-th/0210037].

"Passage of particles through matter," H. Bichsel, D. E. Groom and S. R. Klein, Section 26 in "Review of Particle Physics," Phys. Rev. D **66**, 010001-1 (2002).

"Re-validation of the isobaric mass multiplet equation," M. C. Pyle, A. García, E. Tatar, J. Cox, B. K. Nayak, S. Triambak, B. Laughman, A. Komives, L. O. Lamm, T. Finnessy, L. D. Knutson and P. A. Voytas, Phys. Rev. Lett. **88**, 122501-1 (2002).

"Direct evidence for neutrino flavor transformation from neutral-current interactions in the Sudbury Neutrino Observatory," Q .R. Ahmad and the SNO Collaborators, Phys. Rev. Lett. **89**, 011301 (2002).

"Measurement of day and night neutrino energy spectra at SNO and constraints on neutrino mixing parameters," Q. R. Ahmad and the SNO Collaborators, Phys. Rev. Lett. **89**, 011302 (2002).

"Mid-rapidity lambda and lambda bar production in Au + Au collisions at $\sqrt{s_{NN}} = 130$ GeV," C. Adler and the STAR Collaborators (including H. Bichsel, J. G. Cramer, Q. J. Liu, D. J. Prindle, J. G. Reid, T. A. Trainor and J. M. S. Wu), Phys. Rev. Lett. **89**, 092301 (2002) [nucl-ex/0203016].

"Azimuthal anisotrophy of K_s^0 and $\Lambda + \Lambda$-bar production at mid-rapidity from Au+Au collisions at $\sqrt{s_{NN}} = 130$ GeV," C. Adler and the STAR Collaborators (including H. Bichsel, J. G. Cramer, Q. J. Liu, D. J. Prindle, J. G. Reid, T. A. Trainor and J. M. S. Wu), Phys. Rev. Lett. **89**, 132301 (2002) [hep-ex/0205072].

"Centrality dependence of high p_T hadron suppression in Au + Au collisions at $\sqrt{s_{NN}} = 130$ GeV," C. Adler and the STAR Collaborators (including H. Bichsel, J. G. Cramer, Q. J. Liu, D. J. Prindle, J. G. Reid, T. A. Trainor and J. M. S. Wu), Phys. Rev. Lett. **89**, 202301 (2002), [nucl-ex/0206011].

"Coherent Rho_0 production in ultra-peripheral heavy in collisions," C. Adler and the STAR

Collaborators (including H. Bichsel, J. G. Cramer, Q. J. Liu, D. J. Prindle, J. G. Reid, T. A. Trainor and J. M. S. Wu), Phys. Rev. Lett. **89**, 272303 (2002), [nucl-ex/0206004].

"Azimuthal anisotropy and correlations in the hard scattering regime at RHIC," C. Adler and the STAR Collaborators (including H. Bichsel, J. G. Cramer, Q. J. Liu, D. J. Prindle, J. G. Reid, T. A. Trainor and J. M. S. Wu), Phys. Rev. Lett. **90**, 032301 (2003).

"Disappearance of back-to-back high p_T hadron correlations in central Au + Au collisions at $\sqrt{s_{NN}} = 200$ GeV," C. Adler and the STAR Collaborators (including H. Bichsel, J. G. Cramer, Q. J. Liu, D. J. Prindle, J. G. Reid, T. A. Trainor and J. M. S. Wu), Phys. Rev. Lett. **90**, 082302 (2003), [nucl-ex/0210033].

"Sub-millimeter tests of the gravitational inverse square law," E. G. Adelberger, *Proceedings of the Second Meeting on CPT and Lorentz Symmetry*, ed. V. A. Kostelecky, World Scientific (2002) p. 9, hep-ex/0202008+.

"Extra dimensions, scalars fields, and CPT: tests of the gravitational inverse square law," B. Heckel, *Proceedings of the Eighteenth International Conference on Atomic Physics, ICAP 2002*, World Scientific, 2002.

"The new status of ^{37}Ar artificial neutrino source project," J. N. Abdurashitov *et al.*, Nucl. Phys. B Proceeding Supplements, **110**, 326 (2002).

"Purpose and physics of event-by-event analysis, T. A. Trainor, *AIP Conference Proceedings*, **631**, 599 (2003).

"First results from STAR EbyE analysis at RHIC," T. A. Trainor, *Proceedings Heavy Ion Physics*, **15**, 183 (2002).

Papers submitted or to be published:

"Tests of the gravitational inverse square law," E. G. Adelberger, B. R. Heckel and A. E. Nelson, Ann. Rev. Part Sci. accepted for publication.

"Correlation analysis with scale-local entropy measures," J. G. Reid and T. A. Trainor, submitted to J. Phys. A, math-ph/0304010.

"Scale-local dimension of strange attractors," J. G. Reid and T. A. Trainor submitted to J. Phys. A, math-ph/0305022).

"Strange anti-particle to particle ratios at mid-rapidity in $\sqrt{s_{NN}} = 130$ GeV Au + Au collisions," C. Adler and the STAR Collaborators (including H. Bichsel, J. G. Cramer, Q. J. Liu, D. J. Prindle, J. G. Reid, T. A. Trainor and J. M. S. Wu), submitted to Phys. Lett. B, [nucl-ex/0211024].

"Kaon production and kaon to pion ratio in Au + Au collisions at $\sqrt{s_{NN}} = 130$ GeV," C. Adler and the STAR Collaborators (including H. Bichsel, J. G. Cramer, Q. J. Liu, D. J. Prindle,

J. G. Reid, T. A. Trainor and J. M. S. Wu), to be submitted to Phys. Lett. B, [nucl-ex/0206008].

"Directed and elliptic flow of charged pions and protons in Pb + Pb collisions at 40-A-GeV and 158-A-GeV," C. Alt and the NA49 Collaborators (including H. Bichsel, J. G. Cramer, Q. J. Liu, D. J. Prindle, J. G. Reid, T. A. Trainor and J. M. S. Wu), submitted to Phys. Rev. C, [nucl-ex/0303001].

"Is e^+-e^-pair emission important in the determination of the ^{3}He + ^{4}He S-factor?" K. A. Snover and A. E. Hurd, Phys. Rev. C, in press.

"Jet quenching and event-wise mean-pt fluctuations Au-Au collisions at $\sqrt{s_{NN}} = 200$ GeV in Hijing 1.37," Q. J. Liu and T. A. Trainor, submitted to Phys. Lett. B, hep-ph/0301214.

"Bose-Einstein correlations of charge kaons in central Pb-Pb collisions at E = 158 A GeV," S. V. Afanasiev and the NA49 Collaborators (including H. Bichsel, J. G. Cramer, Q. J. Liu, D. J. Prindle, J. G. Reid, T. A. Trainor and J. M. S. Wu), submitted to Phys. Lett. B.

Erratum: "Midrapidity antiproton-to-proton ratio from Au+Au $\sqrt{s_{NN}} = 130$ GeV," [Phys. Rev. Lett. **86**, 4778 (2001)], C. Adler and the STAR Collaborators (including H. Bichsel, J. G. Cramer, Q. J. Liu, D. J. Prindle, J. G. Reid, T. A. Trainor and J. M. S. Wu), submitted to Phys. Rev. Lett.

"Narrowing of the balance function with centrality in Au+Au collisions at $\sqrt{s_{NN}} = 130$ GeV," C. Adler and the STAR Collaborators (including H. Bichsel, J. G. Cramer, Q. J. Liu, D. J. Prindle, J. G. Reid, T. A. Trainor and J. M. S. Wu), submitted to Phys. Rev. Lett., [nucl-ex/0301014].

"New tests of the strong equivalence principle and of the inverse square law," E. G. Adelberger, *Proceedings of XXV Johns Hopkins Workshop 'A Relativistic Spacetime Odyssey,'* to be published.

Invited talks, abstracts and other conference presentations:

"Fundamental physics and tests of Newton's inverse-square law," and "Fundamental physics and tests of Einstein's equivalence principle," E. G. Adelberger, *Lectures at Lake Louise Winter Institute*, Lake Louise, Canada, February, 2002.

"Sub-millimeter tests of the gravitational inverse-square law," E. G. Adelberger,
Physics Colloquium, Johns Hopkins University, Baltimore, MD, February, 2002;
Physics Colloquium, Iowa State University, Ames, IA, March, 2002;
Distinguished Visitor, Haverford College, Haverford, PA, April, 2002;
Physics Colloquium, University of Chicago, Chicago, IL, April, 2002;
Physics Colloquium, New York University, New York, NY, November, 2002;
Physics Colloquium, Carnegie-Mellon University, Pittsburgh, PA, November, 2002;
William Nordberg Memorial Lecturer, Goddard Space Flight Center, November, 2002;
Physics Colloquium, University of Toronto, Toronto, Canada, February, 2003;

Invited Talk, AAAS Meeting, Denver, CO, February, 2003.

"Experimental searches for equivalence principle violations," J. H. Gundlach, *Physik Zentrum Bad Honnef Workshop, Aspects of Quantum Gravity: From Theory to Experimental Search*, Germany, February, 2002.

"The complexity of RHIC collisions," T. A. Trainor, Nuclear Physics Institute ASCR, Prague, Czech Republic, April, 2002.

"Big G and gravity close up," J. H. Gundlach, colloquium, Tulane University, New Orleans, LA, April, 2002.

"Solving the solar neutrino problem," J. F. Wilkerson, Invited Plenary Talk, American Physical Society, Albuquerque, NM, April, 2002, Bull. Am. Phys. Soc. M1.002 (2002).

"Testing the gravitational inverse-square law at sub-mm length scales," E. G. Adelberger, American Physical Society, Albuquerque, NM, April, 2002, Bull. Am. Phys. Soc. U6.003 (2002).

"Measuring the neutrino interaction rates in SNO for variable fiducial volumes," K. Heeger, American Physical Society, Albuquerque, NM, April, 2002, Bull. Am. Phys. Soc. X7.004 (2002).

"Double beta decay and NUSL," S. R. Elliott and C. Alseth, American Physical Society, Albuquerque, NM, April, 2002, Bull. Am. Phys. Soc. 07.007 (2002).

"Next-generation double-beta decay experiments," C. Alseth and S. R. Elliott, American Physical Society, Albuquerque, NM, April, 2002, Bull. Am. Phys. Soc. 07.008 (2002).

"Direct searches for neutrino mass," J. F. Wilkerson, Invited talk, *Neutrino Masses and Mixing Mini Workshop*, Institute for Nuclear Theory, University of Washington, Seattle, WA, April, 2002.

"Solar neutrino experiments," R. G. H. Robertson, Invited talk, *Neutrino Masses and Mixing Mini Workshop*, Institute for Nuclear Theory, University of Washington, Seattle, WA, April, 2002.

"Status of the National Underground Science Laboratory," J. F. Wilkerson, Triangle Universities, Nuclear Laboratory Seminar, Duke University, Durham, NC, April, 2002.

"The solar neutrino mystery - solved!" J. F. Wilkerson, Physics Colloquium, University of North Carolina, Chapel Hill, NC, April, 2002; Physics Colloquium, Duke University, September, 2002.

"The Seattle - TRIUMF ^{7}Be$(p,\gamma)^8$B experiment," K. A. Snover, Invited talk, *Northwest Section meeting of the APS*, Banff, Canada, May, 2002.

"Electron antineutrino detection at the Sudbury Neutrino Observatory," J. L. Orrell, Contributed talk, *Northwest Section meeting of the APS*, Banff, Canada, May, 2002.

"The surprising saga of the neutrino," J. F. Wilkerson, Invited introductory talk to International KATRIN Review Panel, Karlsruhe, Germany, May, 2002.

"Recent results from the Sudbury Neutrino Observatory," P. J. Doe, Invited talk to International KATRIN Review Panel, Karlsruhe, Germany, May, 2002.

"SNO flies: The solar neutrino problem resolved," R. G. H. Robertson, Colloqiuium, University of Oregon, Eugene, OR, May, 2002; University of Arizona, AZ, October, 2002; Goddard Space Flight Center, November, 2002.

"Torsion balance experiments at the University of Washington," J. H. Gundlach, International Workshop: *Experiments on the Equivalence Principle: from Earth to Space Probing General Relativity*, Pisa, Italy, May, 2002.

'The correlation structure of RHIC Au-Au events," T. A. Trainor, *10th International Workshop on Multiparticle Production*, Istron Bay, Crete, June, 2002.

"Extra dimensions, scalars fields and CPT: tests of the gravitational inverse square law," Invited talk, B. Heckel, *ICAP 2002 Conference*, Cambridge, MA, July, 2002.

"Theory of particle identification (PID) for TPCs," H. Bichsel, Poster presented at *Proceedings of Quark Matter 2002*, Nantes, France, July, 2002.

"Preparation for neutral current detector deployment in the Sudbury Neutrino Observatory," L. C. Stonehill, *Nuclear Physics Summer School*, St. John's College, Santa Fe, NM, August, 2002.

"The Solar Neutrino Puzzle: Mapping a Solution," J. A. Formaggio, Invited talk, Particle Physics and Cosmology, *Proceedings of the Third Tropical Workshop on Particle Physics and Cosmology – Neutrinos, Branes, and Cosmology*, AIP Conference Proceedings, **655**, 3 (2002); San Juan, Puerto Rico, August, 2002.

"How many space dimensions does the universe have?" and "Sub-millimeter tests of the gravitational inverse-square law," E. G. Adelberger, *LIGO Public Lecture*, Pasadena, CA, August, 2002.

"Fundamental physics and tests of Newton's inverse-square law," and "Fundamental physics and tests of Einstein's equivalence principle," E. G. Adelberger, Lecturer at *Villa Mondragone International School on Gravitation and Cosmology*, Frascati, Italy, September, 2002.

"New tests of Einstein's equivalence principle," and "How many space dimensions does the universe have?" E. G. Adelberger, Umeezawa Distinguished Visitor, University of Alberta, Edmonton, Alberta, September, 2002.

"Direct neutrino mass measurements and prospects," R. G. H. Robertson, Invited talk, *Neutrinos and Subterranean Science Conference*, Washington, DC, September, 2002.

"Low-background underground counting facility panel," J. F. Wilkerson, Panel Discussion Leader, *International Workshop on Neutrinos and Subterranean Science*, Washington DC, September, 2002.

"Direct neutrino mass measurements via beta-decay," J. F. Wilkerson, Invited talk, *Neutrino News from the Lab and the Cosmos*, Fermilab, Batavia, IL, October, 2002.

"A new determination of the astrophysical S-factor for the ^{7}Be$(p, \gamma)^8$B reaction," A. R. Junghans, American Physical Society, East Lansing, MI, October, 2002, Bull. Am. Phys. Soc. **47**, No. 6, 18 (2002).

"Design considerations for a large metal-loaded liquid scintillator detector with applications for solar neutrino and double beta decay studies," P. J. Doe, R. G. H. Robertson, V. Gehman, G. Gehring, H. Iwamoto and D. I. Will, American Physical Society, East Lansing, MI, October, 2002, Bull. Am. Phys. Soc. **47**, No. 6, 49 (2002).

"Update on the day-night measurements in SNO," K. Miknaitis and the SNO Collaborators, American Physical Society, East Lansing, MI, October, 2002, Bull. Am. Phys. Soc. **47**, No. 6, 84 (2002).

"University of Washington lab report to SNEAP," G. C. Harper, *Symposium for Northeastern Accelerator Personnel*, Lafayette, GA, October, 2002.

"Tandem terminal ion source, tandem beam tube problems, and tandem post-earthquake alignment," G. C. Harper, *Symposium for Northeastern Accelerator Personnel*, Lafayette, GA, October, 2002.

"Solving the solar neutrino problem," L. C. Stonehill, *The American Association of Physics Teachers Washington Section conference*, Eastern Washington University, Cheney, WA, October, 2002.

"The MOON double-beta decay, experiment," R. G. H. Robertson, Invited presentation, *SNOLAB Workshop*, Ottawa, Canada, November, 2002.

"Fundamental physics from lunar laser-ranging experiments," E. G. Adelberger, William Nordberg Memorial Lecturer, Goddard Space Flight Center, November, 2002.

"Going deep – discovery opportunities at a National Underground Science and Engineering Laboratory," J. F. Wilkerson, Physics Colloquium, Indiana University, January, 2003; Physics Division Colloquium, National Institute of Standards and Technology, Gaithersburg, MD, January, 2003.

"Was Newton right? New tests of the inverse square law," B. Heckel, Colloquiums, Columbia University, New York, NY, April, 2002; University of Chicago, Chicago, IL, January 2003.

"Interactions of fast charged particles with matter," H. Bichsel, Invited lecture at *Frontier Symposium on the Interaction between Particle Beams and Matter at OUS*, Okayama University of Science, Okayama, Japan, January, 2003.

"Next generation 0-neutrino double beta-decay detectors," J. F. Wilkerson, presentation to NSAC Orbach Sub-committee, New Brunswick, NJ, February, 2003.

“The neutral current detector phase of the Sudbury Neutrino Observatory,” L. C. Stonehill, Contributed talk, *Western Regional Nuclear and Particle Physics Conference*, Lake Louise, Canada, February, 2003.

“Search for the ^{8}B$(2^{+}) \rightarrow$ ^{8}B(0^{+}) ground state transition,” M. Bacrania, Contributed talk, *Western Regional Nuclear and Particle Physics Conference*, Lake Louise, Canada, February, 2003.

“Neutral current detectors in the Sudbury Neutrino Observatory,” L. C. Stonehill, Contributed talk, *Lake Louise Winter Institute*, Lake Louise, Canada, February, 2003.

“Nuclear beta decay as a tool to search for new physics,” A. García, Invited colloquium at the Physics Department, Idaho State University, Pocatello, ID, April, 2003.

“Prospects of nanopore DNA sequencing,” J. H. Gundlach, Condensed Matter Seminar, University of Washington, Seattle, WA, April, 2003.

“Majorana and MEGA: A proposed germanium-based search for $0\nu\beta\beta$ decay,” K. Kareem and the Majorana Collaborators, American Physical Society, Philadelphia, PA, April, 2003, Bull. Am. Phys. Soc. **48**, No. 2, 32 (2003).

“Status of the MOON ^{100}Mo double beta decay and solar neutrino project,” R. G. H. Robertson and the MOON Collaborators, American Physical Society, Philadelphia, PA, April, 2003, Bull. Am. Phys. Soc. **48**, No. 2, 32 (2003).

“Short distance tests of the inverse square law,” Invited talk, B. Heckel, *April Meeting of the APS*, E. Adelberger, D. Kapner, J. Gundlach, E. Swanson, C. D. Hoyle and U. Schmidt, American Physical Society, Philadelphia, PA, April, 2003, Bull. Am. Phys. Soc. **48**, No. 2, 85 (2003).

“Search for time reversal violation in neutron beta decay,” H. P. Mumm and the emiT Collaborators (including A. García, R. G. H. Robertson and J. F. Wilkerson), American Physical Society, Philadelphia, PA, April, 2003, Bull. Am. Phys. Soc. **48**, No. 2, 77 (2003).

“Short-range tests of Newton’s inverse square law,” E. G. Adelberger, J. H. Gundlach, B. R. Heckel, D. J. Kapner, H. E. Swanson and C. D. Hoyle, American Physical Society, Philadelphia, PA, April, 2003, Bull. Am. Phys. Soc. **48**, No. 2, 171 (2003).

Conference presentations by collaborators of CENPA personnel:

“An ultra low background counting facility at NUSL,” A. Hamer and the NUSL Collaborators (including J. F. Wilkerson), American Physical Society, Albuquerque, NM, April, 2002, Bull. Am. Phys. Soc. 07.008 (2002).

“Measurement of the PNC spin-rotation of transversely polarized neutrons travelling with liquid ^{4}He,” C. Bass and the Spin-Rotation Collaborators (including B. Heckel, E. G. Adelberger and H. E. Swanson), American Physical Society, East Lansing, MI, October, 2002, Bull. Am. Phys. Soc. **47**, No. 6, 85 (2002).

"Non-identical particle correlation analysis as a probe of transverse flow," F. Retiere and the STAR Collaborators;
"Correlations, fluctuations, and flow measurements from the STAR experiment, R. L. Ray and the STAR Collaborators;
"Measurement of source chaoticity for particle emission in Au+Au collisions at $\sqrt{s_{NN}} = 130$ GeV using 3-particle HBT correlations," R. Willson and the STAR Collaborators;
"Identical particle interferometry at STAR, M. Lopez Noriega and the STAR Collaborators;
"Results on correlations and fluctuations," C. Blume and the NA49 Collaborators;
"Directed and elliptic flow in Pb+Pb collisions at 40-A-GeV and 158-A-GeV," A. Wetzler and the NA49 Collaborators;
Proceedings of Quark Matter 2002, Nantes, France, July, 2002, to appear in Nucl. Phys. A.

"Azimuthally-sensitive pion HBT at RHIC," M. Lisa and the STAR Collaborators, presented at the *XXXII International Symposium on Multiparticle Dynamics*, (ISMD2002), Alushta, Ukraine, [nucl-ex/0301005].

"Recent results from STAR," M. Oldenburg and the STAR Collaborators, *Proceeding of the 14th Topical Conference on Hadron Collider Physics, (HCP 2002)*, Karlsruhe, Germany, [nucl-ex/0211033].

"Recent results of NA49," H. G. Fischer and the NA49 Collaborators, *Proceedings of 30th International Workshop on Gross Properties of Nuclei and Nuclear Excitation*, Hirschegg, Austria, published in Hirschegg 2002, Ultrarelativistic heavy-ion collisions, 39-44, 2002.

11.1 Degrees Granted, Academic Year, 2002-2003

Model-Independent Measurement of the Neutral-Current Interaction Rate of Solar ^{8}B Neutrinos with Deuterium in the Sudbury Neutrino Observatory, Karsten Miklas Heeger (2002).

Event-by-Event Analysis Methods and Applications to Relativistic Heavy-Ion Collision Data, Jeffrey Gordon Reid (2002).

An Investigation of Matter Enhanced Neutrino Oscilation with the Sudbury Neutrino Observatory, Miles Walter Eldon Smith (2002).